1-1-1994

Phase behavior, crystallization kinetics and morphologies of poly([epsilon]-caprolactone) (PCL)/polycarbonate (PC) blends/

Yunwa Wilson Cheung
University of Massachusetts Amherst

PHASE BEHAVIOR, CRYSTALLIZATION KINETICS AND MORPHOLOGIES OF POLY(ε-CAPROLACTONE) (PCL)/ POLYCARBONATE (PC) BLENDS

A Dissertation Presented

by

YUNWA WILSON CHEUNG

Submitted to the Graduate School of the
University of Massachusetts Amherst in partial fulfillment
of the requirements for the degree of

DOCTOR OF PHILOSOPHY

February 1994

Department of Polymer Science and Engineering

PHASE BEHAVIOR, CRYSTALLIZATION KINETICS AND MORPHOLOGIES OF POLY(ε-CAPROLACTONE) (PCL)/ POLYCARBONATE (PC) BLENDS

A Dissertation Presented

by

YUNWA WILSON CHEUNG

Approved as to style and content by:

Richard S. Stein, Chairperson of Committee

William J. MacKnight, Member

Henning H. Winter, Member

William J. MacKnight, Department Head
Polymer Science and Engineering

ACKNOWLEDGMENTS

It has been a tremendous honor for me to work and learn under my advisor Prof. Richard S. Stein. I am deeply grateful for his guidance, support and patience. His incisive physical insight and dedication have been truly inspirational. I would also like to thank Profs. MacKnight and Winter for serving on my committee. Their valuable comments and suggestions are greatly appreciated.

This work would not have been possible without the assistance and collaboration of many people. It gives me great pleasure to acknowledge the help of Drs. Wignall and Lin of ORNL and Dr. Hammouda of NIST for their help with the SANS and SAXS measurements. Special thanks to Prof. Chu and Mr. Wu of SUNY at Stony Brook for their help with the synchrotron experiments. I would also like to acknowledge Dr. Yang and Mr. Yazobucci of Kodak for their help with the synthesis of deuterated polycarbonate. Financial support from Novacor Inc. is greatly appreciated.

I would like to say thanks to the members of Stein's group and friends (too many to mention here) who made my graduate study at Amherst so enjoyable and memorable.

Finally and above all, I would like to extend my deepest appreciation for my family for their love, support and encouragement.

ABSTRACT

PHASE BEHAVIOR, CRYSTALLIZATION KINETICS,

AND MORPHOLOGIES OF POLY(ε-CAPROLACTONE) (PCL)/

POLYCARBONATE (PC) BLENDS

FEBRUARY 1994

YUNWA WILSON CHEUNG, B.E., THE COOPER UNION

M.S., NORTHWESTERN UNIVERSITY

Ph. D., UNIVERSITY OF MASSACHUSETTS AMHERST

Directed by: Professor Richard S. Stein

Small-angle neutron and X-ray scattering (SANS and SAXS) coupled with thermal analysis, optical microscopy and FTIR have been employed to probe the phase behavior, crystallization kinetics and crystalline morphologies of PCL/PC blends.

The composition dependence of the glass transition temperature T_g exhibited a discontinuity and was critically analyzed using the classical equations of Gordon-Taylor and Fox, and the free volume theory of Kovacs. Results derived from the random phase approximation (RPA) analysis of the SANS profiles measured at 30 °C for the deuterated PC-rich blends and those obtained from the melting point depression analysis of the PCL-rich blends suggested favorable blend interactions.

The effects of composition, crystallization temperature and PC crystallinity on the athermal and isothermal crystallization kinetics of PCL in PCL-rich blends have been examined. Combination of the overall crystallization rate measurements and the radial growth rate results unequivocally demonstrated that PC is an effective nucleating medium

for PCL crystallization. Evolution of the PCL lamellar growth was monitored by synchrotron SAXS. The interlamellar spacing initially varied with time and then approached a plateau value at the later stage of crystallization. An insertion mechanism is proposed in which PCL is crystallized in the amorphous intralamellar phase of PC.

Crystalline morphologies of deuterated PC/PCL blends were studied by SANS and SAXS in the semicrystalline/amorphous state (above T_m of pure PCL). A two-correlation length model provided an excellent fit for the SANS data over the entire composition range. The long range correlation length (~ 10^2 Å) and the short range correlation length (~ 10 Å) derived from this model were inferred to be associated with the crystalline PC domain and the local cluster in the amorphous phase, respectively.

Quantitative SAXS analysis suggested that random mixing of PCL and PC lamellae occurred in the semicrystalline/semicrystalline state. Two distinct regions of incorporation were identified in the semicrystalline/amorphous state. It was found that PCL was rejected from the interlamellar region in the PCL-rich blends. In contrast, PCL was incorporated into the amorphous phase between the crystalline lamellae in the PC-rich blends.

TABLE OF CONTENTS

LIST OF TABLES

LIST OF FIGURES

CHAPTER 1

GENERAL INTRODUCTION

Fundamental to any polymer blend study is the elucidation of the structure-property relationships of the resulting material produced by mixing of two or more polymers. Academically, polymer blend study occupies an important place in the condensed matter physics hierarchy due to the unique molecular architecture of polymers. Commercially, blending is still one of most cost-effective and efficient means of producing "tailored-made" materials. Polymer blend thermodynamics remains to be one of the most challenging areas in statistical mechanics and is extremely important in the design of useful polymeric materials. Phase separation is often found in miscible systems where demixing occurs at a lower critical solution temperature (LCST) or an upper critical solution temperature (UCST). The dynamic interplay between thermodynamics and kinetics determines the morphologies and thus the properties of the resulting materials.

Poly(ε-caprolactone) (PCL) is an aliphatic polyester containing five-methylene units and is known to be miscible with numerous polymers[1] including poly(vinyl chloride) (PVC), poly(hydroxy ether) prepared from bisphenol A and epichlorohydrin, chlorinated polyether, and bisphenol A polycarbonate (PC). PCL is also biodegradable and exhibits a relatively low glass transition temperature T_g (~ -60 °C) and melting temperature T_m (~ 60 °C). Bisphenol A polycarbonate (PC) is one of the toughest polymers and exhibits a fairly high T_g (~ 150 °C) and T_m (~ 230 °C). The chemical and crystal structures of these two polymers are illustrated in Table 1.1. Blends of PCL/PC have been shown to undergo multiple phase transitions and to exhibit very complex morphologies.[2-4] Therefore, it is the major focus of this investigation to explore the complex phase behavior, crystallization kinetics, and morphologies of the PCL/PC blends.

Before delineating the scope of our investigation, the PCL/PVC system will be briefly reviewed and contrasted against the PCL/PC system. Extensive morphological investigations of the PCL/PVC system have been conducted using small-angle light scattering (SALS) and small-angle X-ray scattering (SAXS).[5-7] It was found that PCL crystallization in the blends was completely suppressed with the presence of more than 50% PVC. Blends rich in PCL showed that PCL formed volume filling spherulites incorporating PVC within the spherulites. Spherulitic size was found to be almost independent of composition. SAXS revealed that PVC was trapped within the amorphous region between the PCL lamellae as the long period increased with increasing PVC. Additionally, Guinier analysis on dilute blend of PCL in PVC indicated that the PCL radius of gyration R_g was expanded in the PVC matrix and the second virial coefficient A_2 was approximately zero. These two observations strongly supported the conclusion that PCL was molecularly dispersed in the PVC matrix.

The phase behavior of the PCL/PC blends has been examined by differential scanning calorimetry (DSC) and dynamic mechanical analysis (DMA),[2] Fourier transform infrared spectroscopy (FTIR),[3] and analyzed with melting point depression analysis.[4] On the basis of these studies, this blend system was found to be miscible over the entire composition range as evidenced by the presence of a single T_g. Additionally, the blends exhibited a lower critical solution temperature (LCST ~ 260 °C) where phase separation was observed. PC is traditionally classified as an amorphous polymer and can only crystallize at temperatures above its T_g or when mixed with a plasticizer such as a low molecular weight solvent. Interestingly, PC was found to crystallize even at room temperature in blends containing more than 50% PCL. Hence, the PCL-rich blends are semicrystalline/semicrystalline at room temperature. Similar to the PCL/PVC system, both PCL and PC crystallization were greatly suppressed in blends containing more than 50% PC.

Calorimetric study of low molecular weight analogs of PC and PCL[8] revealed negative heat of mixing indicating the presence of specific interactions. This exothermic interaction was attributed to the n-π complex formation between the electrons of the ester carbonyl and the aromatic ring of the carbonate molecule. Results derived from the FTIR studies[9] suggested the presence of specific interactions between these two polymeric components in the amorphous state. The nature of the specific interactions is analogous to that for the PCL/PVC system[10] where frequency shifts for both the crystalline and amorphous υ_S(C=O) as a function of PVC were observed.

A much more quantitative method to characterize miscibility is to measure the Flory interaction parameter χ. Various techniques including melting point depression analysis,[11] inverse gas chromatography,[12] and small-angle neutron scattering (SANS)[13-14] have been employed to measure χ. Due to its simplicity and convenience, melting point depression based on DSC measurements, still remains to be one of the most widely used techniques for χ determination. This approach is based on the assumption that the melting point depression is solely caused by the thermodynamics of mixing of miscible polymers. However, changes in lamellar thickness due to blending, the degree of crystalline perfection, and the physical nature of the amorphous phase surrounding the crystalline phase can profoundly affect the melting point and thus rendering the analysis questionable.

On the basis of the assumption that the observed melting point depression of the crystalline PCL component in the PCL/PC blends was entirely due to polymer-polymer interaction, Varnell et. al.[3] concluded from their DSC study that the χ parameter lies between -1 and -2. From the exothermic heats of mixing between small molecular analogs of PC and PCL, Cruz et. al.[8] estimated χ to be between -0.2 and -0.3. However, Jonza and Porter[4] reported an equilibrium melting temperature, obtained from Hoffman-Weeks extrapolation, of 71-73 $^{\circ}$C for PCL. This study indicated that the PCL-rich blends

yielded identical melting endotherms and Hoffman-Weeks extrapolations as the PCL homopolymer. This result leads to an interaction parameter $0 \sim \chi \leq \chi_{crit}$ (0.024) suggesting that there are no specific interactions between the two polymers. The sources of the differences in the reported χ values probably arise from the inherent deficiency and uncertainty in the melting point depression analysis.

Depending on the composition, temperature and the processing conditions, the PCL/PC blends could be a semicrystalline/semicrystalline, semicrystalline/amorphous, amorphous/amorphous and immiscible material. Unique to the PCL-rich blends is the three-phase morphology in which two distinct crystalline phases (PCL and PC) coexist with a mixed amorphous phase. As described earlier, studies on this system have been primarily confined to examining the phase behavior with thermal analysis and FTIR. In order to establish a better understanding of this complex blend system, the focus of this investigation will be directed at elucidating the phase behavior including miscibility and thermal stability, crystallization kinetics and mechanisms, and the crystalline blend morphologies primarily using small-angle scattering coupled with thermal analysis and optical microscopy. Table 1.2 summarizes the properties of small-angle scattering measurements based on the various types of radiation. It can be seen that small-angle scattering is extremely powerful as it probes both the thermodynamics and structure of materials.

Specifically, the thesis is organized into seven chapters. Chapter 2 will examine the miscibility and thermal stability of the blends. Differential scanning calorimetry, and cloud point measurements based on the total internal reflection geometry will be employed to identify the various phase transitions. Melting point depression analysis coupled with Hoffman-Weeks extrapolations will be used to evaluate blend miscibility. The composition dependence of the glass transition temperature will be critically analyzed using the classical equations of Gordon-Taylor and Fox, and the free volume formulation

of Kovacs. Thermal stability of the blends at temperatures close to the LCST will be assessed with FTIR and thermogravimetric analysis (TGA). Due to the thermal instability of PCL at elevated temperatures close to the LCST, the blends may undergo chain scission and/or transesterification. Nuclear magnetic resonance (NMR) spectroscopy will be used to evaluate the chemical integrity of the blends. Miscibility between PCL and deuterated PC (d-PC) in the amorphous/amorphous state will be probed with small-angle neutron scattering (SANS). In most SANS studies of polymer blends, one component is normally deuterated and the other is hydrogenated to create scattering contrast. It has been observed that deuteration may perturb the thermodynamics of the system.[15] Therefore, it is important to stress that the results derived from this study may not truly reflect the behavior of the corresponding hydrogenated system.

Chapters 3 and 4 will focus on the evolution of PCL crystalline structures in the PCL-rich blends as probed by DSC, optical microscopy, and synchrotron small-angle X-ray scattering (SAXS), respectively. In addition to the traditional variables of composition and crystallization temperature, the effects of PC crystallinity on the PCL crystallization kinetics will be explored. This comprehensive study is one of the first attempts at unraveling the complex crystallization kinetics and mechanisms of a semicrystalline/semicrystalline blend system at both the microscopic and macroscopic levels.

In Chapter 3 the overall crystallization rate and the radial growth rate will be measured by DSC and optical microscopy, respectively. Both athermal and isothermal crystallization kinetics will be critically examined. On the basis of these results, the composite effects of nucleation and growth can be decoupled and analyzed with the nucleation and growth theory. In order to investigate the crystallization kinetics and mechanisms at a microscopic level, time resolved synchrotron SAXS will be employed to monitor the PCL lamellar evolution in the PCL-rich blends. Chapter 4 will focus on the

isothermal crystallization kinetics of PCL measured in terms of the PCL lamellar development.

Chapters 5 and 6 will examine the crystalline blend morphologies as revealed by SANS, SAXS and SALS. The main focus of this part of the investigations is to elucidate the blend morphologies, at both the lamellar and spherulitic levels, in both the semi-crystalline/semicrystalline and semicrystalline/amorphous states. Attention will be directed at a critical analysis of the SANS results for the d-PC/PCL blends in Chapter 5. Application of SANS and SAXS for studying polymer blend morphology has been demonstrated to be highly effective in yielding unambiguous structural information.[16-17] This synergism comes about because the contrast mechanism in SAXS is very different from that of SANS. SAXS arises from the difference in electron density difference (e.g. amorphous and crystalline region), whereas SANS arises from scattering length density (SLD) differences. The latter are dominated by the substitution of deuterium for hydrogen, due to the change of sign in the scattering length (b_D = 0.667 X 10^{-12} cm; b_H = -0.374 X 10^{-12} cm). Since PC is deuterated in the work reported here, SANS directly probes the spatial arrangement between PC and PCL whereas SAXS probes the amorphous/crystalline region.

Quantitative analysis of the SAXS profiles measured both in the semicrystalline /semicrystalline and semicrystalline/amorphous states will be discussed in Chapter 6. Correlation function analysis, absolute invariant calculation and Porod analysis will be used to determine the characteristic morphological parameters including the crystal- and amorphous-phase thickness and the transition layer thickness. Small-angle light scattering (SALS) coupled with polarized optical microscopy will be used to probe the spherulitic structure.

General conclusions and future work will be described in the last chapter. Inevitably, results derived from this study will probably lead to more questions than answers. As in most dissertations, the purpose of the final chapter is to stimulate more questions and to stage an open forum for more intellectual discussion.

Table 1.1

Chemical and Crystal Structures of PC and PCL

Polymer	Chemical Structure	Crystal Structure
Bisphenol A Polycarbonate (PC)	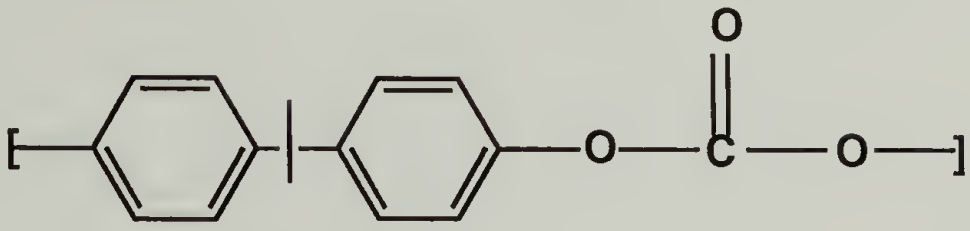	Monoclinic a = 12.3 Å b = 10.1 Å c = 20.8 Å γ = 84 °
Poly(ε-caprolactone) (PCL)	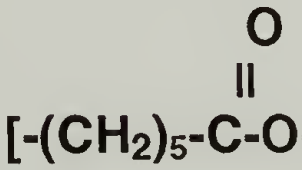	Orthorhombic a = 7.496 Å b = 4.974 Å c = 17.297 Å

Table 1.2

Characteristic Properties of Small-Angle Scattering

Radiation	Power	λ	q-Range	Contrast	Structure
SALS	Few mW	632 nm	0.05 μm^{-1} - 1.5 μm^{-1}	Δ(Refractive Index)	Spherulite
SAXS	40 KeV	1.54Å	0.005$Å^{-1}$ - 0.12$Å^{-1}$	Δ(Electron Density)	Lamellae
SANS	85 MW	4.75Å	0.007$Å^{-1}$ - 0.07$Å^{-1}$	Δ(SLD)	Domain ζ and χ
Synchrotron SAXS	2.6 GeV	1.54Å	0.003$Å^{-1}$ - 0.15$Å^{-1}$	Δ(Electron Density)	Evolution of Lamellae

SALS- Small Angle Light Scattering

SAXS- Small Angle X-Ray Scattering

SANS- Small Angle Neutron Scattering

SLD - Neutron Scattering Length Density

ζ- Correlation Length

χ- Flory Interaction Parameter

References

1. Koleske, J.V. In *Polymer Blends*; Paul, D.R. and Newman, S., Ed.; Academic Press, New York, 1978.

2. Cruz, C.A.; Paul, D.R. and Barlow, J.W. *J. Appl. Polym. Sci.* **23**, 589 (1979).

3. Varnell, D.F.; Runt, J.P. and Coleman, M.M. *Macromolecules* **14**, 1350 (1981).

4. Jonza, J.M. and Porter, R.S. *Macromolecules* **19**, 1946 (1986).

5. Khamatta, F.B.; Warner, F.; Russell, T.B. and Stein, R.S. *J. Polymer Sci., Phys. Ed.* **14**, 1391 (1976).

6. Khamatta, F.B., Ph.D. Thesis, University of Massachusetts, Amherst, 1976.

7. Russell, T.P., Ph.D. Thesis, University of Massachusetts, Amherst, 1979.

8. Cruz, C.A.; Barlow, J.A. and Paul, D.R. *Macromolecules* **12**, 726 (1979).

9. Coleman, M.M. and Painter, P.C. *J. Appl. Spect. Reviews* **20(3&4)**, 255 (1984).

10. Coleman, M.M. and Zarian, J. *J. Polym. Sci., Polym. Phys. Ed.* **17**, 837 (1979).

11. Nishi, T. and Wang, T.T. *Macromolecules* **8**, 909 (1975).

12. Olabisi, O. *Macromolecules* **8(3)** 316 (1975).

13. Shibayama, M.; Yang, H.E.; Stein, R.S. and Han, C.C. *Macromolecules* **18** 2179 (1985).

14. Han, C.C.; Baurer, B.J.; Clark, J.C.; Muroga, Y.; Okada, M.; Tran-Cong, Q. and Sanchez, I.C. *Polymer* **29**, 2002 (1988).

15. Bates, F.S. *J. Appl. Cryst.* **21**, 681 (1988).

16. Russell, T.P.; Ito, H. and Wignall, G.D. *Macromolecules* **21**, 1703 (1988).

17. Wignall, G.D.; Farrar, M. and Morris, S. *J. Mater. Sci.*. **25**, 69 (1990).

CHAPTER 2

PHASE BEHAVIOR AND MISCIBILITY

2.1 Introduction

Studies conducted on the PCL/PC blends have been limited to the examination of the phase behavior with thermal analysis and Fourier transform infrared spectroscopy (FTIR). There are many conflicting reports on the sign and magnitude of the interaction parameter. Thermal stability of the blends has never been systematically investigated. Due to the crystallinity effects, the real composition of the amorphous phase could be very different from the blend composition. This effect is generally ignored in the measurement of the glass transition temperature. Additionally, the composition dependence of the glass transition temperature has never been vigorously analyzed.

In order to clarify these ambiguities and to establish a better understanding of this complex blend system, the phase behavior and the miscibility will be critically examined. DSC and cloud point measurements will be employed to identify the various phase transitions. The composition dependence of the glass transition temperature will be analyzed using the classical equations based on the free volume hypothesis and the Kovacs free volume theory. Thermal stability of the blends at temperatures close to the LCST will be assessed with FTIR and thermogravimetric analysis (TGA). Due to the thermal instability of PCL at elevated temperatures close to the LCST, the blends may undergo chain scission and/or transesterification. Nuclear magnetic resonance (NMR) spectroscopy will be used to evaluate the chemical integrity of the blends. Attempts will be made to re-examine the equilibrium melting point of the PCL-rich blends. Miscibility between PCL and deuterated PC in the PC-rich blends will be probed with small-angle neutron scattering.

2.2 Experimental

Both PCL and PC were obtained from Scientific Polymer Products. The deuterated PC was synthesized by solution polymerization of deuterated bisphenol with phosgene at 0 °C in methylene chloride.[1] Pyridine was used to neutralize the hydrochloric acid generated from the condensation reaction. The resulting polymer was then washed in water and precipitated out of methanol. The molecular weights of the these homopolymers, determined from gel permeation chromatography, are shown in Table 2.1. The two homopolymers were dissolved and mixed in methylene chloride yielding a 5 wt. % solution. The blends were subsequently recovered from solution by precipitating them in methanol. The blends were first air dried overnight and then vacuum dried at 90 °C for two days. Pure PCL was subjected to the similar purification procedures and thermal treatments. In order to promote solution-induced crystallization, PC was first dissolved in methylene chloride yielding a 5 wt. % solution. The sample was then solution cast on a Teflon-coated surface. The cast films were dried in a similar manner as the blends.

Thermal transitions of the blends were measured with a Dupont-10 differential scanning calorimeter at a heating rate of 20 °C/min. The glass transition temperatures were obtained from the second heating scan and determined from the midpoint of the change in heat capacity. The melting endotherms of both components were recorded from the first heating scan and the melting point was obtained from the peak temperature of the endotherm. Based on the values of the of heat of fusion for 100% crystalline PC[2] (35.3 cal/g) and PCL[3] (32.4 cal/g), the degree of crystallinity of both PC and PCL was calculated from the melting endotherm and normalized with respect to the composition of each component in the blend.

Due to the large difference in the refractive index between PCL (n = 1.149) and PC (n = 1.586), the optical cloud point method based on the turbidity measurement was used

to determine the phase separation temperature. The cloud point apparatus consisted of a He-Ne laser, hot stage, photo-multiplier tube interfaced to a computer. The scattered light produced from total internal reflection was collected with a photo-multiplier tube as shown in Figure 2.1. This geometry is much more superior than the conventional turbidity technique as a much wider angular range of scattered light was sampled by this apparatus. The sample was heated to above the blend T_g and cast between two glass slides. The sample was first equilibrated at 240 °C for 3 min on a hot stage and then ramped at 4 °C/min to above the cloud point while the intensity of the scattered light was simultaneously monitored. The temperature at which the scattered light intensity increased significantly was recorded as the phase separation temperature (cloud point). In order to examine the reversibility of the phase separation, the sample was cooled at 4 °/min to below the cloud point.

Thermal stability of the blends was assessed with a Perkin-Elmer TGS2 thermo-gravimetric analyzer (TGA). The sample was first ramped to 100 °C and then heated at 10 °/min to 600 °C. Measurements were conducted in air. FTIR was performed on samples cast on NaCl plates with an IBM-32 spectrometer averaging 128 scans. ^{13}C NMR was performed on samples dissolved in chloroform with a Varian 300 XL spectrometer.

SANS samples were prepared by dissolving the two components, PCL and d-PC, in methylene chloride. The blend solution was then cast on an aluminum surface. The samples were first dried under ambient conditions overnight and then vacuum dried at 90 °C for two days to ensure complete removal of residual solvent. Crystalline h-PC was also prepared in an identical manner as the blends where PC crystallinity was enhanced by means of solution-induced crystallization. In order to render the blends amorphous, the samples were heated to 250 °C for 3 min under vacuum. Scattering samples were compression molded typically at T_g+50 °C under vacuum. Samples were then rapidly

transferred to a metal surface and quenched to room temperature. Sample disc dimension was about 1 mm in thickness and 15 mm in diameter.

SANS experiments were performed at the National Institute of Standards and Technology (NIST) in Maryland. Measurements were conducted on the 30 meter CHRNS SANS instrument. The neutron wavelength was 5 Å ($\Delta\lambda/\lambda = 0.34$) and the source and sample slits were separated by a distance of 14.77 m. The sample-detector distance was 12.5 m and the data were corrected for instrumental backgrounds and detector efficiency on a cell-by-cell basis, prior to radial averaging to give a q-range of 0.0013 to 0.044 $Å^{-1}$. The net intensities were converted to an absolute (±5%) differential cross section per unit sample volume (in units of cm^{-1}) by comparison with pre-calibrated secondary standards.[4] Incoherent scattering backgrounds were estimated from the scattering of the hydrogeneous polymers and were subtracted from the sample scattering.

2.3 Results and Discussion

2.3.1 Phase Transitions

The "quasi-equilibrium" (due to kinetic effects) phase diagram for the PCL/PC blends is depicted in Figure 2.2. As discussed earlier, the phase transitions were measured at 20 °/min with the exception of the lower critical solution temperature (LCST) which was measured at 4 °/min. In accord with previous results,[5-7] this blend system is miscible in the amorphous phase, as demonstrated by the presence of a single glass transition temperature, over the entire composition range. Both PCL and PC in the PCL-rich blends readily undergo crystallization under ambient conditions. Therefore, PCL is an effective macromolecular plasticizer for PC as pure PC cannot crystallize at temperatures below 150 °C. Figure 2.3 shows the normalized PCL and PC crystallinities as determined by DSC, obtained from quenching the blends from above T_m of PC to room temperature, for the PCL-rich blends. At about 30% PC incorporation, it was observed

that the PCL crystal-linity showed a marked reduction and whereas the PC crystallinity approached a maximum. Crystallization of both components was strongly suppressed in the PC-rich blends.

Cloud point measurements indicated that the blends undergo phase separation above the LCST. As the sample approached its phase separation temperature, the integrated scattering intensity increased sharply as depicted in Figure 2.4. This temperature is termed the cloud point and is related to the locus of the binodal curve. In the limit of infinitely slow heating rate and monodisperse molecular weight distribution, the cloud point curve corresponds to the binodal curve.[8] As indicated in this figure, the integrated scattering intensity decreased as the sample was cooled below the cloud point and such reversibility was a strong signature of a true LCST.

2.3.2 Glass Transition Temperature Analysis

Blend miscibility is often quantified by measuring the blend T_g and by analyzing its dependence with composition. Traditionally equations[9-12] based on the free volume hypothesis have been used to model the composition dependence of the glass transition temperature. The two mostly used expressions are the Fox[9] and the Gordon-Taylor[12] equations. The Fox equation shown below

$$\frac{1}{T_g} = \frac{W_1}{T_{g1}} + \frac{W_2}{T_{g2}} \qquad (2.1)$$

where W_i is the weight fraction of component i and T_g is the blend T_g, assumes the specific heats of the two components are identical. The Gordon-Taylor equation

$$T_g = \frac{W_1 T_{g1} + k W_2 T_{g2}}{W_1 + k W_2} \qquad (2.2)$$

where $\mathbf{k} = \Delta\alpha_2/\Delta\alpha_1$, and $\Delta\alpha_i$ is the thermal expansion difference between the liquid and glassy states at T_{gi}, accounts for the effects of thermal expansion on the T_g. In general, **k** is often used as a fitting parameter. These classical equations predict that T_g increases continuously (smoothly) and monotonically with composition.

However, it has been observed that the T_g-composition variation of several polymer blend systems is not monotonic and exhibits a cusp at a certain critical composition.[13] This phenomenon becomes very prominent when the T_g difference between the two homopolymers exceeds 50 deg. The classical equations become invalid below a critical temperature T_c as the free volume of the high T_g component becomes zero. According to Kovacs,[14] the critical temperature and composition are given by

$$\mathbf{T_c = T_{g2} - (f_{g2}/\Delta\alpha_2) \quad if \quad T_{g2} > T_{g1}} \tag{2.3}$$

$$\phi_c = \frac{\mathbf{f_{g2}}}{[\Delta\alpha_1(\mathbf{T_{g2}-T_{g1}}) + \mathbf{f_{g2}}(1-\Delta\alpha_1/\Delta\alpha_2)]} \tag{2.4}$$

where $\Delta\alpha_2$ is the difference between the volume expansion coefficients in the glassy and liquid states of component 2, f_{g2} is the free volume fraction of polymer 2 at T_{g2}. Below T_c, the T_g is described by

$$\mathbf{T_g = T_{g1} + \left(\frac{f_{g1}}{\Delta\alpha_1}\right)\left(\frac{\phi_2}{\phi_1}\right)} \tag{2.5}$$

According to this equation, the blend T_g is uniquely determined by the properties of the low T_g polymer at temperatures below T_c or at compositions below ϕ_c. If there is excess volume between the two polymers upon mixing, Braun and Kovacs[15] have derived the following

$$T_g = T_{g1} + \frac{\phi_2 f_{g2} + g\phi_1\phi_2}{\phi_1 \Delta\alpha_1} \qquad (2.6)$$

where g is an interaction term defined as

$$g = \frac{(V_e/V)}{\phi_1\phi_2} \qquad (2.7)$$

where V_e is the excess volume and V the volume of the blend. The excess volume or g is positive if blend interactions are stronger than those between the homopolymers. Effectively, g is obtained by fitting the T_g-composition data to the Braun-Kovacs equation.

The overall weight fraction, normalized PCL and PC crystallinities, volume fraction and the corresponding T_g are listed in Table 2.2. From the degree of crystallinities and the density value of 1.095 g/cm^3 for amorphous PCL[3] and 1.196 g/cm^3 for PC,[2] the real composition, expressed in terms of the volume fraction of PC, of the amorphous phase was calculated and is plotted in Figure 2.5. Three different equations were applied to model the composition dependence of T_g. The Gordon-Taylor fit to the data yielded a **k** value of 0.27 and failed to reproduce the cusp observed in the T_g-composition variation. Based on the classical value of 0.025 for f_{g2} and 0.00048 K^{-1} for $\Delta\alpha_2$, the critical temperature and volume fraction (with respect to PC) are 372 K and 0.72, respectively. The Fox equation was used to fit the data above ϕ_c and the Braun-Kovacs equation was applied to the data below ϕ_c. Combination of the Fox equation and the Kovacs theory accurately predicted the T_g-composition variation. It was found that the Braun-Kovacs fit yielded a g value of -0.0227. This negative value suggested that the blend interactions are fairly weak. Additionally, the cross-over from the classical (Fox) limit to the free volume (Kovacs) regime occurred at about 0.76, in close agreement with the value of 0.72

predicted by Kovacs equation. It should be noted that this is one of the first successful applications of the Kovacs theory to predict the T_g-composition dependence for a semi-crystalline/semicrystalline blend system.

2.3.3 Melting Point Depression

As discussed earlier, melting point depression is extensively used to evaluate the miscibility of polymer blends. There are two basic origins of melting point depression: 1) morphological and 2) thermodynamic. Morphological variables such as lamellar thickness and crystal perfection can profoundly affect the melting point. Two different approaches are often employed to obtain the equilibrium melting point $T_m°$. The first is the Gibbs-Thompson approach in which the $T_m°$ is obtained from the intercept of a plot of reciprocal of lamellar thickness versus T_m. The more popular approach is the Hoffman-Weeks extrapolation in which $T_m°$ is derived from a plot of T_m versus T_c. Specifically, the equilibrium melting point is obtained from the intercept of the experimental T_m versus T_c curve with the $T_m = T_c$ equation. A series of Hoffman-Weeks plots is depicted in Figure 2.6 and the corresponding $T_m°$, derived from the extrapolation, as a function of composition is illustrated in Figure 2.7. The uncertainty associated with the equilibrium melting point could be fairly significant as errors in both the melting point measurement and the extrapolation could yield low precision.

According to the Nishi and Wang formulation,[16] the interaction energy density B, defined as

$$B = \frac{\chi V_{1u}}{RT} \tag{2.8}$$

where χ is the polymer-polymer interaction parameter, V_{1u} is molar volume of the amorphous polymer, is related to the melting point depression by the following expression

$$\frac{1}{V_1}\left[\frac{1}{T_m} - \frac{1}{T_m^0}\right] = -\frac{BV_{2u}}{\Delta H_{2u}}\left(\frac{V_1}{T_m}\right) \qquad (2.9)$$

where T_m° is the equilibrium melting point of the pure polymer, T_m is the equilibrium melting point of the blend, and ΔH_{2u} is the enthalpy of fusion per mole of repeating unit and V_1 is the volume fraction of the amorphous polymer. Assuming B or χ is composition independent, a plot of $(1/V_1)[(1/T_m)-(1/T_m^\circ)]$ versus (V_1/T_m) should yield a straight line with a slope which is proportional to B and a zero y-intercept. Figure 2.8 shows such a melting point depression plot. An examination of this figure indicates that the curve deviates from linearity and has a non-zero y-intercept. This non-linear behavior could imply that χ is composition dependent. As discussed and demonstrated by many groups,[7, 17] the errors associated with the melting point depression analysis could be significant and a small uncertainty in the melting point could profoundly affect the χ value. Hence, no attempts were made to extract χ from the melting point depression analysis as the melting point measurements and the Hoffman-Weeks extrapolations are plagued with many problems. However, Figure 2.7 indeed shows a melting point depression and this could suggest a negative value for χ.

2.3.4 Thermal Stability

In order to investigate the thermal stability of the blends, TGA was used to measure the onset degradation temperature of the blends in air. FTIR and ^{13}C NMR were employed to probe the chemical integrity of the blends after exposure to elevated temperatures. Elucidation of the exact nature of the degradation products and mechanisms

of the PCL/PC blends is highly complex and is beyond the scope of this study. Hence, the focus of the following discussion is to illustrate some basic qualitative features pertaining to the thermal stability of the blends.

The TGA scans recorded in air are depicted in Figure 2.9 and the corresponding onset degradation temperature as a function of composition is summarized in Figure 2.10. A cursory examination of these figures reveals that the onset temperature increased with increasing PC. It is observed that the onset temperature increased almost linearly with increasing PC for the PCL-rich blends and increased very modestly for the PC-rich blends. According to Figure 2.9, the PCL-rich blends exhibited similar weight loss profiles as the pure PCL. Interestingly, a two-step weight loss mechanism was observed in the PC-rich blends. Addition of even 10% PCL to PC strongly modified the degradation profile and significantly lowered the degradation temperature.

It was observed that the blends liberated a large amount of bubbles when they were heated to temperatures close to the LCST (~ 260 °C). The chemical nature of these bubbles was identified by FTIR. Figure 2.11 shows the FTIR spectra for pure PCL and 25%PC/75%PCL blends. Strong carbon dioxide (CO_2) absorption at 2340 cm^{-1} was observed for samples heated at 280 °C for 5 min. At elevated temperatures close to the LCST, it is known that PCL undergoes chain scission resulting in the formation of CO_2. Furthermore, polyester blends[18] can undergo transesterification which could also produce CO_2 as a by-product. In order to suppress thermally-induced chain scission, a 50%PCL/50%PC blend was prepared at 250 °C for 10 min in the presence of a 2 wt. % titanium butoxide trans-reaction catalyst under nitrogen for NMR study. Results derived from the ^{13}C NMR study indicated no signs of transesterification as the spectrum for the samples exposed to elevated temperature and the trans-reaction catalyst remained intact. The FTIR results coupled with the NMR findings suggested that the blend degradation,

as detected by the evolution of CO_2, primarily came from chain scission of PCL. This hypothesis is consistent with the thermooxidative chain branching mechanism previously proposed.[7]

2.3.5 Small-Angle Neutron Scattering

Since the LCST for the PCL/PC system overlaps with the degradation temperatures, determination of the cloud point curve using the conventional optical measurement is complicated by the evolution of CO_2. Generally, the spinodal curve could be obtained by examining the temperature dependence of the correlation length derived from the SANS profiles.[19] Additionally, the interaction parameter χ may be calculated from the SANS profiles using the random phase approximation (RPA)[20] analysis as illustrated below:

$$\frac{K_n}{I(q)} = \frac{1}{N_A V_A \phi_A D_A(qR_{gA})} + \frac{1}{N_B V_B \phi_B D_B(qR_{gB})} - \frac{2\chi}{V_0} \qquad (2.10)$$

where I(q) is the absolute scattering intensity, $q = 4\pi\lambda^{-1}\sin(\theta/2)$, θ being the scattering angle, N_i the degree of polymerization of component i, V_i the monomer volume, ϕ_i the volume fraction, V_0 the "cell" or the reference volume, K_n and $D_i(qR_{gi})$ are the contrast factor and the Debye scattering function, respectively, which are defined as

$$K_n = \left(\frac{a_A}{V_A} - \frac{a_B}{V_B}\right)^2 N_{av} \qquad (2.11)$$

$$D_i(qR_{gi}) = \frac{2}{U_i^2}\left[\exp(-U_i) - 1 + U_i\right] \qquad (2.12)$$

where (a_i / V_i) is the scattering length density, N_{av} the Avogadro's number, $U_i = q^2 R_{gA}^2$ and $R_{gi} = (N_A b_A^2/6)$, b_i is the segment length of component i. In order to reduce the number of floating parameters, an average segment length b_{av} is often used and defined as

$$b_{av} = b_i \sqrt{\frac{V_0}{V_i}} \tag{2.13}$$

Effectively, the RPA analysis reduces to fitting the SANS profiles with two adjustable parameters (χ/V_0) and b_{av}.

As discussed earlier, the PC in the PCL-rich blends is semicrystalline and becomes totally amorphous at about 230 °C. Since the PCL/PC blends were not thermally stable at these elevated temperatures, SANS studies of the amorphous/amorphous blends were limited to the PC-rich blends where PC crystallization was highly suppressed. The SANS profiles as a function of temperature for three d-PC-rich blends are shown in Figures 2.12-2.14. It is readily observed that the scattering intensity first remained fairly constant with increasing temperature and then increased significantly at temperatures above the blend T_g. This sudden rise in the scattering intensity was mainly caused by crystallization of PC resulting from prolonged annealing, since the temperature was ramped in a step-wise fashion. This finding implies that χ cannot be easily extracted from the SANS profiles measured above the blend T_g due to PC crystallization.

Attempts were made to estimate χ from SANS recorded below the blend T_g. The analysis assumes that the scattering predominantly arises from concentration fluctuations. Figure 2.15 shows the RPA fit to the SANS profiles recorded at 30 °C. The corresponding $(2\chi/V_0)$ and b_{ave} are plotted in Figure 2.16. These RPA results suggested

a composition- dependent χ and that the blend interactions are favorable as reflected by the negative sign of the interaction parameter. Assuming the cell volume to be approximated by $V_0 = \sqrt{V_A V_B}$, χ is estimated to be of the order of -1 which is in agreement with previous results[6] derived from the melting point depression analysis. However, it is extremely important to stress that the χ measured below T_g represents a non-equilibrium value which may not reflect the true value. Additionally, the interpretation of the RPA results is complicated by the possible residual crystallinity in the samples.

2.4 Conclusions

The PCL/PC blends exhibited multiple phase transitions and highly complex phase behavior. It was found that the PCL-rich blends are semicrystalline/semicrystalline at room temperature in which both components readily undergo crystallization. At about 30% PC incorporation, the PCL crystallinity showed a marked reduction and whereas the PC crystallinity approached a maximum. Based on the degree of crystallinity of both components measured from DSC, the real composition of the amorphous phase was calculated. The composition dependence of T_g exhibited a discontinuity (cusp) and was critically examined using the classical equations of Gordon-Taylor and Fox, and the free volume formulation of Braun-Kovacs. The Gordon-Taylor equation failed to reproduce the cusp observed in the T_g-composition dependence. However, combination of the Fox and Braun-Kovacs equations accurately reproduced the cusp and yielded a very good fit to the T_g-composition data. The experimental cross-over volume fraction (of PC) from the classical (Fox) limit to the free volume (Kovacs) regime was about 0.76, in very good agreement with the critical value of 0.72 predicted by Kovacs theory. This is one of the first successful applications of Kovacs theory to a semicrystalline/semicrystalline blend system.

Thermal stability of the blends was evaluated with TGA. The onset degradation temperature increased with increasing PC. At temperatures close to the LCST (~ 260 °C), carbon dioxide evolution was observed and detected by FTIR. ^{13}C NMR studies indicated that the blends were not susceptible to transesterification as the spectrum remained virtually unchanged for samples exposed to elevated temperature and a titanium butoxide catalyst which is known to promote trans-reaction in polyester blends. These findings suggested that the blends degraded primarily via chain scission of PCL as evidenced by the evolution of carbon dioxide.

In contrast to other study,[7] the PCL-rich blends showed melting point depression as revealed by the Hoffman-Weeks extrapolations. SANS studies on the d-PC-rich blends indicated that the scattering intensity first remained fairly constant with increasing temperature and then increased sharply at temperatures above the blend T_g. This rise in the intensity was attributed to the crystallization of PC resulting from prolonged annealing. Attempts were made to estimate χ from the SANS profiles measured at 30 °C (below T_g) using the RPA analysis. The SANS results coupled with the melting point depression analysis suggested favorable blend interactions as reflected by the negative sign of the interaction parameter.

Table 2.1

Molecular Weights for Poly(ε-caprolactone) (PCL), Hydrogeneous Polycarbonate (h-PC), and Deuterated Polycarbonate (d-PC)

Polymer	M_w	M_n	M_w/M_n
PCL	23,700	16,500	1.44
h-PC	23,100	36,400	1.57
d-PC[1]	109,000	52,800	2.06
d-PC[2]	134,000	15,600	8.59

1- Used for Amorphous Blend Study in the Present Chapter.

2- Used for Crystalline Blend Morphologies Study in Chapters 5 and 6.

Table 2.2

Composition, Degree of Crystallinity and Glass transition Temperature of PCL/PC Blends

wt % PC	% PC Crystallinity	% PCL Crystallinity	ϕ_{PC}*	T_g, K
0.0	0.0	58.6	0.0	213.8
0.1	4.3	53.0	17.10	227.5
0.2	8.8	51.3	29.91	226.0
0.3	13.1	25.6	31.33	227.7
0.4	15.6	25.5	40.76	233.0
0.5	3.5	17.3	51.53	235.9
0.6	0	1.9	57.28	256.0
0.7	0	0	68.02	299.8
0.8	0	0	78.47	355.6
0.9	0	0	89.14	384.2
1.0	0	0	100	424.0

*Volume Fraction of PC in the Mixed Amorphous Phase.

References

1. Cheung, Y.W.; Stein, R.S.; Wignall, G.D. and Yang, H.E. *Macromolecules* **26**, 5365 (1993).

2. Branddrup, J. and Immergut, E.H. *Polymer Handbook*, 2nd ed., Wiley, New York, 1975.

3. Khamatta, F.B.; Warner, F.; Russell, T.B. and Stein, R.S. *J. Polymer Sci., Phys. Ed.* **14**, 1391 (1976).

4. Wignall, G.D. and Bates, F.S. *J. Appl. Cryst.* **20**, 28 (1987).

5. Cruz, C.A.; Paul, D.R., and Barlow, J.W. *J. Appl. Polym. Sci.* **23**, 589 (1979).

6. Varnell, D.F.; Runt, J.P. and Coleman, M.M. *Macromolecules* **14**, 1350 (1981).

7. Jonza, J.M. and Porter, R.S. *Macromolecules* **19**, 1946 (1986).

8. Solc, K. Ed. *Polymer Compatibility and Incompatibility: Principles and Practices*; Harwood Academic, New York, 1982.

9. Fox, T.G. and Flory, P.J. *J. Polym. Sci.***14**, 315 (1954).

10. Couchman, P.R. and Karasz, F.E. *Macromolecules* **11**, 117 (1978).

11. Utracki, L.A. *Adv. Polym. Technol.***5**, 33 (1985).

12. Gordon, M. and Taylor, J.S. *J. Appl. Chem.***2**, 493 (1952).

13. Aubin, M. and Prud'homme, R.E. *Macromolecules* **21**, 2945 (1988).

14. Kovacs, A.J. *Adv. Polym. Sci.***3**, 394 (1963).

15. Braun, G. and Kovacs, A.J. In *Physics of Non-Crystalline Solids*; Prins, J.A. Ed.; North-Holland, Amsterdam, 1965.

16. Nishi, T. and Wang, T.T. *Macromolecules* **8**, 909 (1975).

17. Private Communications with Koningsveld, R.

18. Godard, P.; Dekoninck, J.M. and Devlesavedr, J. *J. Polym. Sci., Polym. Chem.* **24**, 3315 (1986).

19. Beaucage, G., Ph.D. Thesis, University of Massachusetts, Amherst, 1991.

20. de Gennes, P.G. *Scaling Concepts in Polymer Physics*; Cornell University, Ithaca, 1979.

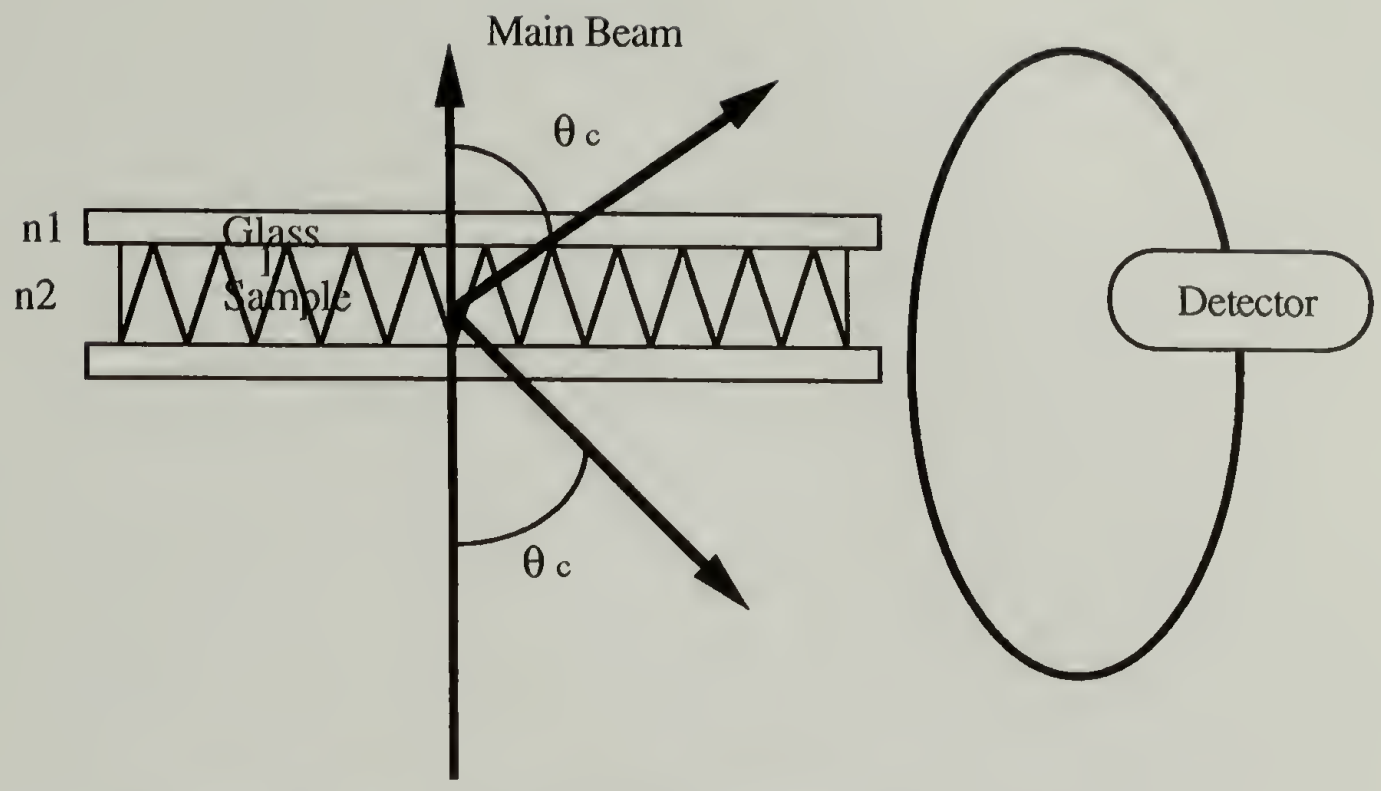

Critical Angle for Total Internal Reflection: $n_1 \sim 1.5$, $n_2 \sim 1.2$

$\theta_c = \sin^{-1}(n_2/n_1) = 53\ °$

Total Internal Reflection Occurs at : $\theta_c < \theta < 180° - \theta_c$ or $53° < \theta < 127°$

$q = (4n\pi/\lambda_0) \sin(\theta/2) = 13.3 - 26.7\ \mu m^{-1}$

Figure 2.1 Cloud point apparatus analysis: schematic drawing of the wide-angle scattering generated from total internal reflection.

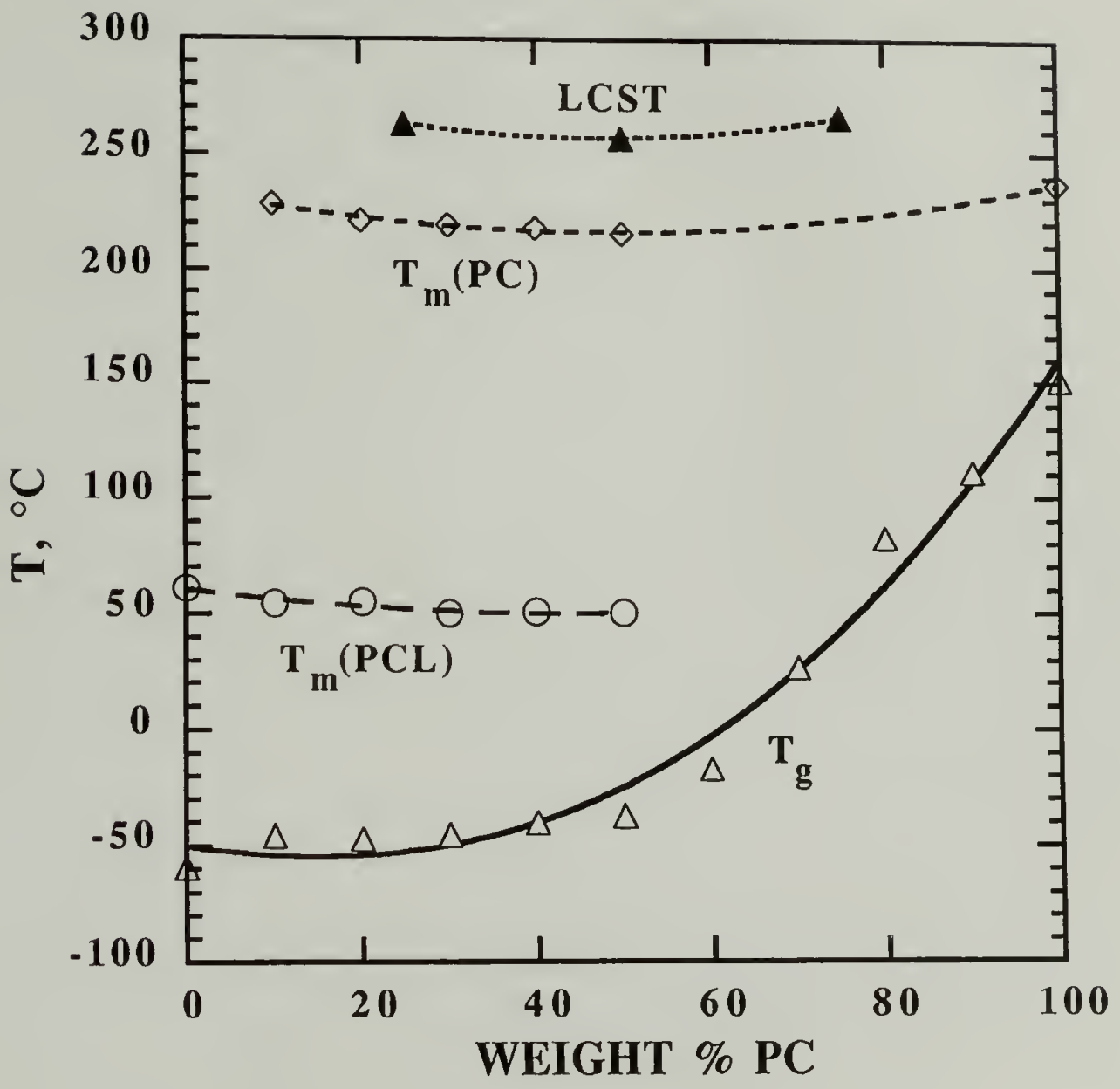

Figure 2. 2 Phase transition temperatures for PCL/PC blends measured at 20 °C/min. The lower critical solution temperature (LCST) was obtained at 4 °C/min.

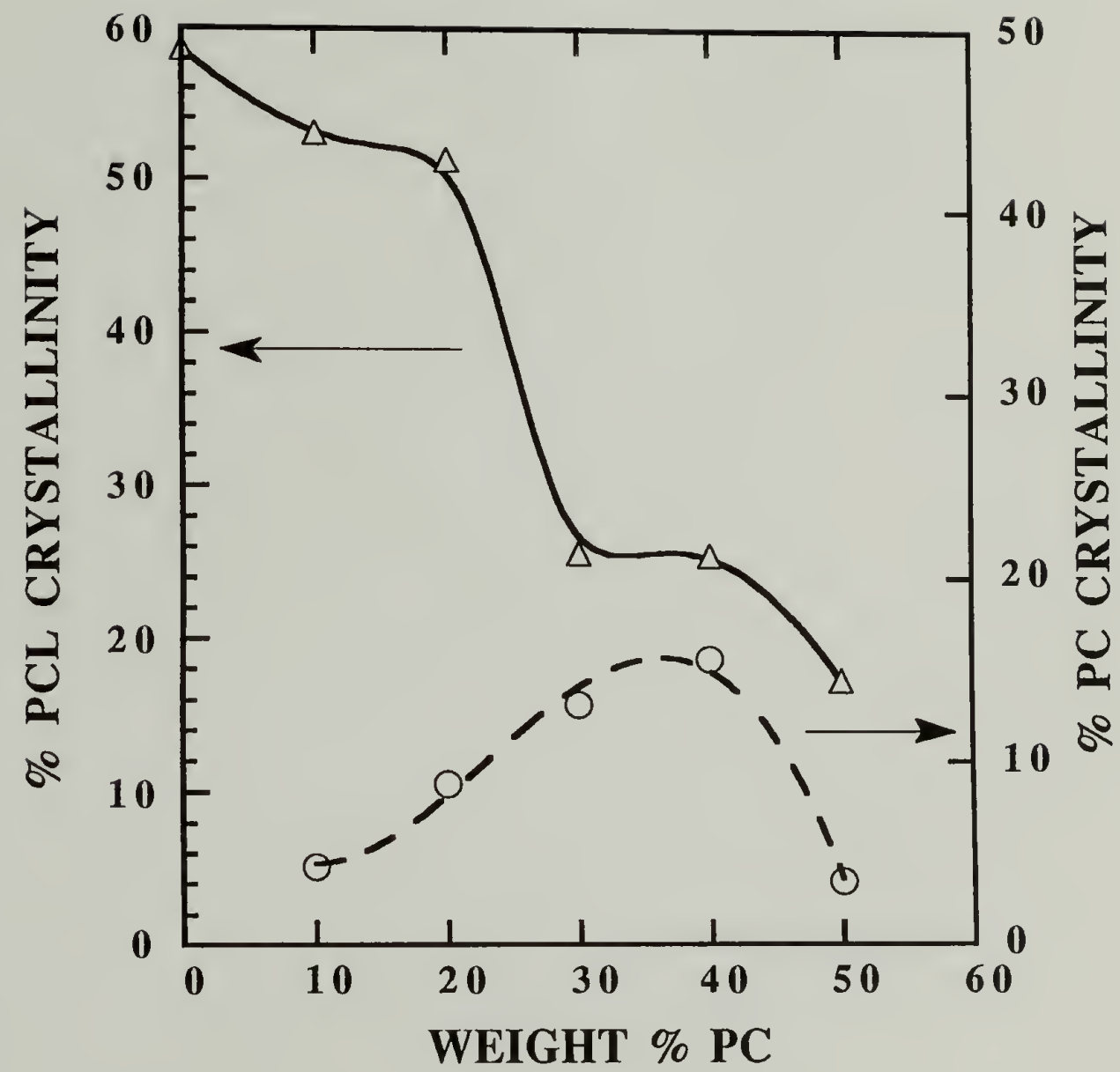

Figure 2.3 Normalized PCL and PC crystallinity, obtained from quenching the samples from above the melting point of PC to the room temperature, for the PCL-rich blends.

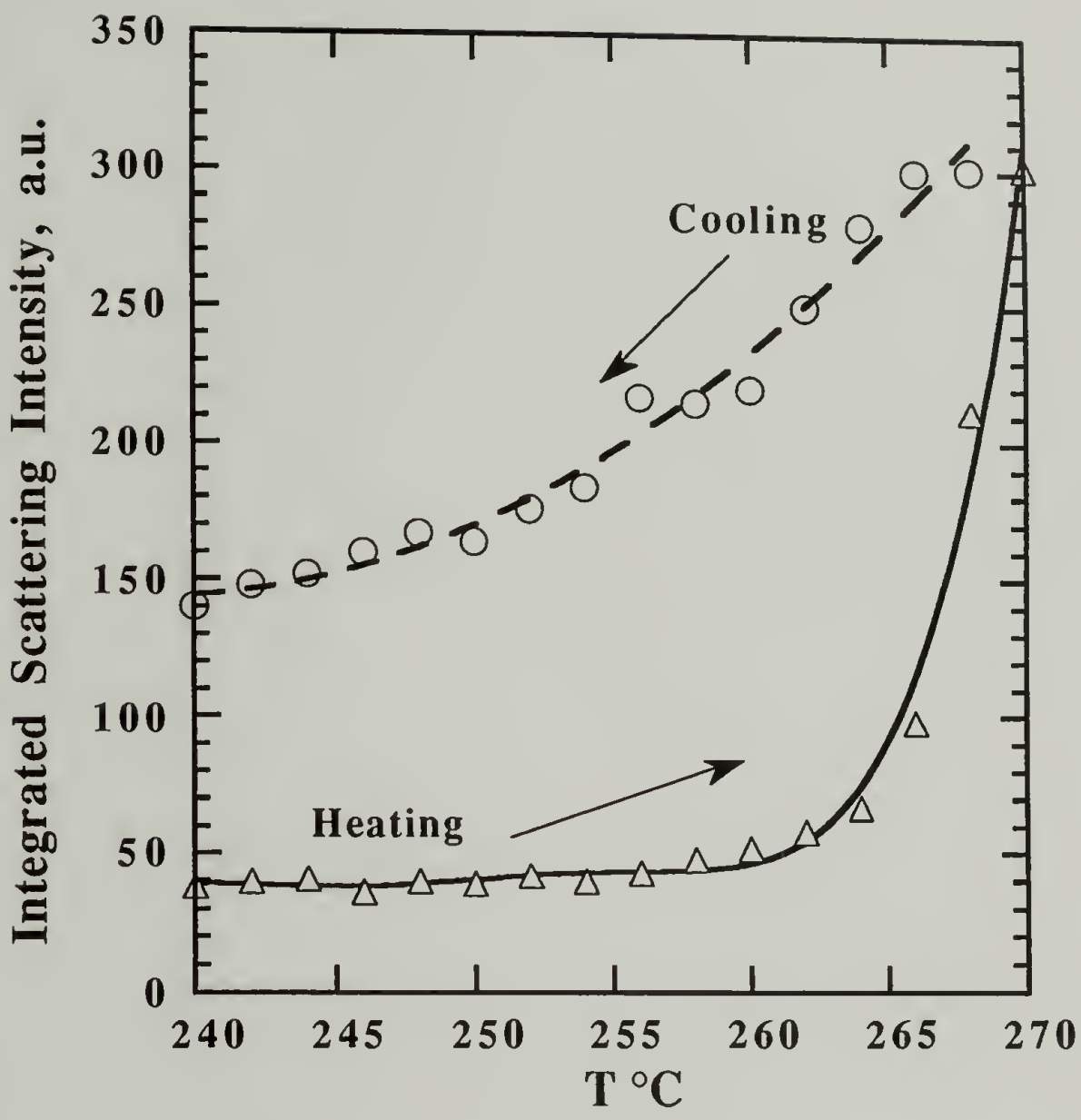

Figure 2.4 Cloud point curve for a 75%PCL/25%PC blend ramped at 4 °C/min.

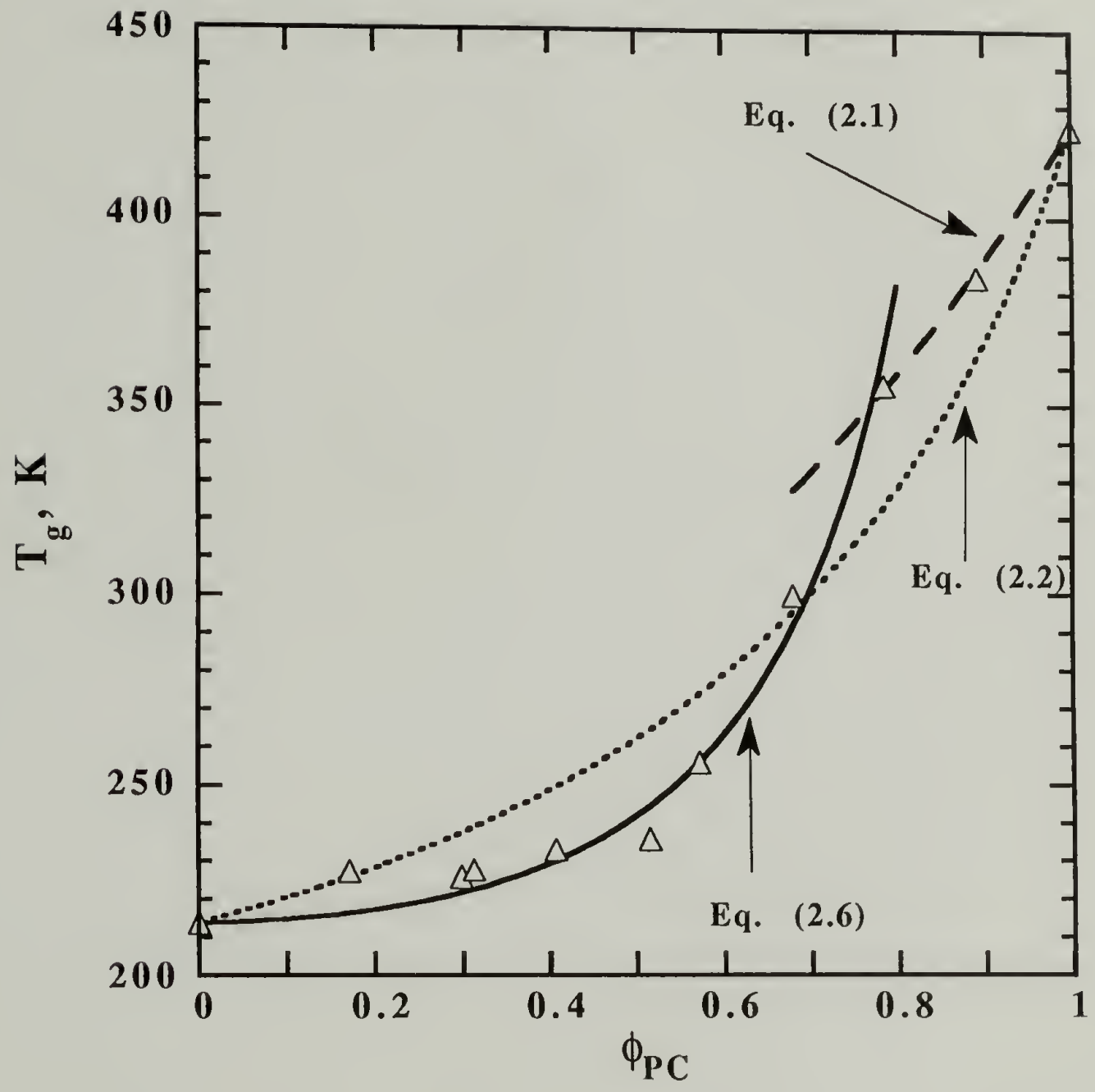

Figure 2.5 Glass transition temperature for PCL/PC blends as a function of volume fraction of amorphous PC in the mixed amorphous phase. T_g-composition dependence analysis: Eq. (2.1)- Fox; Eq. (2.2)- Gordon-Taylor with **k** = 0.27; Eq. (2.6)- Braun-Kovacs with g = -0.0227.

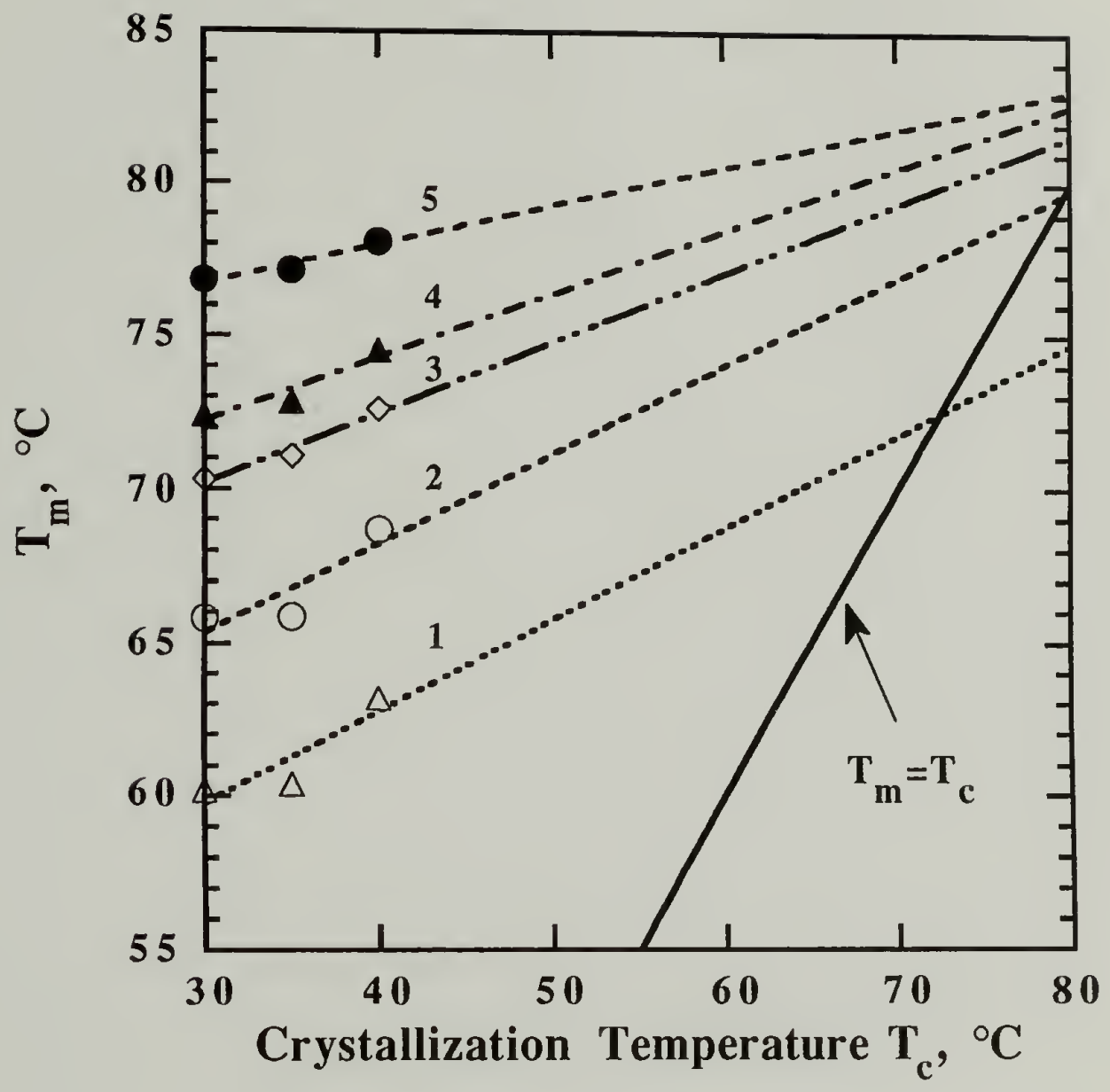

Figure 2.6 Determination of equilibrium melting $T_m°$ from Hoffman-Weeks extrapolation. The data are successively displaced by 5 °C to be able to discern the different composition. 1- 100%PCL, 2- 90%PCL, 3- 80%PCL, 4- 70% PCL, 5- 60% PCL.

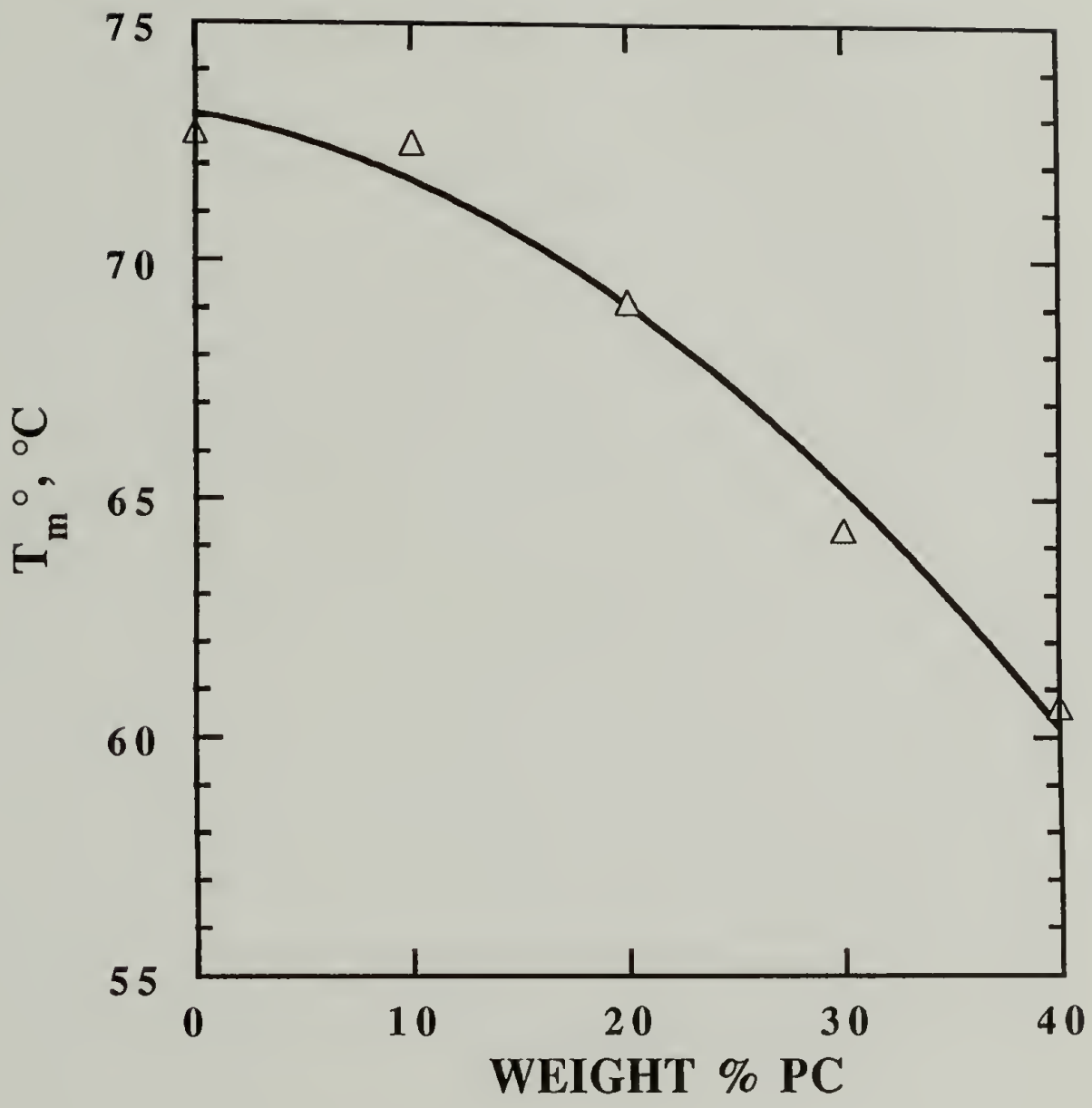

Figure 2.7 Equilibrium melting point $T_m°$ versus volume fraction of PC.

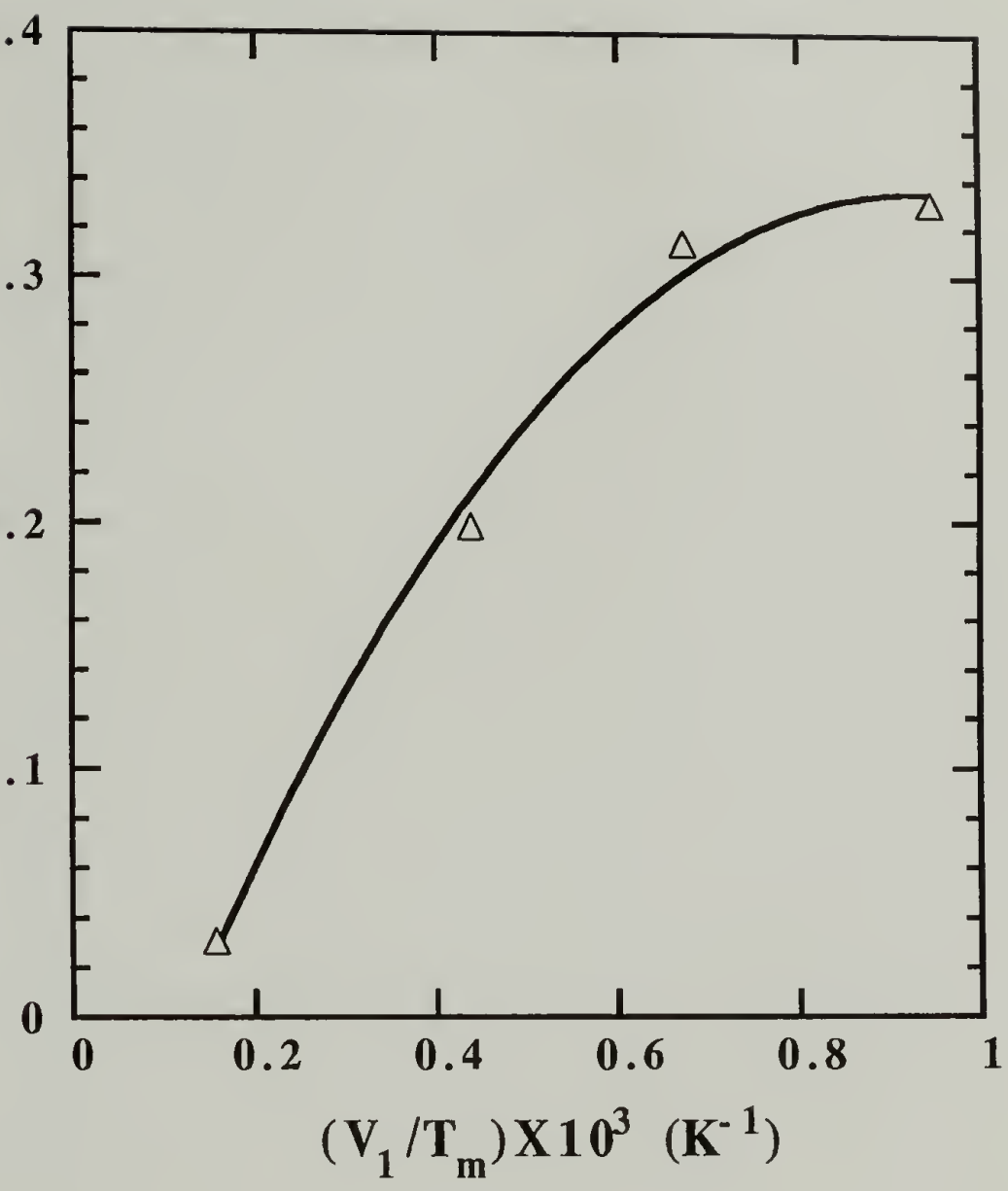

Figure 2.8 Melting point depression plot, where T_m is the melting point of PCL crystals in the blends, $T_m°$ is the melting point of pure PCL, and V_1 is the volume fraction of PC.

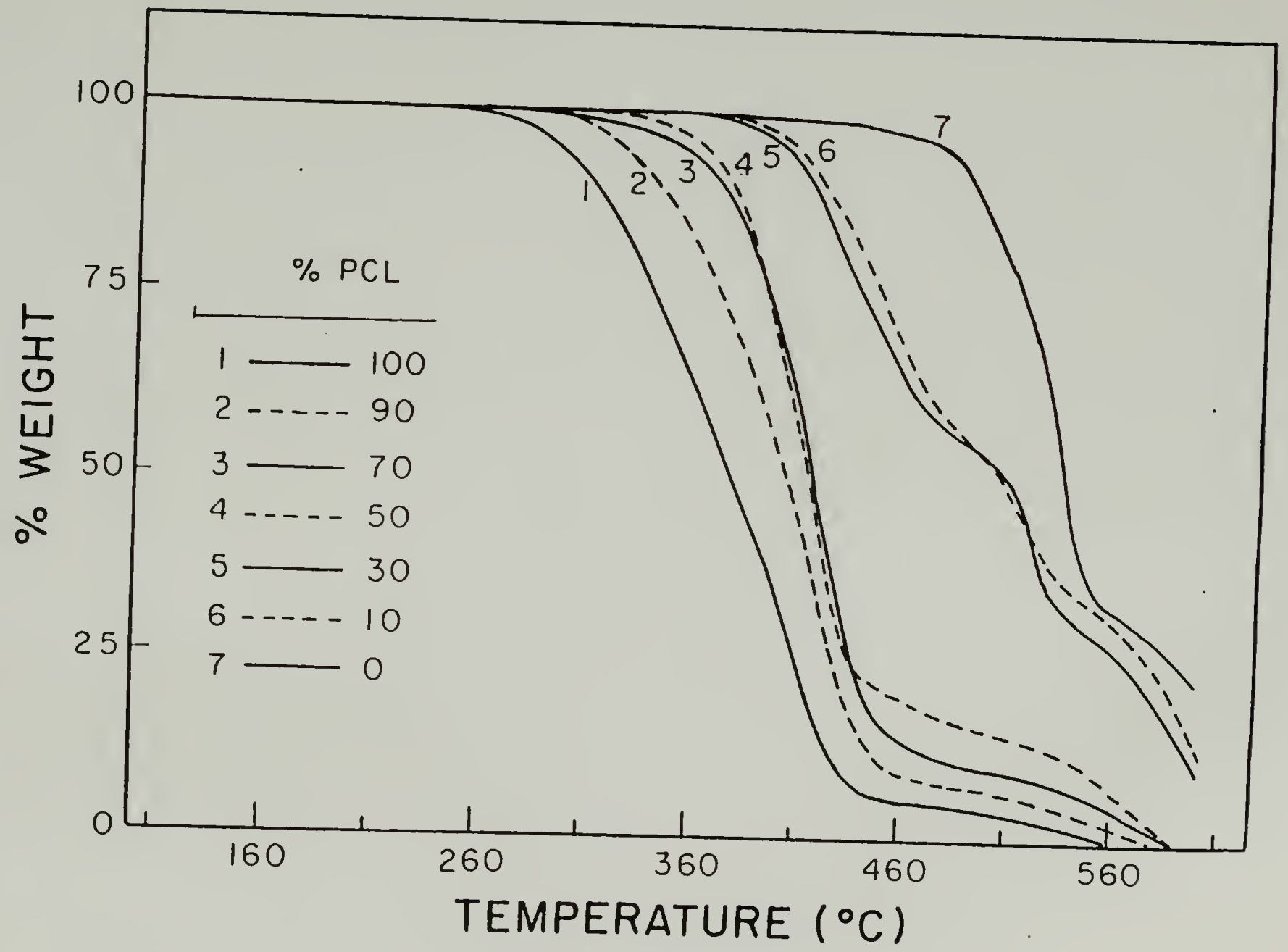

Figure 2.9 TGA curves for PCL/PC blends heated at 10 °C/min in air.

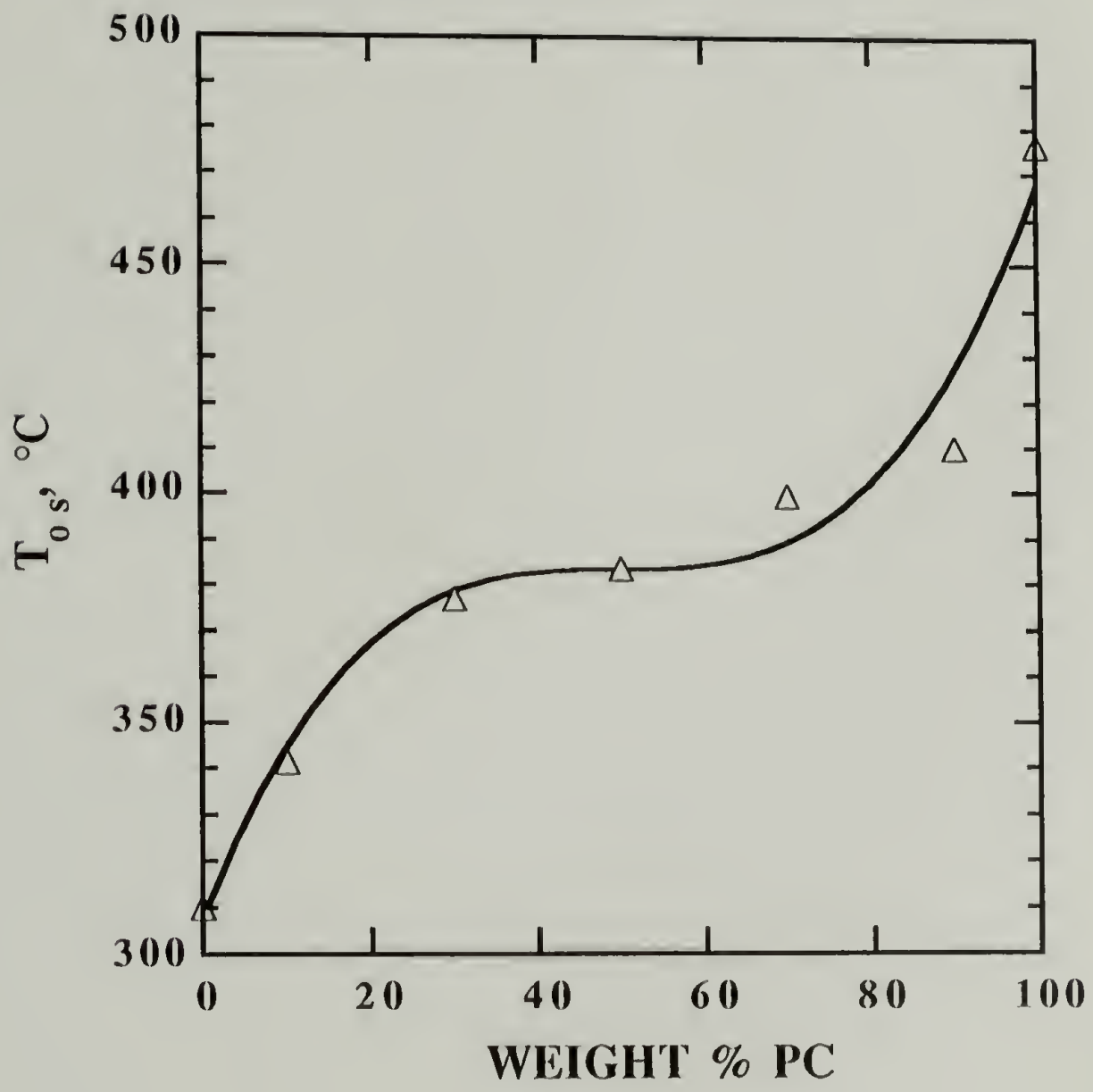

Figure 2.10 The onset degradation temperature for PCL/PC blends in air.

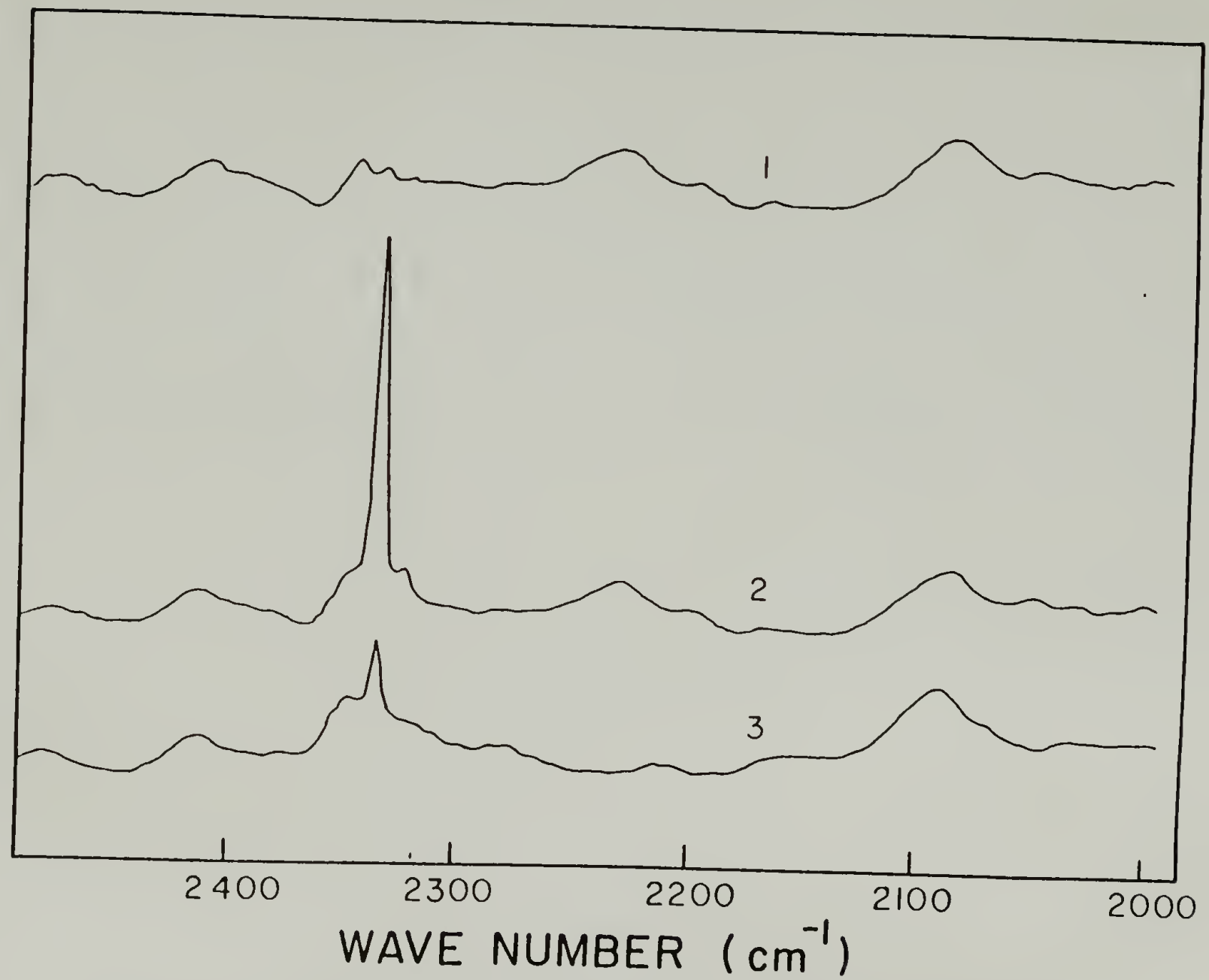

Figure 2.11 FTIR spectra for (1) pure PCL and (2) 75%PCL/25%PC blend, both exposed to 280 °C for 5 min , (3) 75%PCL/25%PC blend without exposure to elevated temperatures. Carbon dioxide absorption occurs at 2340 cm^{-1}.

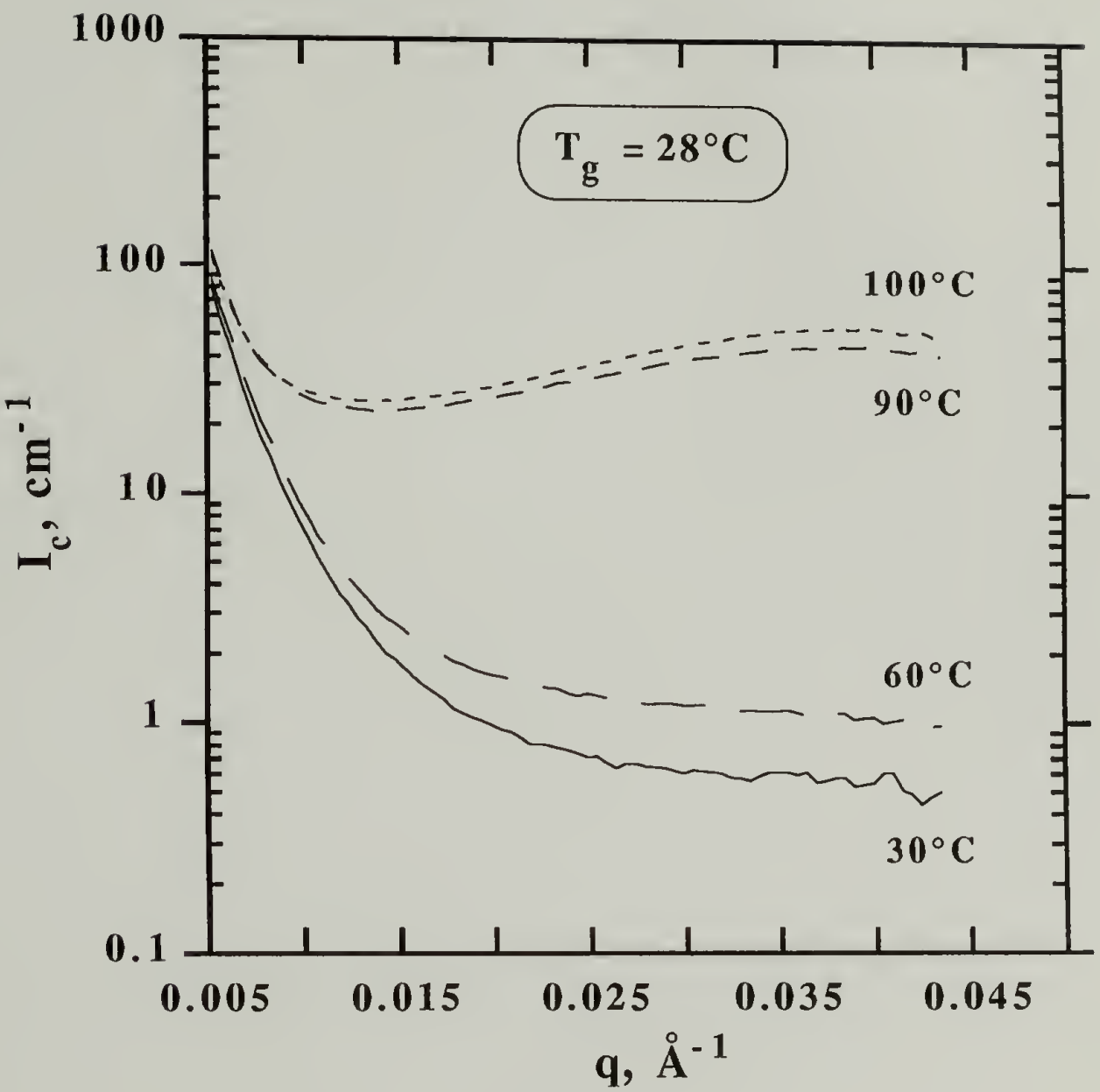

Figure 2.12 SANS profiles for a 70%d-PC/30%PCL blend.

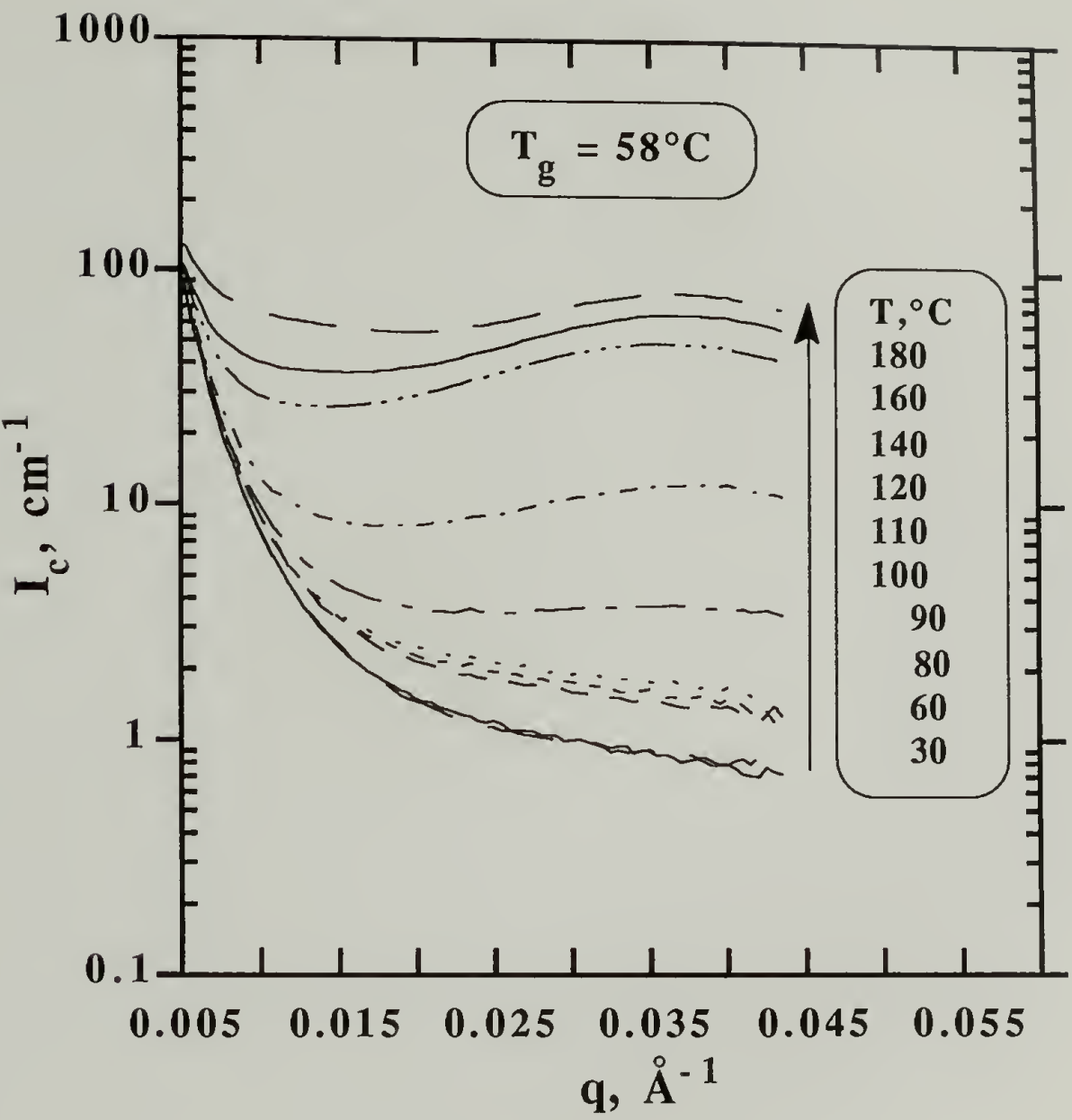

Figure 2.13 SANS profiles for a 80%d-PC/20%PCL blend.

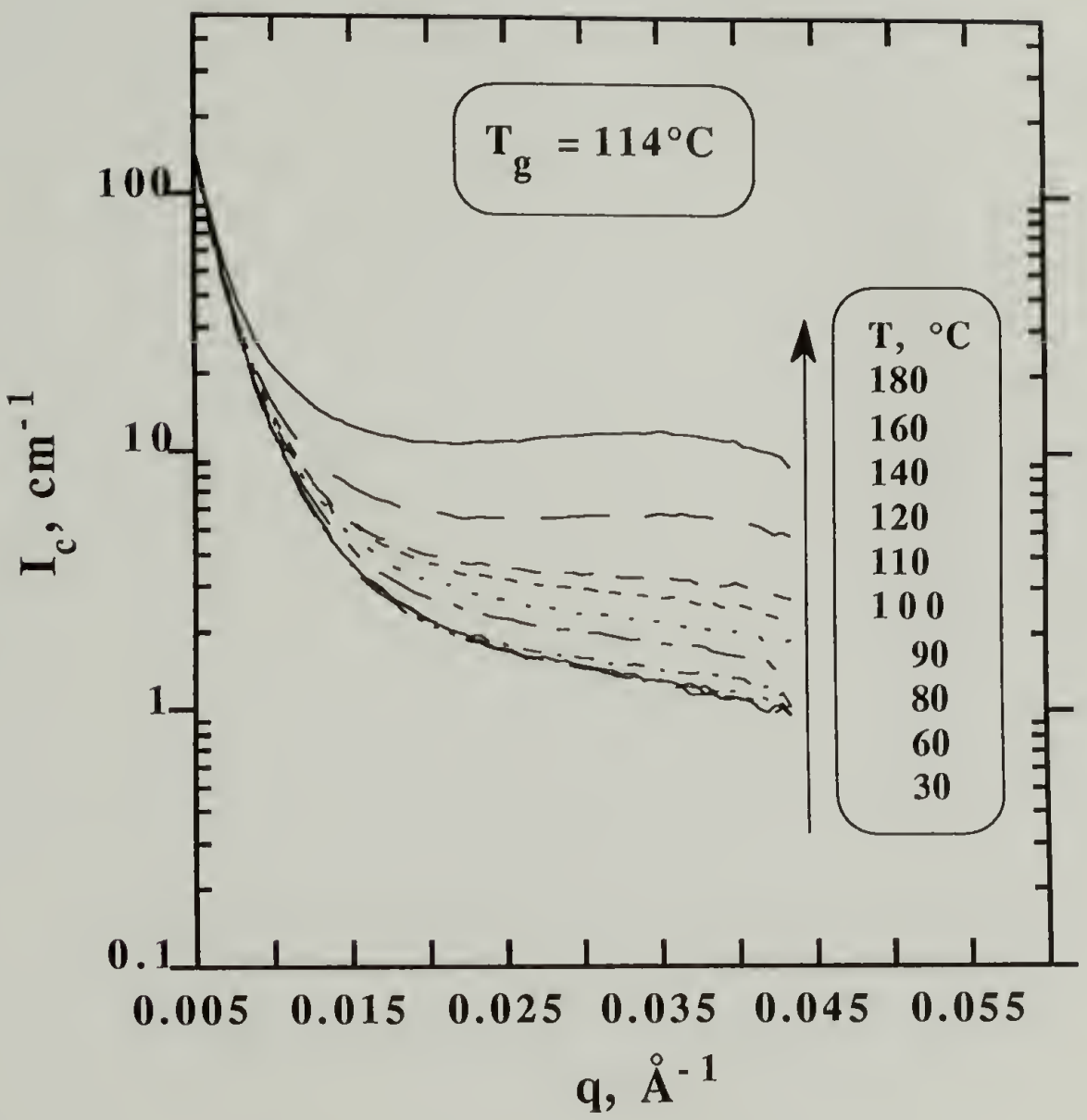

Figure 2.14 SANS profiles for a 90%d-PC/30%PCL blend.

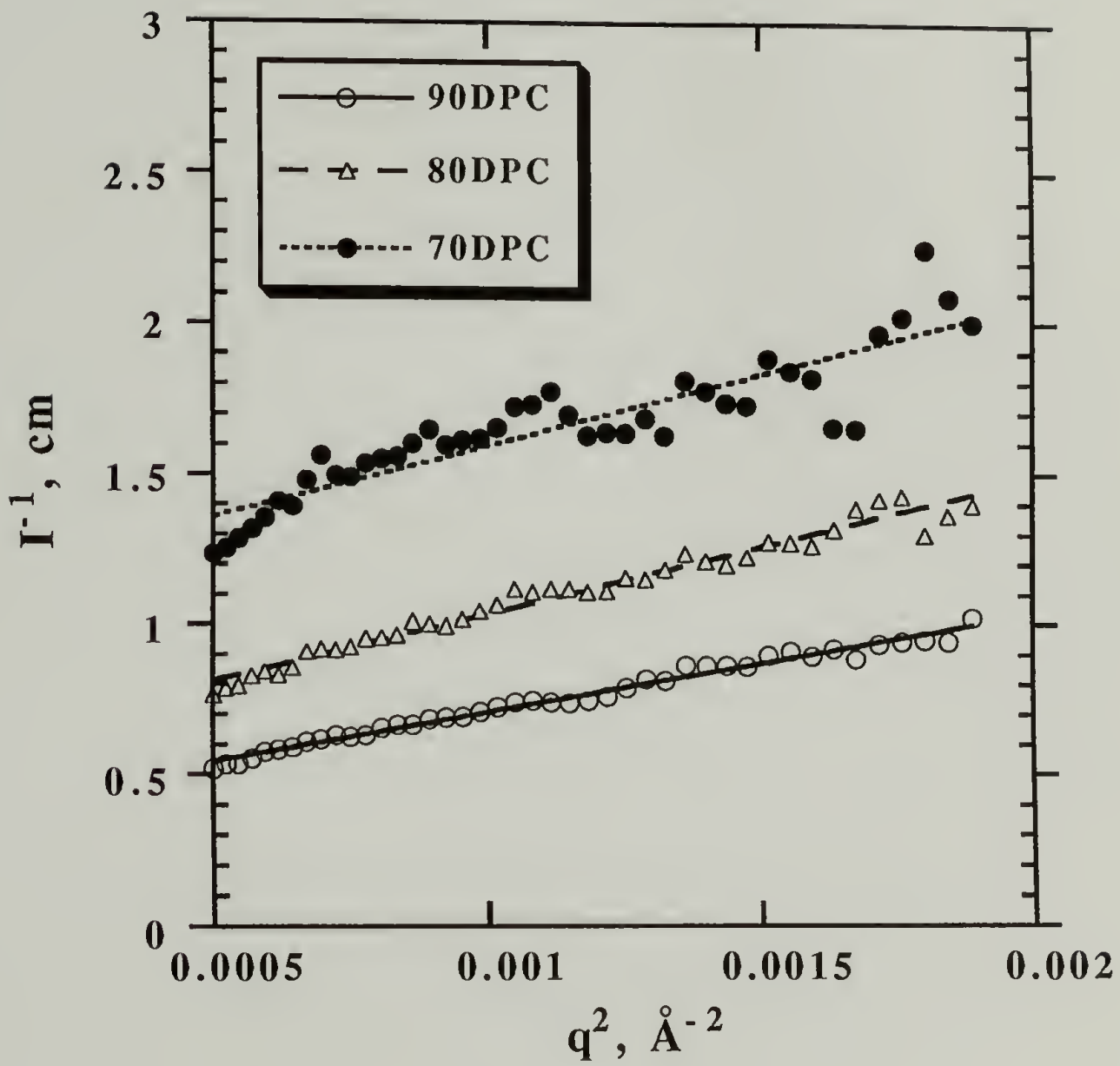

Figure 2.15 Random phase approximation (RPA) fit to the SANS profiles measured at 30 °C.

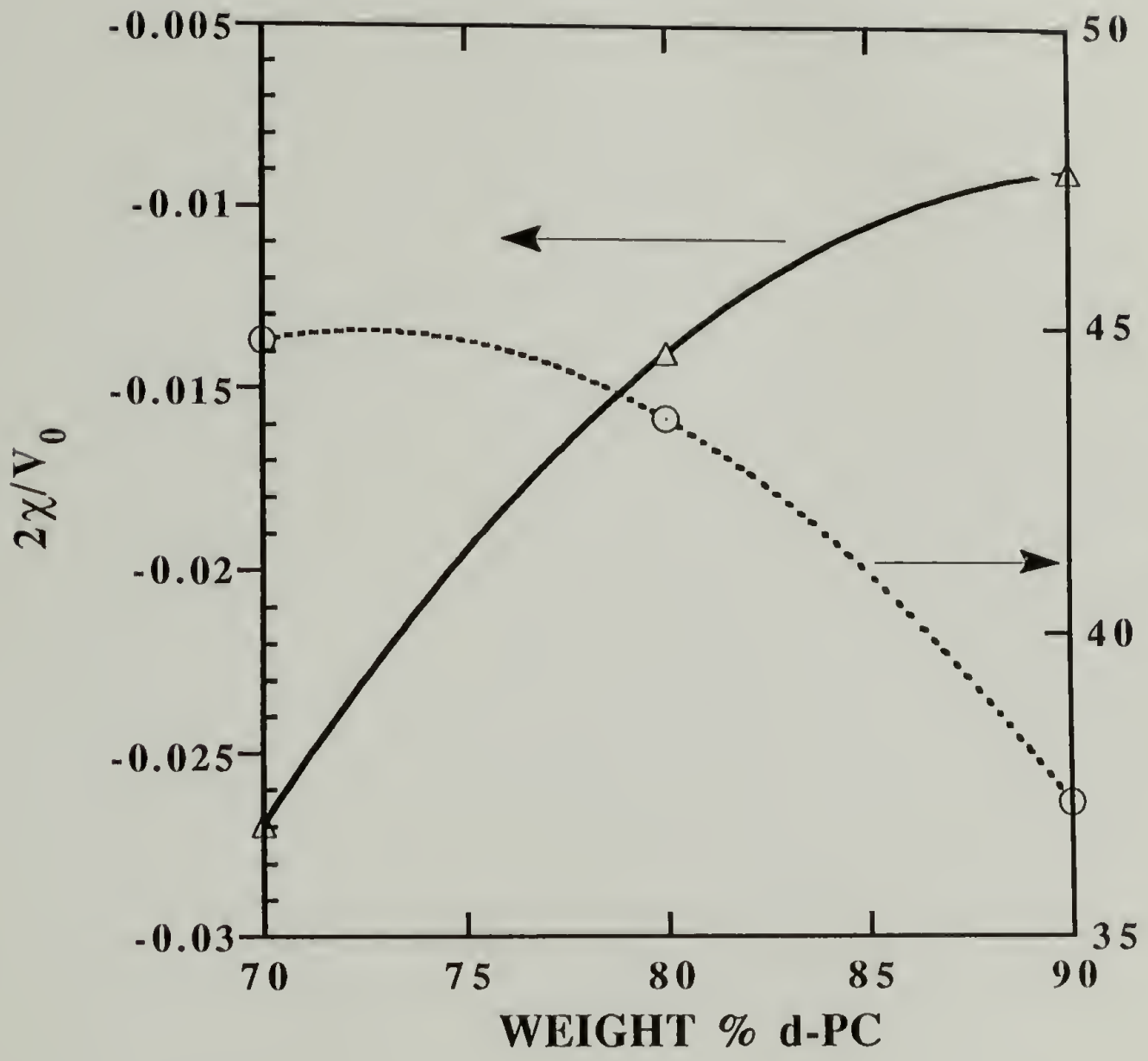

Figure 2.16 ($2\chi/V_0$) and average segment length b_{ave} as a function of composition at 30 °C, where V_0 is the "cell" volume.

CHAPTER 3

ATHERMAL AND ISOTHERMAL CRYSTALLIZATION KINETICS AS MEASURED BY DSC AND OPTICAL MICROSCOPY

3.1 Introduction

Elucidation of the crystallization mechanisms and kinetics of semicrystalline polymers is central to the control of polymer morphologies and hence its physical properties. The presence of a non-crystallizing component in a semicrystalline/amorphous blend exerts a profound influence on the kinetics of crystallization. Modification in the crystallization kinetics is usually mediated by the change in the rate of diffusion resulting from a shift in the glass transition temperature T_g upon blending. An upward shift in the blend T_g relative to the semicrystalline component T_g leads to a narrowing of the crystallization window. Correspondingly, a downward shift results in a widening of the crystallization window. Therefore, the rate of crystallization of the resulting blends may be accelerated or retarded depending on the T_g of the amorphous component.

In the case of semicrystalline/semicrystalline blends, both components may undergo cocrystallization as found in blends of linear low density polyethylene (LLDPE) and high density polyethylene (HDPE).[1] The necessary conditions for cocrystallization are based on 1) miscibility in the melt, 2) similarity in the crystal structure of the individual polymers, 3) nearly identical crystallization window (similar T_g and T_m). Most polymer pairs do not exhibit propensity for cocrystallization. Two most probable scenarios are encountered in which either two polymers crystallize simultaneously into two different crystal lattices or each polymer crystallizes separately to form two distinct crystalline phases. The latter is found in blend system where the two polymers have widely different

crystallization windows. If the two polymers crystallize in a sequential fashion, the rate of crystallization of the second component is not only altered by diffusion but also by the presence of the crystalline phase of the first component. It is envisioned that the second component has to disentangle itself from an inhomogeneous (semicrystalline) phase to form an ordered phase. Effectively, the second component is crystallizing in a medium with highly confined geometry. Epitaxial crystallization of the second component may occur on the surface of the existing crystallites of the first component.

Since the crystallization window and the crystal lattice parameters for PCL[2] (orthorhombic) and PC[3] (monoclinic) are fundamentally different, these two polymers are expected to crystallize in a sequential fashion where PC first crystallizes then follows by PCL. In addition to the commonly studied variables of composition and temperature, one can explore the effects of PC crystallinity on the crystallization kinetics of PCL in the PCL-rich blends.

Differential scanning calorimetry (DSC),[4] small-angle light scattering (SALS),[5] turbidity measurement, optical microscopy and synchrotron small-angle X-ray scattering (SAXS)[6] are very effective in monitoring the crystal growth at various structural levels depending on the probes used. DSC provides a direct measure of the overall crystallization rate as commonly expressed in terms of the half crystallization time or the crystallization rate constant derived from the Avrami analysis.[7] Optical microscopy and SALS are often used to determine the radial growth rate. Additionally, the nucleation density may be determined from the spherulite number distribution. The overall crystallization rate is simply equal to the product of the radial growth and the nucleation density. Conventional X-ray scattering usually requires very long exposure time (order of several hours) and thus rendering dynamic measurements very difficult or impossible. Synchrotron SAXS, due to its highly intense source, can be used to monitor crystallization in real

time. This technique is ideally suited for probing the lamellar development in a time resolved manner.

In order to explore the complex crystallization process at a macroscopic level, the present chapter will concentrate on the overall crystallization rate and the radial growth measurements as obtained by DSC and optical microscopy, respectively. Both athermal and isothermal crystallization kinetics will be monitored by DSC. Synchrotron SAXS studies of PCL lamellar evolution in the PCL-rich blends will be discussed in the next chapter.

3.2 Experimental

Homogeneous methylene chloride solutions containing about 5 wt % polymer were prepared. Blend samples were recovered by precipitating the solution into methanol. Blends were first dried under ambient conditions overnight and then dried in a vacuum oven at 90 °C for two days. Quenched (Q) blends were prepared by first heating the samples to 250 °C for three min and rapidly cooled to room temperature. As-precipitated (AP) blends were used for the crystallization studies without further thermal treatments.

Athermal and isothermal crystallization kinetics were monitored with a Dupont-10 DSC. Athermal studies were conducted by melting the PCL crystals at 80 °C for 5 min and cooling the sample at a rate of 5 °C/min. Isothermal studies were performed by destroying the PCL crystallinity at 80 °C for 5 min on a hot stage and then rapidly transferred to the DSC equilibrated at the crystallization temperature. Since the thermal mass of the sample was relatively low and the temperature jump was fairly shallow (~ 30 °C), it was estimated that the sample reached the crystallization temperature in less than a minute. This time scale was generally shorter than the induction time for PCL crystallization. The heat of crystallization was then recorded as a function of time. Spherulitic

growth rate was measured by heating the samples at 250°C for 3 min, and then rapidly transferring to a hot stage equilibrated at the crystallization temperature. The isothermal time variation of the spherulitic radius was studied using a Zeiss polarized optical microscope.

3.3. Results and Discussion

3.3.1 Crystallinity of AP and Q Blends

The degree of crystallinity is an important determinant of physical properties. In addition to the traditional variables of temperature and composition, the effects of PC crystallinity on the PCL crystallization kinetics will be examined. By tuning the thermal treatments, different degrees of PC crystallinity may be obtained as shown in Figure 3.1. Due to solution-induced crystallization, the PC crystallinity for the AP blends is always higher than that for the corresponding Q blends. Hence, the PC crystallinity for the Q blends may be viewed as the "quasi-equilibrium" crystallinity attained at room temperature since these blends were rapidly cooled to and annealed at room temperature.

The normalized PCL crystallinity for blends crystallized at various temperatures is shown in Figure 3.2. It is observed that the crystallinity showed a marked reduction at about 30% PC incorporation. This "transition" is not commonly found in other blend systems. Generally, the crystallinity of a semicrystalline/amorphous blend either decreases linearly or remains fairly constant with the addition of a non-crystallizing component. The origin of this phenomenon may be related to the 30% percolation threshold limit[8], where both PC and PCL phases become bicontinuous, at which the matrix amorphous phase experiences significant stiffening. Retardation of the amorphous phase mobility results in a corresponding reduction of the crystallizability of PCL.

3.3.2 Athermal Crystallization Kinetics

Figure 3.3 shows a series of DSC scans for the pure PCL and the PCL-rich Q blends recorded at a cooling rate of 5 °C/min. A cursory examination of these crystallization exotherms reveals that the peak temperature did not decrease monotonically with the addition of PC. The crystallization peak temperatures for both the Q and AP blends are shown in Figure 3.4. On the basis of diffusion, the PCL crystallization rate should be retarded with the addition of PC as the blend T_g was higher than the pure PCL T_g. Hence, the crystallization peak temperature should decrease with increasing PC. The non-monotonic dependence of the peak temperature with the addition of PC may be related to the nucleating effects of crystalline PC on PCL crystallization. In order to isolate the crystallinity effects, the peak temperatures for the two different types of blends are plotted as a function of the amorphous PC composition in the mixed amorphous phase as shown in Figure 3.5. To a first order of approximation, the crystallization rate was governed by the amount of amorphous PC in the blend as indicated by the master plot. However, it is found that the Q blends still crystallized slower than the corresponding AP blends. Therefore, it is postulated that the presence of crystalline PC enhances nucleation (increase crystallization rate) and the amorphous PC retards mobility (decrease crystallization rate). Superposition of these two competing forces results in a non-monotonic variation of crystallization peak temperature with PC.

3.3.3 Isothermal Crystallization Kinetics

3.3.3.1 Half Crystallization Time

In an athermal kinetics measurement both the nuclei concentration N and the growth rate G vary during the course of crystallization. In the case of an isothermal kinetics study the only variable is the nuclei concentration N since G is constant. By examining the isothermal crystallization kinetics results, the effects of nucleation and growth may be decoupled and analyzed. The subsequent discussion will direct at the study of isothermal

crystallization kinetics analyzed in terms of the half crystallization time, $\tau_{1/2}$, and the Avrami parameters.

The half crystallization time, $\tau_{1/2}$ as measured by DSC, defined as the time required to achieve 50% of the overall crystallinity, for blends crystallized at 35 °C is plotted as a function of PC concentration as illustrated in Figure 3.6. In agreement with the athermal crystallization kinetics results, $\tau_{1/2}$ increased in a non-monotonic fashion with the addition of PC. In accord with the crystallization peak temperature results, $\tau_{1/2}$ for the Q blends was invariably larger than that for the corresponding AP blends. This phenomenon may be rationalized on the basis of diffusion in which the mixed amorphous phase mobility of the AP blends was higher than that of the corresponding Q blends. This enhancement in the mobility resulted from the depletion of PC in the amorphous phase resulting from crystallization. In addition to the diffusion effects as manifested by the changes in blend T_g, the crystal-line PC may act as an effective nucleating surface for PCL crystallization. This also leads to an further enhancement in crystallization rate for the AP blends.

Attempts have been made to account for the PC crystallinity by expressing the blend composition in terms of the amorphous PC concentration in the mixed amorphous phase. Figure 3.7 shows the half crystallization time dependence on the amorphous PC composition at two different crystallization temperatures. It is observed that the crystallization rate decreased with increasing crystallization temperature indicating that the temperature range under investigation is in the nucleation-controlled regime. At 35 °C the half crystallization time for both the AP and Q blends can be almost superimposed into one master curve. However, the non-monotonic trend was still readily observable. In the case of higher crystallization temperature (40 °C) the $\tau_{1/2}$ for the AP blends was significantly lower than that for the corresponding Q blends. This finding indicates that the PC

nucleation effects became more pronounced and rate-determining as the growth rate at this degree of undercooling was relatively small.

According to the Hoffman-Lauritzen theory,[9] the overall rate of crystallization is governed by the product of growth rate and nucleation density. In the nucleation-controlled regime both the nucleation density and the growth rate increase with the degree of undercooling. At a small degree of undercooling the growth rate is relatively small and a slight increase in the nucleation density resulting from blending could significantly increase the crystallization rate. The AP blends, with higher PC crystallinity, exhibited substantially higher crystallization rate than the Q blends at 40 °C. On the basis of this finding, it is postulated that crystalline PC offers an effective surface for PCL nucleation. At a larger degree of undercooling the overall crystallization rate was dominated by growth as the effects of PC crystallinity as manifested by the increases in nucleation density became less important.

3.3.3.2 Avrami Analysis

The Avrami analysis is often used to model the overall rate of isothermal crystallization as depicted below

$$1 - \Phi(t) = \exp(-kt^n) \qquad (3.1)$$

where $\Phi(t)$ is the crystalline fraction developed after time t, k is the rate constant, n is the Avrami exponent which characterizes the nucleation process and the dimensionality of growth. The intercept of the Avrami plot yields the rate constant and the slope yields the Avrami exponent. Nucleation may be classified either as homogeneous or heterogeneous. Furthermore, it is subdivided according to the crystal size distribution. Athermal nucleation describes the process by which the crystals are growing at the same time

resulting in a narrow crystal size distribution. Thermal nucleation occurs when the crystals start growing throughout the course of the crystallization leading to a non-uniform size distribution. For three-dimensional growth coupled with thermal nucleation,[10] the Avrami exponent n assumes a value of 4. Generally, n increases with increasing dimensionality. Additionally, the rate constant may be related to the half crystallization time by

$$\tau_{1/2} = [\ \ln (2) / k\ ]^{1/n} \qquad (3.2)$$

It is often found that n changes during crystallization. Hence, the half crystallization time computed from the above equation may be very different from that obtained directly from the crystallinity curve.

A series of fractional crystallinity curves for the AP blends crystallized at 45 °C is shown in Figure 3.8 and the corresponding Avrami plots are illustrated in Figure 3.9. In order to discern the different composition, each curve is successively displaced by one decade in the time domain. Several features are readily observable from these plots. The conversion curves, with the exception of the highest PC (60%PCL/40%PC) blend, exhibited sigmoidal time dependence. The onset of the linear region generally increased with increasing PC. In the case of the highest PC blend, the crystallinity grew almost linearly with time. Based on Figure 3.9 and the analysis of other blends, it was observed that the Avrami exponent generally decreased with increasing PC. The n value ranged from 2.5 to 1.5. Figure 3.10 shows a series of Avrami plots for a 90%PCL/10%PC Q blend crystallized at various temperatures. A cursory examination of this figure indicates that the Avrami exponent is roughly about 2.0 and is almost independent of the crystallization temperature. Additionally, Avrami exponents obtained from the AP blends and those derived from the corresponding Q blends were virtually identical.

Quantitative interpretation of the Avrami exponent is not possible due to the uncertainty associated with and the deficiency in the Avrami analysis. However, the Avrami parameters could still serve as a convenient means for describing the crystallization process. Unique to the crystallization of a polymer blend system is that the T_g of the amorphous phase changes during the course of the crystallization. In particular with the present blend system, the presence of crystalline PC may modify the energetics of the nucleation and growth process. These effects are clearly manifested in the shape of the Avrami plots and the values of the kinetic parameters. The reduction in the Avrami exponent with increasing PC coupled with the half crystallization time results suggest that the crystallization mechanism for the pure PCL is fundamentally different from that for the blends. A reduction in the Avrami exponent could result either from a modification in the mode of nucleation or a decrease in the dimensionality of growth. It is postulated that PCL nucleates on the surface of crystalline PC in which the growth path is confined by the pre-existing PC crystallites. This restriction in the growth path could account for the reduction in the Avrami exponent as the dimensionality of growth decreases with increasing PC.

3.3.3.3 Radial Growth Rate

As discussed earlier, the overall crystallization rate is determined by the product of growth rate and nucleation density. In order to decouple theses two effects, the radial growth rate of the blends was measured by optical microscopy and compared to that of the pure PCL. Figure 3.11 shows the radial growth rate as a function of the blend composition and crystallization temperature. In agreement with the DSC results, the radial growth rate decreased with increasing crystallization temperature indicating that the crystallization temperature range is in the nucleation-controlled regime. In contrast to the overall crystallization rate, the growth rate decreased monotonically with increasing PC. This retardation in the growth rate may be rationalized on the basis of the reduction in

mobility resulted from blending. This finding clearly demonstrates that the non-monotonic variation in the overall crystallization rate as measured by DSC is a direct consequence of the nucleation effects of PC on the PCL crystallization. In agreement with this nucleation hypothesis, optical microscopy also revealed that the PCL spherulitic size decreased with the addition of PC.

3.3.3.4 Crystal Nucleation

It has been shown that the nucleation mechanisms involved in polymer crystallization have both physical and chemical origin.[11] Three different mechanisms of heterogeneous nucleation have been identified. The first mechanism is self-nucleation in which the nucleation sites are the fragments of the polymer crystals in the melt. The second is epitaxial nucleation of polymers on inorganic or organic substrates.[12-13] The third mechanism involves the dissolution of organic salts in the molten polymers producing ionic chain ends which precipitate and form aggregates serving as nucleating sites. The epitaxial nucleation mechanism is the most probable means through which PCL couples to the PC crystallites.

On the basis of the DSC results coupled with the optical microscopy findings, crystalline PC appears to be a very effective nucleating medium for PCL crystallization. It is postulated that PCL crystallizes on the surface of PC crystals. These crystals are extremely small and are beyond the resolution of optical microscopy. This picture is also consistent with the small-angle light scattering results, described in Chapter 6, which indicated that the PCL spherulitic size decreased with the addition of PC. Hence, it is proposed that the physical state of PC may have a profound impact on PCL crystallization. Amorphous PC retards the mixed amorphous phase mobility as manifested by an increase in T_g. This effect leads to a reduction in the rate of diffusion and consequently the rate of crystal growth. In contrast, crystalline PC enhances nucleation and thereby

increasing the rate of crystallization. The competition between these two forces, as schematically depicted in Figure 3.12, results in a non-monotonic variation of the half crystallization time with PC. It remains to be a challenge to elucidate the detailed mechanism of the crystalline PC-PCL epitaxial interactions.

3.4 Conclusions

Both athermal and isothermal crystallization kinetics of PCL in PCL-rich blends have been examined. The overall crystallization rate and the radial growth rate were measured by DSC and optical microscopy, respectively. The PCL crystallization peak temperature decreased in a non-monotonic fashion with the addition of PC. AP blends with higher PC crystallinity displayed faster crystallization rate as reflected by the higher crystallization peak temperature than the corresponding Q blends with lower PC crystallinity. Similar trends were observed for the isothermal crystallization kinetics results. To a first order of approximation, the overall crystallization rate was governed by the amount of amorphous PC in the blends. The isothermal crystallization rate as measured in terms of the half crystallization time decreased with increasing crystallization temperature and decreased in a non-monotonic fashion with the addition of PC. In contrast, the radial growth rate decreased monotonically with increasing PC. The radial growth rate measurements coupled with the DSC results unequivocally demonstrated that PC, probably the crystalline phase, is an effective nucleating medium for PCL crystallization. The mechanism by which PCL couples to PC is postulated to be through epitaxial interaction in which PCL crystallizes on the surface of the PC crystallites.

References

1. Tashiro, K; Satkowski, M.M.; Stein, R.S.; Li, Y; Chu, B. and Hsu, S.L. *Macromolecules* **25**, 1809 (1992).

2. Bittiger, H. and Marchessault, R.H. *Acta. Cryst.* **B26**, 1923 (1970).

3. Bonart, V.A. *Die Makromolekulare* **92**, 146 (1966).

4. Philips, P.J. and Rensch G. *J. Polym. Sci. Polym. Phys. Ed.***27**, 155 (1989).

5. Tabar, R.J., *Ph.D. Thesis*, University of Massachusetts, Amherst, 1983.

6. Song, H.H.; Wu, D.Q.; Chu, B.; Satkowski, M.; Ree, M.; Stein, R.S. and Philips, J.C. *Macromolecules* **23**, 2380 (1990).

7. Mandelkern, L. *Crystallization of Polymers;* McGraw-Hill, New York, 1964.

8. Stauffer, D. *Introduction to Percolation Theory*; Taylor and Francis, London, 1985.

9. Hoffman, J.D., Davis, G.T. and Lauritzen Jr, J.I. in "Treaties on Solid State Chemistry" (Ed. N.B. Hanny), Vol. 3, Plenum, New York, 1976, P. 497.

10. Wunderlich, B. *Macromolecular Physics*; Vol 2, Academic Press, New York, 1976.

11. Mercier, J.P. *Polym. Sci. Eng.* **30(5)**, 270 (1990).

12. Wittmann, J.C. and Lotz, B. *J. Polym. Sci. Polym. Phys. Ed.***19**, 1837 (1981).

13. Wittmann, J.C.; Hodge, A. M. and Lotz, B. *J. Polym. Sci. Polym. Phys. Ed.* **21**, 2495 (1983).

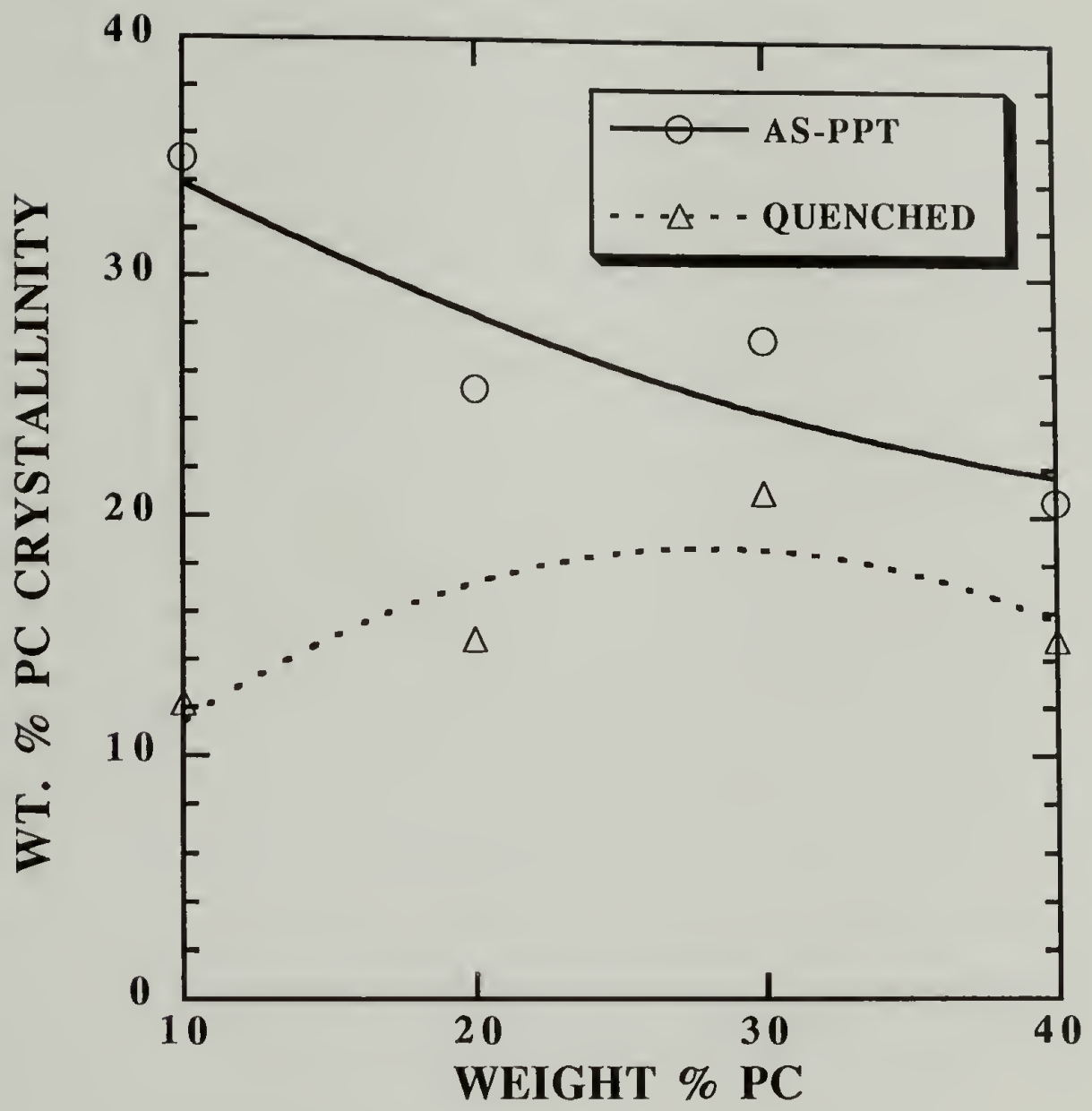

Figure 3.1 Normalized PC crystallinity for as-precipitated and quenched blends.

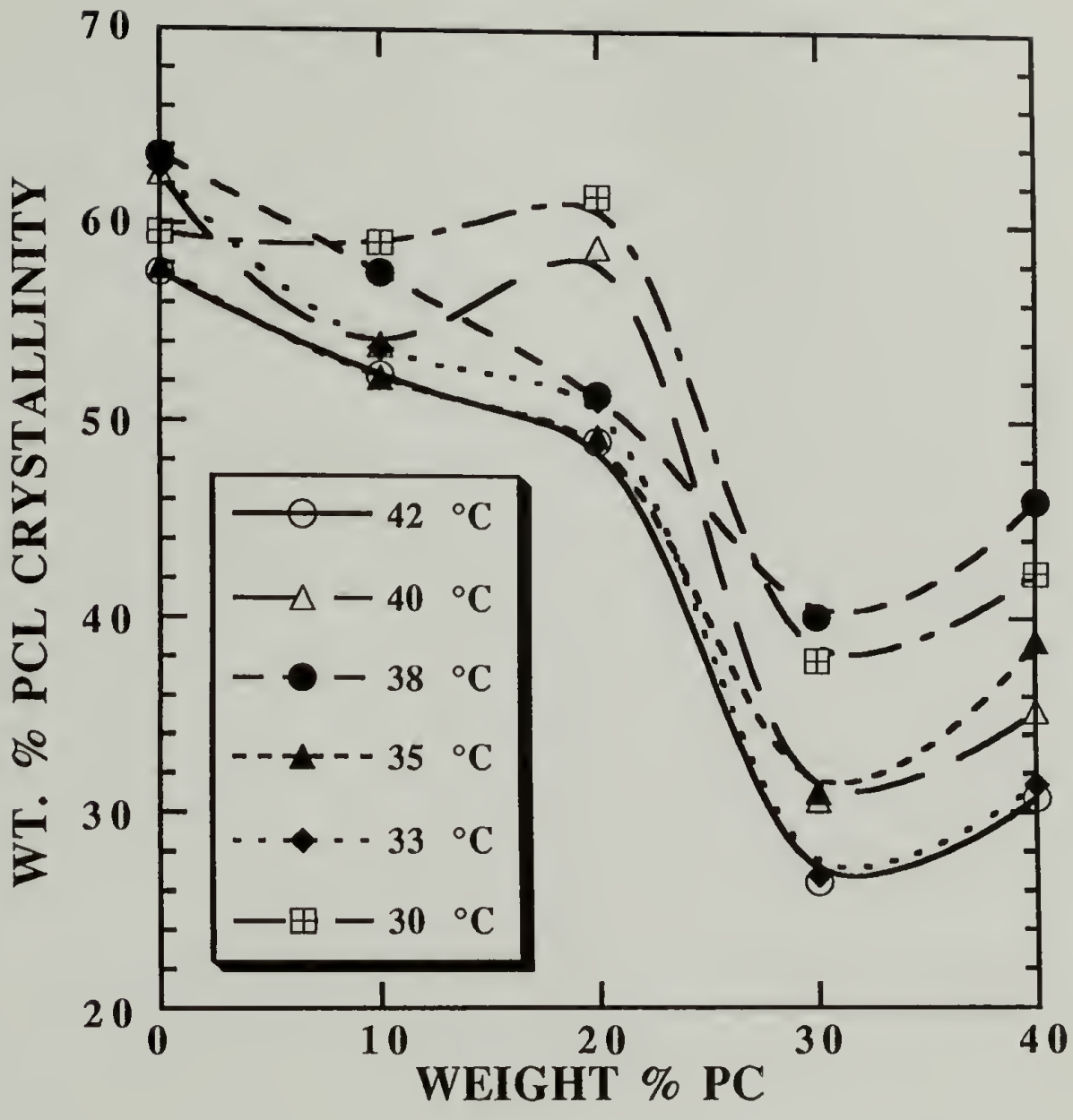

Figure 3.2 Normalized PCL crystallinity for PCL-rich blends crystallized at various temperatures.

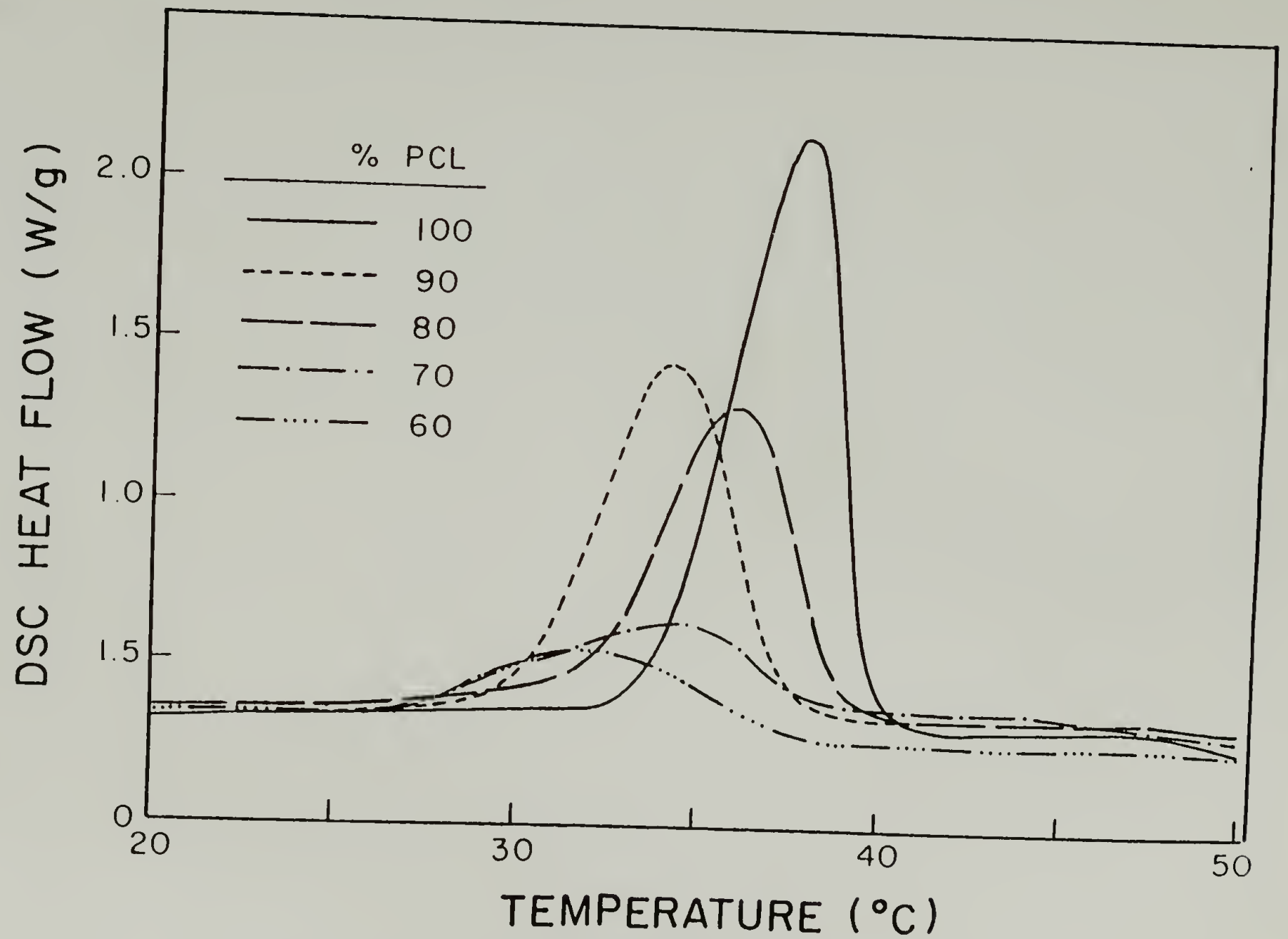

Figure 3.3 Non-isothermal crystallization exotherms for pure PCL and quenched blends measured at a cooling rate of 5 °C/min.

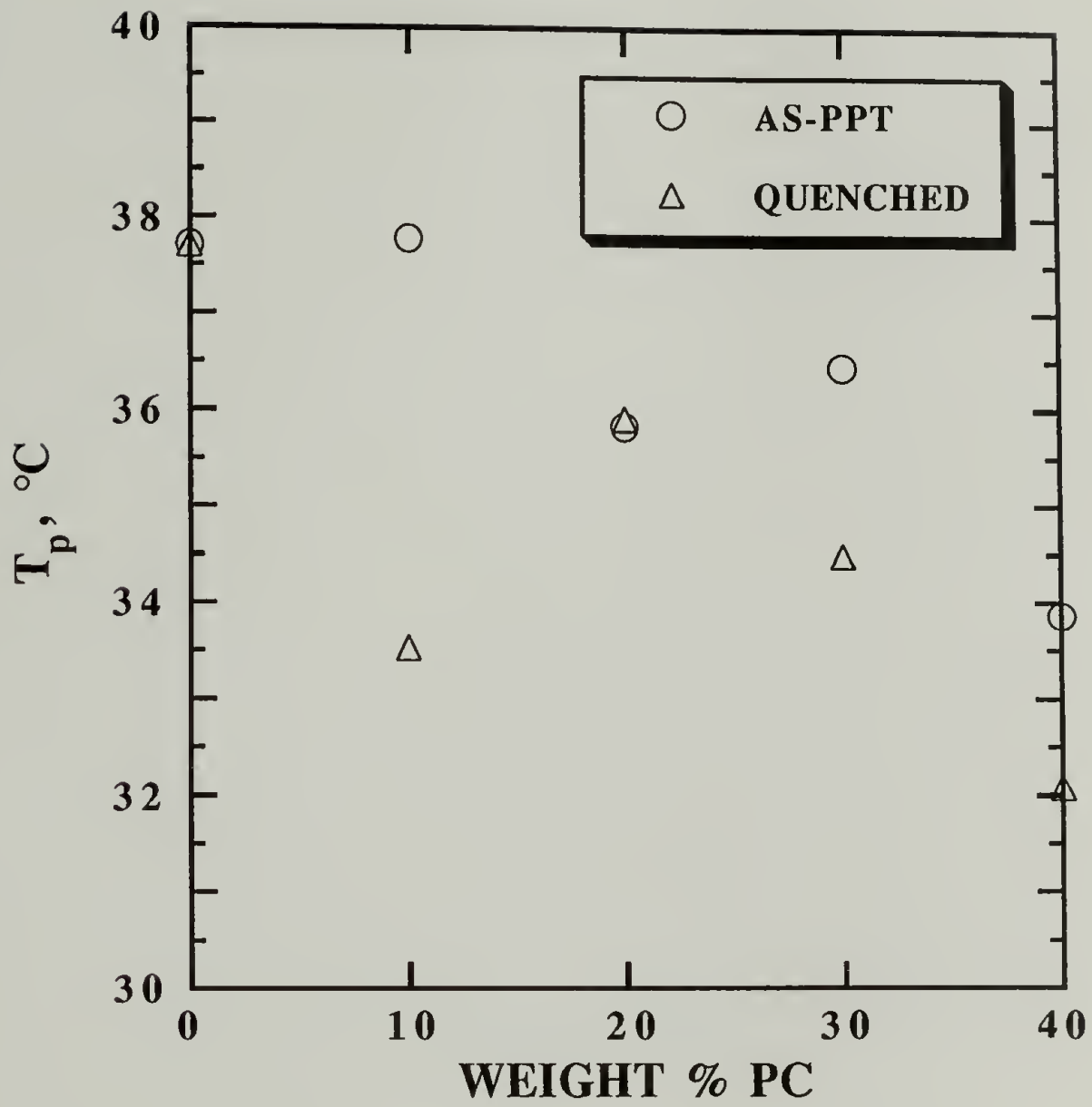

Figure 3.4 Crystallization peak temperatures for as-precipitated and quenched blends.

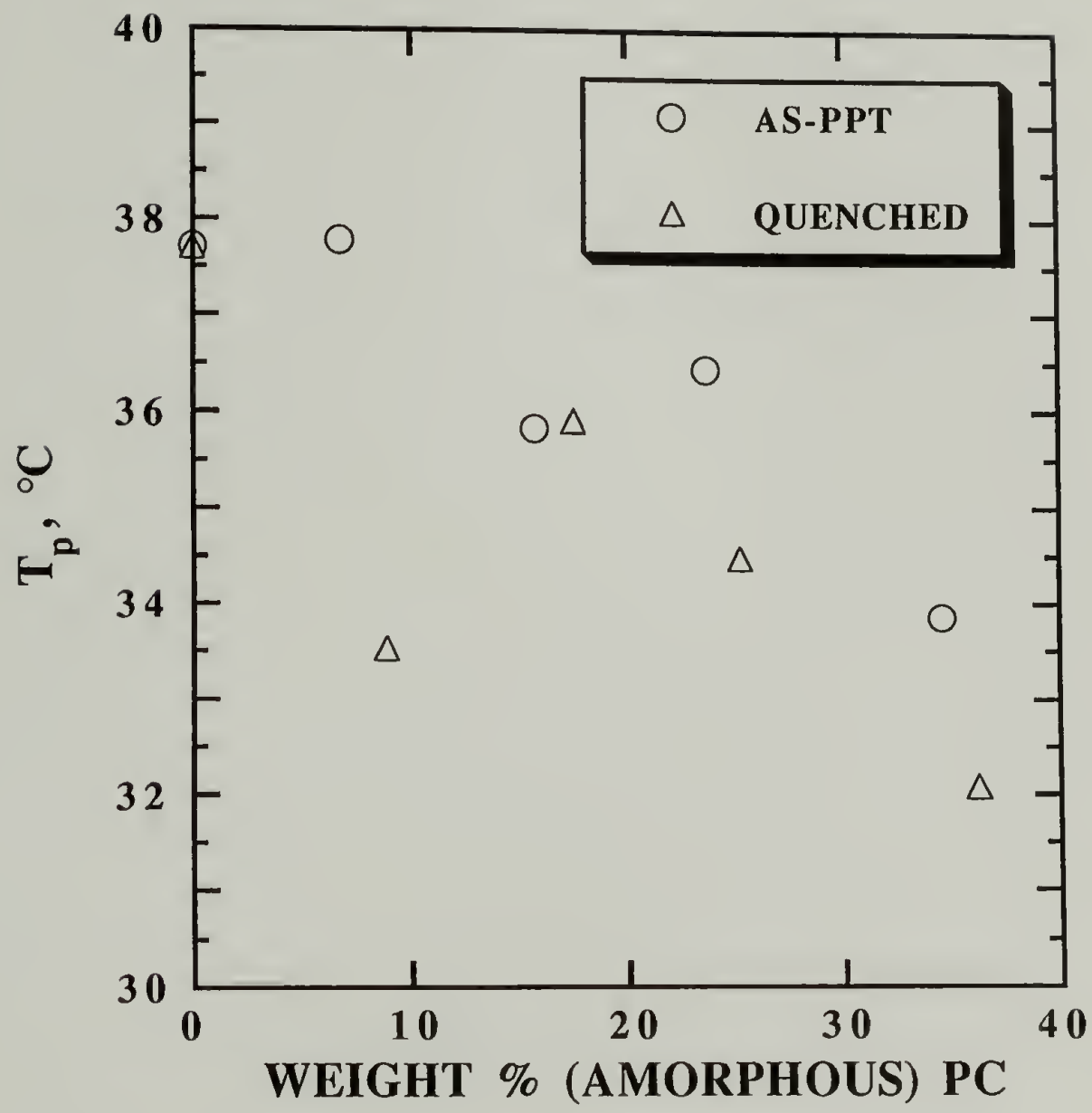

Figure 3.5 Crystallization peak temperatures for as-precipitated and quenched blends as a function of amorphous PC composition in the mixed amorphous phase.

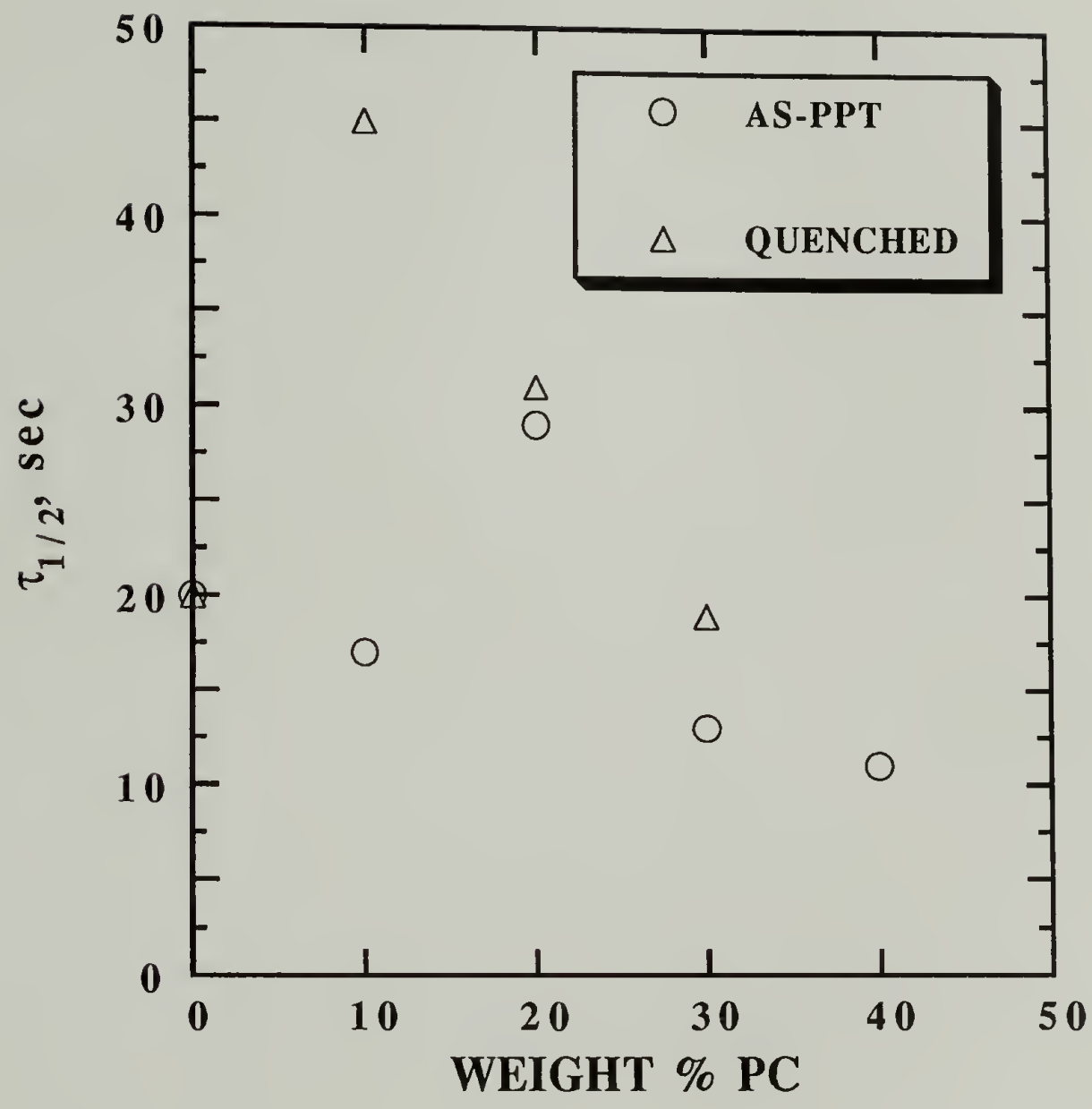

Figure 3.6 Half crystallization time for as-precipitated and quenched blends crystallized at 35 °C.

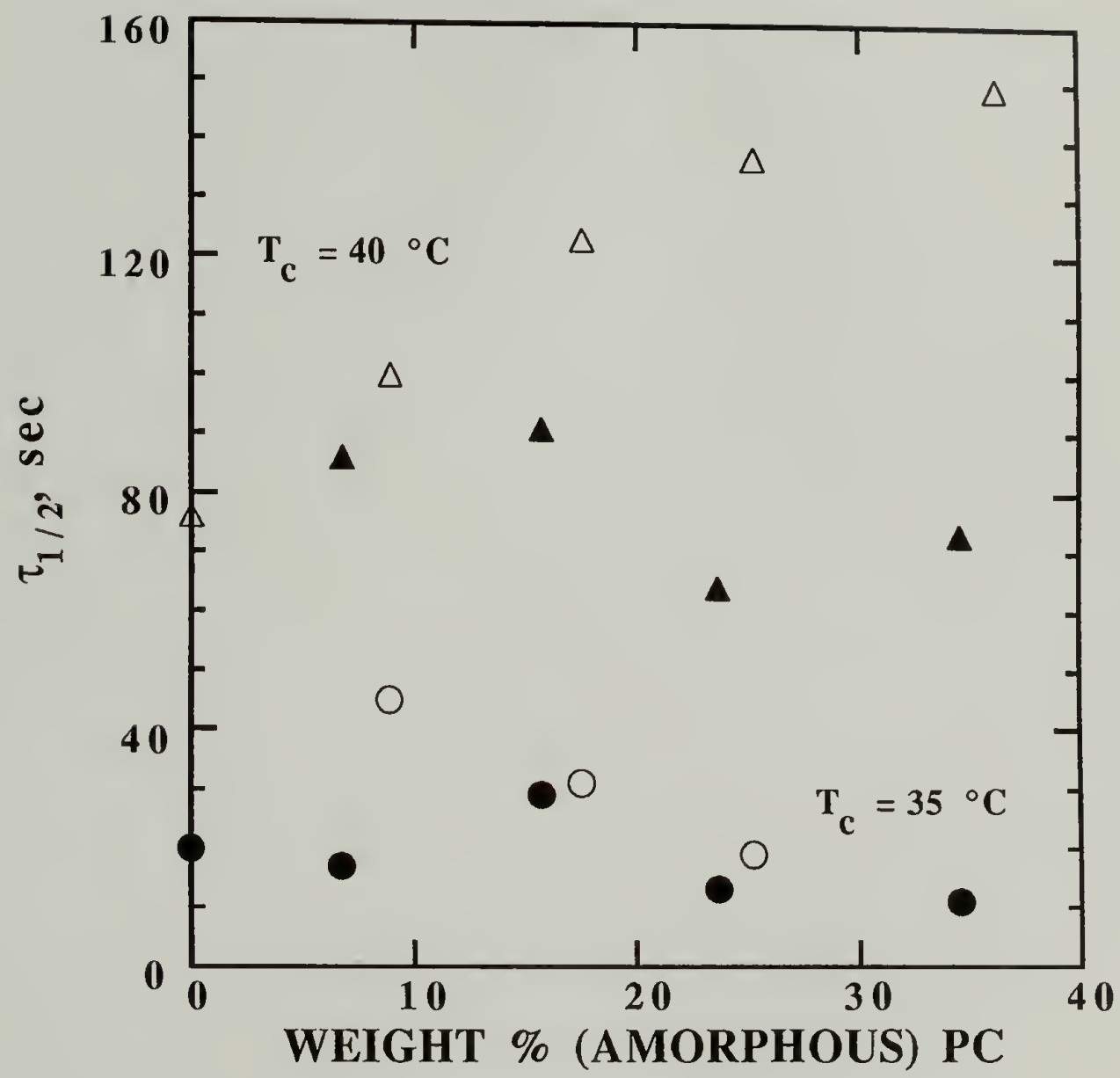

Figure 3.7 Half crystallization time for as-precipitated and quenched blends, crystallized at 35 °C and 40 °C, as a function of amorphous PC composition in the mixed amorphous phase. Fill symbols represent AP blends and open symbols denote Q blends.

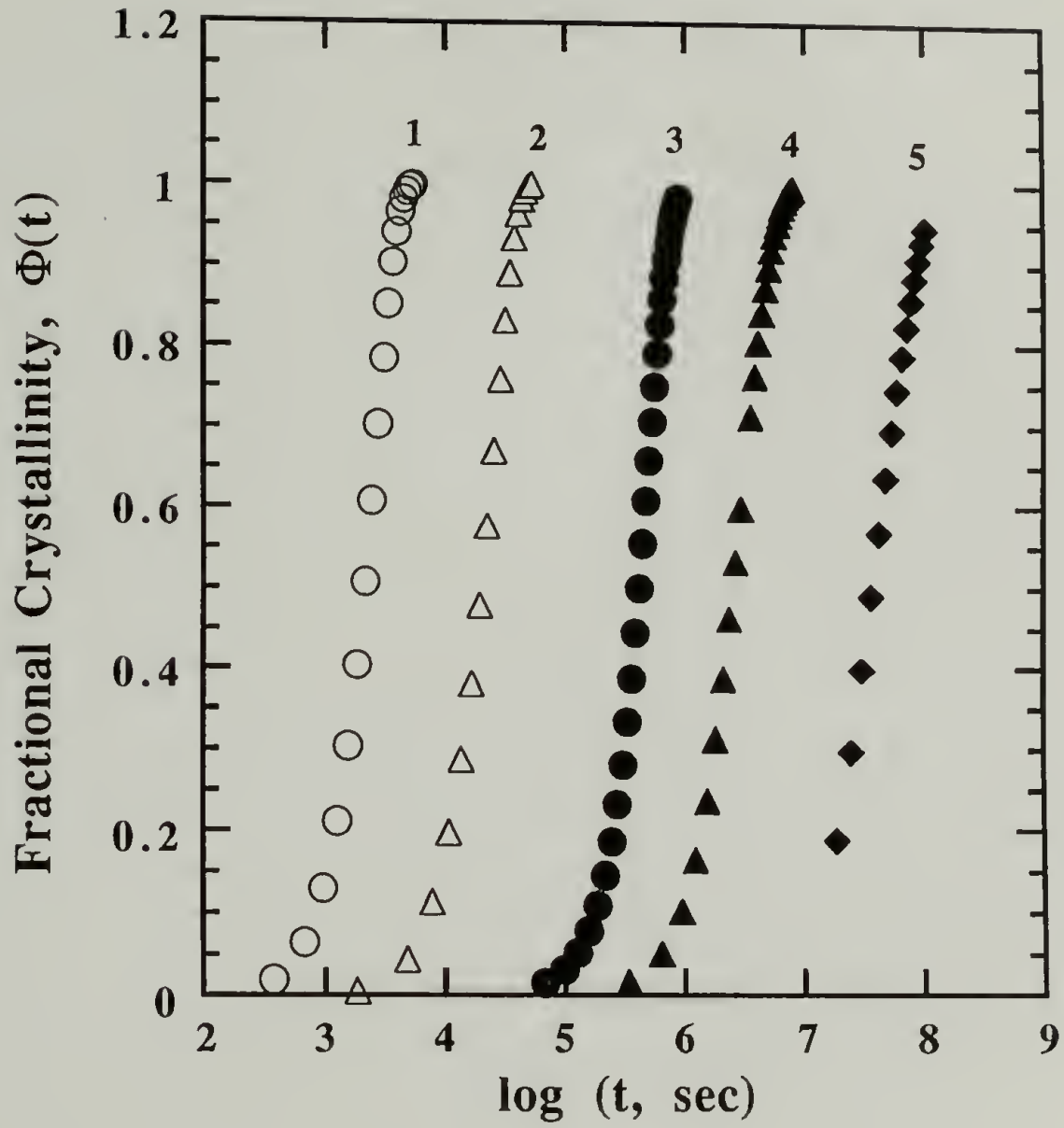

Figure 3.8 Fractional crystallinity for as-precipitated blends crystallized at 45 °C. In order to discern the different composition, each curve is successively displaced by one decade in the time axis. 1- 100% PCL, 2- 90% PCL, 3- 80% PCL, 4- 70% PCL, 5- 60% PCL.

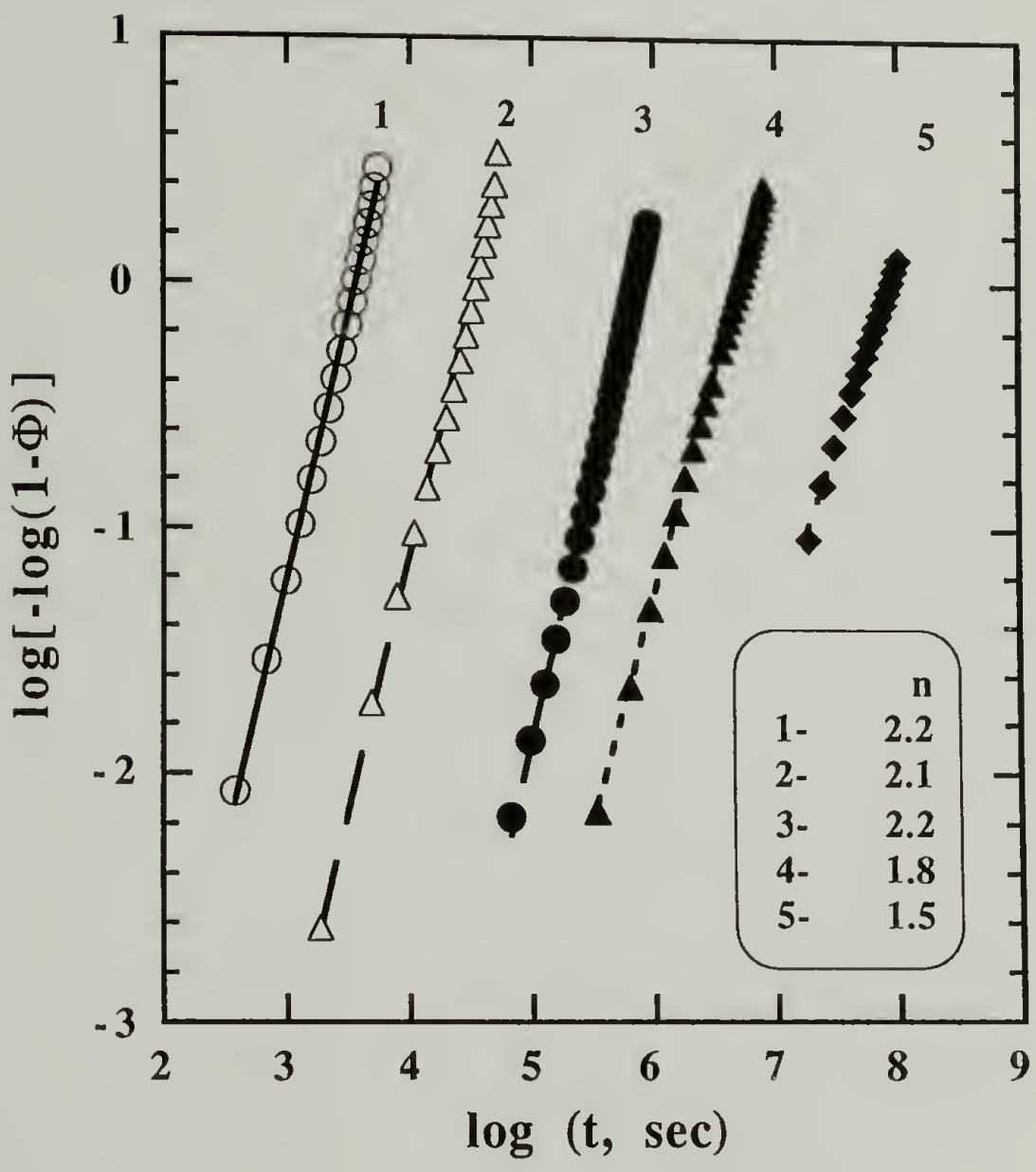

Figure 3.9 Avrami plots for as-precipitated blends crystallized at 45 °C. Each curve is successively displaced by one decade in the time axis. 1- 100% PCL, 2- 90% PCL, 3- 80% PCL, 4- 70% PCL, 5- 60% PCL, where n denotes the Avrami exponent.

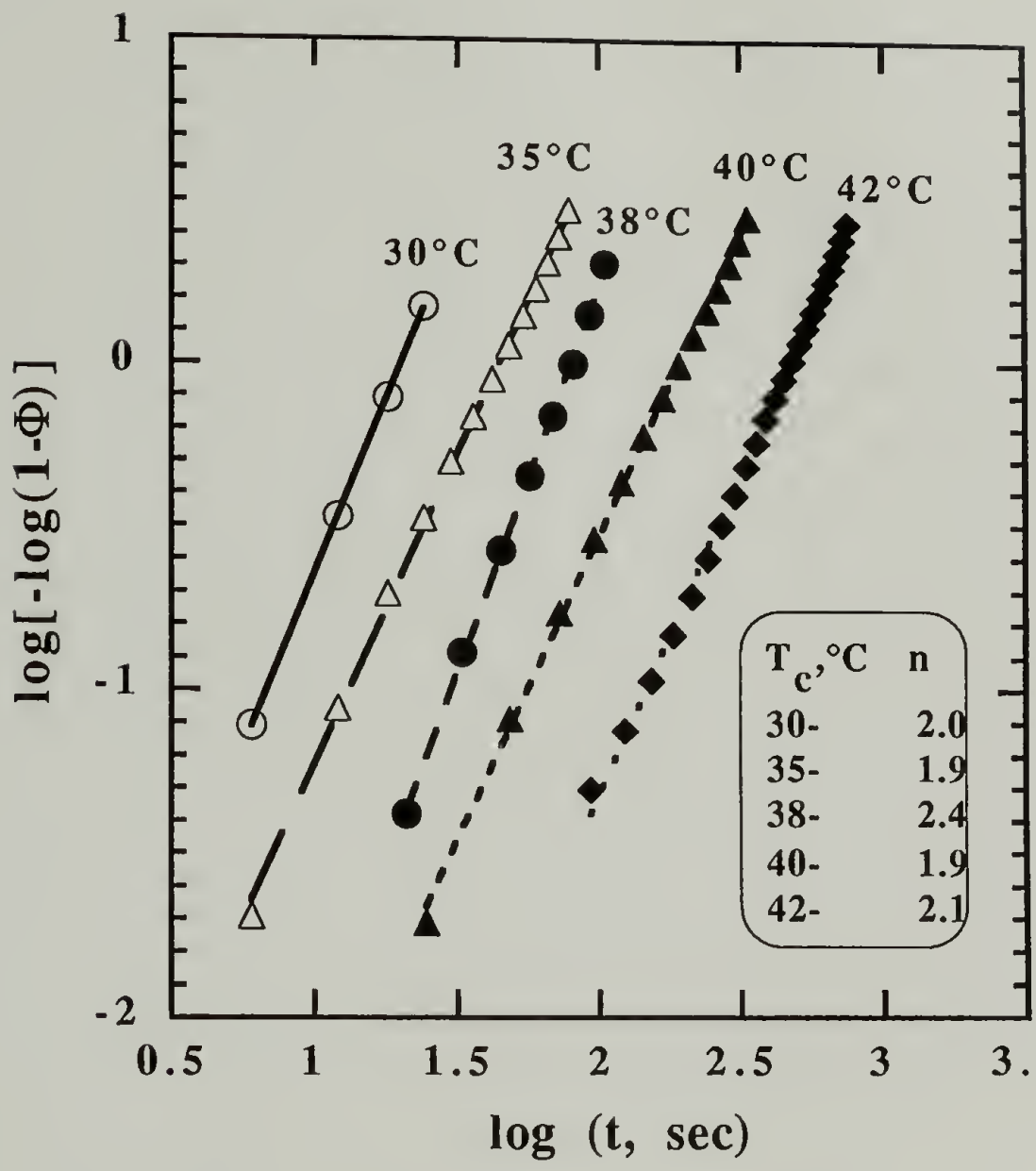

Figure 3.10 Avrami plots for a 90%PCL/10%PC quenched blend, where n denotes the Avrami exponent.

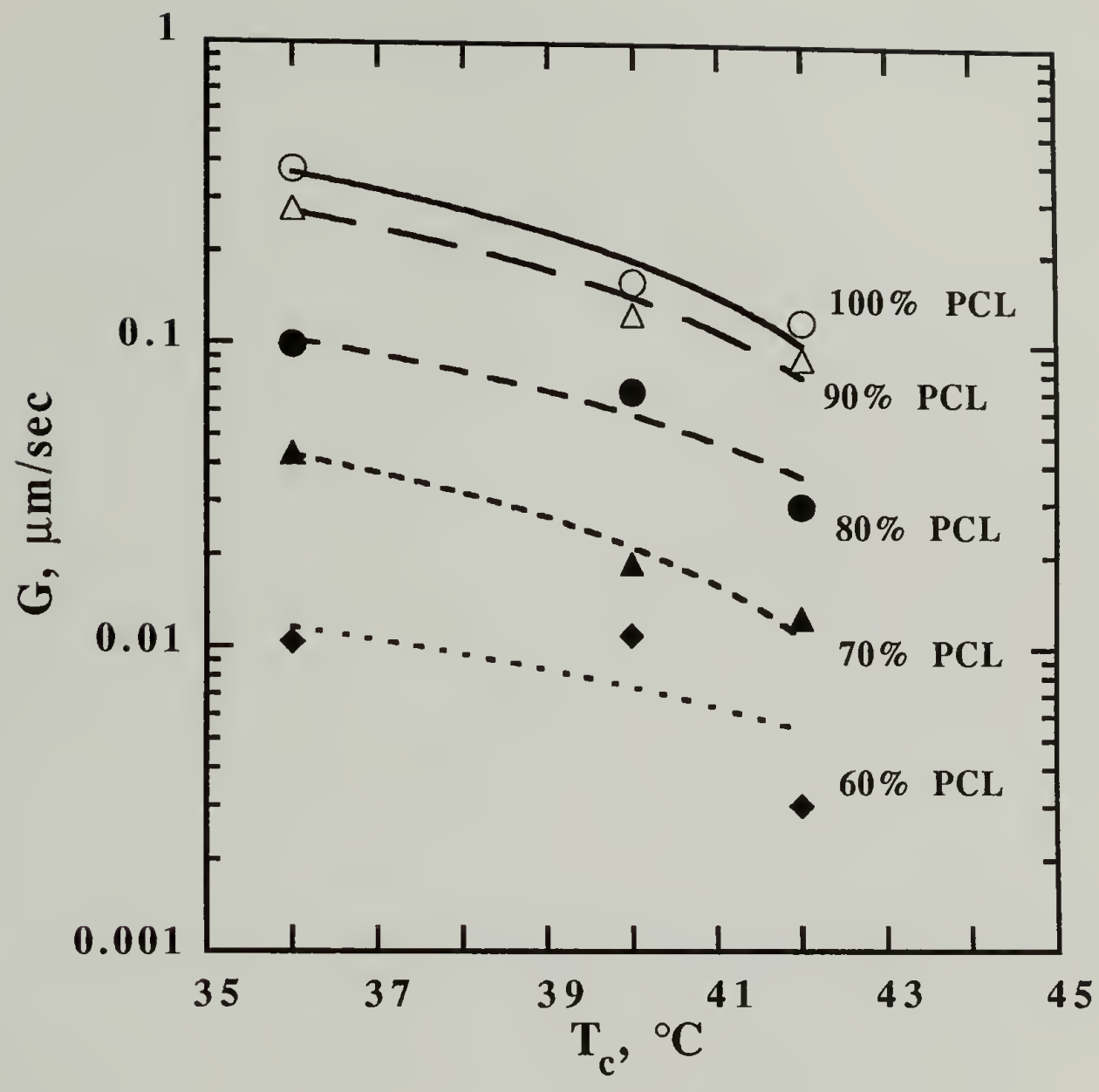

Figure 3.11 Radial growth rate as a function of composition and crystallization temperature.

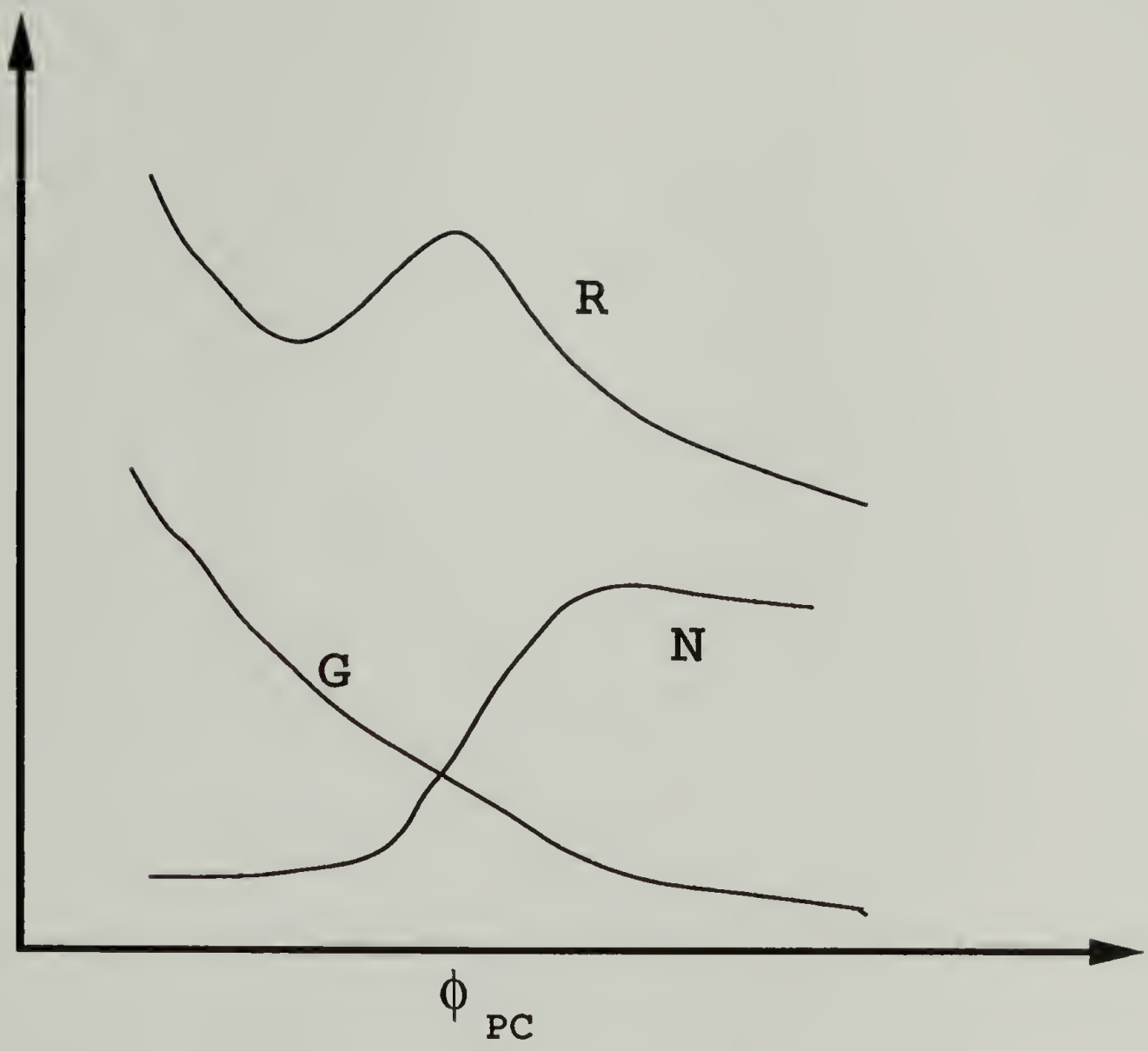

Figure 3.12 Schematic representation of the PCL crystallization kinetics for the PCL-rich blends. R is the overall rate of crystallization, N is the nucleation density, and G is the radial growth rate, where R is the equal to the product of N and G.

CHAPTER 4
ISOTHERMAL CRYSTALLIZATION KINETICS AS PROBED BY SYNCHROTRON SAXS

4.1 Introduction

In order to probe the crystallization kinetics at a microscopic level, time resolved synchrotron small-angle X-ray scattering (SAXS) was employed to monitor the PCL lamellar evolution in the PCL-rich blends. This chapter will focus on the isothermal crystallization kinetics of PCL in the PCL-rich blends containing various amounts of PC crystallinity. The effects of crystallization temperature and PC composition will also be examined. There are three basic parameters which could be easily obtained from synchrotron SAXS. Lamellar development is normally described in terms of the time evolution of the long period as measured by the peak position of the scattering profile. It has been observed that the long period increased with time for polyethylene,[1] decreased for poly(ethylene terephthalate) (PET),[2] and remained constant for poly(β-hydroxybutyrate).[3] The changes in the long period during the course of crystallization are usually related to lamellar reorganization as the lamellae may undergo isothermal thickening or flattening. The nature and magnitude of these lamellar rearrangements are not well understood. The second parameter is the intensity of the peak which reflects the growth of the crystalline phase. The third parameter is the invariant which is proportional to the product of the volume fractions of the two phases and the electron density difference between the crystal and the amorphous region, and is often used as a measure of crystallinity.

Dynamic studies[4] of isothermal crystallization kinetics of PCL and 90% PCL/10% poly(vinyl chloride) (PVC) blend by synchrotron SAXS indicated that the long period for

both the pure PCL and the blend remained virtually constant with time. Kinetic parameters such as the half crystallization time $\tau_{1/2}$ and the Avrami exponent n were derived from the time dependence of the peak intensity. The blend showed a higher $\tau_{1/2}$ than the pure PCL for a given crystallization temperature. Similar to this behavior, the crystallization rate for the PCL/PC blends is slower than that for the pure PCL. The degree of PC crystallinity is expected to have a profound impact on the lamellar development. The focus of this study will be directed at elucidating the effects of crystalline PC on the lamellar evolution and structure of PCL in the PCL-rich blends.

4.2 Experimental

As in the DSC measurements, both Q and AP blends were examined in this study. The blend samples were deposited into a copper cell contained between two 25-mm-thick Kapton films. The sample dimension was about 7 mm in diameter and 2 mm in thickness. Synchrotron SAXS measurements were performed at the State University of New York (SUNY) X3A2 Beamline, National Synchrotron Light Source (NSLS), Brookhaven National Laboratories (BNL) using a modified Kratky block collimation system.[5] The storage ring of the synchrotron was operated at an energy level of 2.6 GeV with a beam current of 110-180 mA. The X-ray wavelength used for the measurement was 1.54 Å. The scattered intensity was collected by a linear position sensitive photodiode array detector coupled to an optical multichannel analyzer.[5] The scattering profiles were corrected for detector non-uniformity, sample absorption, background, and incident X-ray intensity fluctuations.[6-7]

Temperature quenching experiments were conducted in a device consisting of two thermal chambers equilibrated at temperatures T_C and T_H.[8] The sample cell could be transferred rapidly from one chamber to the other chamber by means of a metal rod connected to a pneumatic pressure device. Isothermal crystallization was achieved by

preheating the sample at 75 °C in the T_H chamber for about 5 min in order to render PCL completely amorphous and then rapidly transferred to the T_C chamber equilibrated at the crystallization temperature. Since the thermal chambers were well insulated and the temperature jump was fairly shallow (~ 30 °C), it was estimated that the sample reached the crystallization temperature in about a minute. This time scale was generally shorter than the induction time for PCL crystallization. The scattered intensity during the crystallization was recorded every 10-50 sec until the integrated intensity ceased to change. The temperature fluctuation in the chamber was within ± 0.3 °C during the course of the measurement.

4.3 Results and Discussion

4.3.1 Pure PCL

The time evolution of $q^2I(q)$ for pure PCL crystallized at 41 °C as measured by synchrotron SAXS is shown in Figure 4.1. The integrated SAXS intensity or the invariant Q(t) for a two-phase system with sharp interface boundaries is defined as[9]

$$Q = \int_0^\infty q^2 I(q)\, dq \propto \phi_c (1-\phi_c)(\rho_c - \rho_a)^2 \qquad (4.1)$$

where ρ_a and ρ_c are the electron densities of the amorphous and the crystalline phases, respectively, ϕ_c is the degree of crystallinity and $q = (4\pi\sin\theta/\lambda)$ with 2θ being the scattering angle, and λ, the X-ray wavelength. Based on this equation, the invariant attains a maximum at 50 volume % of crystallinity and could be used as a measure of crystallinity. The normalized invariant, $[Q(t)/Q_{max}]$, as shown in Figure 4.2, revealed a maximum indicating that the degree of crystallinity had exceeded the 50% value. The interlamellar spacing and the peak intensity I_{max} are shown in Figure 4.3. The PCL interlamellar spacing remained fairly constant during the course of crystallization, in agreement with

other studies.[4] Similar to the invariant, the peak intensity exhibited a sigmoidal time dependence reflecting the development of crystallinity. Therefore, both the normalized invariant and the peak intensity could be used to monitor the crystallization process.

4.3.2 Quenched Blends

A series of Lorentz-corrected SAXS profiles for a 80%PCL/20%PC blend also crystallized at 41 °C is shown in Figure 4.4. Two striking features were readily observed from these SAXS profiles. First, there was finite scattering at time zero indicating pre-existing structure. Second, the peak position changed with time reflecting some kind of lamellar rearrangement. Figures 4.5 illustrates these two unusual behaviors. The excess scattering mainly came from the PC lamellae in the blends. As PCL was being crystallized, the long period initially decreased with time and finally approached a plateau value as indicated by Figure 4.5. Similar patterns were observed in other quenched blends crystallized at various temperatures.

A series of crystallization isotherms (I_{max} versus time) for blends crystallized at 37 °C is plotted in Figure 4.6. A cursory examination of these plots revealed that the scattering at time zero increased with increasing PC whereas the magnitude of the change in peak scattering intensity, as measured by $[I_{max}(\infty) - I_{max}(0)]$, decreased with increasing PC. It is clearly observed that the excess scattering generally increased with increasing PC crystallinity and predominantly came from the PC lamellae. The reduction in the change of the peak scattering intensity reflected a corresponding decrease in the PCL crystallinity. The half crystallization times, $\tau_{1/2}$, defined as the time required to achieve 50% of the normalized crystallinity measured in terms of the peak scattering intensity, as a function of the PC composition and crystallization temperature are shown in Figure 4.7. Similar to the overall crystallization rate results, $\tau_{1/2}$ increased with crystallization temperature and generally increased with the addition of PC. Invariably,

the value of the half crystallization time derived from synchrotron SAXS is always larger than that obtained from DSC. On the basis of the DSC results coupled with the present findings, it is found that there exists a very close correspondence between the overall rate of crystallization and the lamellar growth as the kinetics for these two processes are comparable.

The composition and crystallization temperature dependence of the "equilibrium" long period, obtained at the end of the crystallization, are summarized in Figure 4.8. Due to the difference in the degree of undercooling, the long period increased with the crystallization temperature. Furthermore, the long period remained fairly independent of the PC composition. Additionally, the long periods obtained at 75 °C are somewhat larger than those measured at lower temperatures. The scattering at 75 °C arose mainly from PC as the PCL (T_m ~ 60 °C) became amorphous at this temperature. Hence, the long periods measured at 75 °C represented the actual interlamellar spacing for PC. These values were similar to those measured during the induction period of the PCL crystallization. It was found that the actual PCL long period could not be isolated as the SAXS measured at various crystallization temperatures (below the T_m of PCL) came from a superposition of the PC and PCL lamellar scattering. Effectively, the long period derived at temperatures below the T_m of PCL could be viewed as the average long period for the PC and PCL lamellae.

As discussed earlier, the time dependence of the long period reflects the lamellar organization during the crystallization. For all the Q blends investigated, the long period initially decreased with time and then approached a plateau value characteristic of the average interlamellar spacing for the PC and PCL lamellae. On the basis of these findings, an insertion mechanism is proposed in which the PCL is crystallized in the amorphous intralamellar region. According to this insertion model, the new PCL lamellae

are formed in the amorphous phase between the existing PC lamellae. This model can easily account for the initial reduction in the long period and the absence of multiple peaks. It is also consistent with the results derived from the quantitative SAXS studies of the PCL-rich blends in the semicrystalline/semicrystalline state, described in Chapter 6, which suggested a random mixing of PCL and PC lamellae. In other words, PCL and PC lamellae are randomly dispersed in the amorphous phase and the SAXS profiles measured in the semicrystalline/semicrystalline state could be modeled as scattering originating from composite entities consisting of PCL and PC lamellae. The reduction in the PC long period could be attributed to the formation of the PCL lamellae. As crystallization proceeded, the scattering became dominated by the PCL lamellae and the long period ceased to change as was observed for the pure PCL. The "equilibrium" long periods for the blends differed from those of the pure PCL due to the composite nature of the lamellar scattering and the differences in the thermodynamic forces for PCL crystallization arising from blending.

4.3.3 As-Precipitated Blends

In addition to the PC composition and crystallization temperature, the effects of PC crystallinity on the PCL lamellar growth were also examined. According to Figure 3.2, the PC crystallinities for the AP blends were always higher than those for the corresponding Q blends. For a given blend composition, it was found that the AP blends always crystallized faster than the corresponding Q blends as revealed by DSC. This difference was attributed to the depletion of PC in the mixed amorphous phase due to crystallization and thereby resulting in a higher mobility. To a first order of approximation, the PCL crystallization kinetics were governed by the total amount of amorphous PC present in the blends. The PC crystallinity effects on the lamellar development will be discussed with respect to and contrasted against the Q blends.

The evolution of the long period and I_{max} for a 80%PCL/20%PC blend crystallized at 43 °C is shown in Figure 4.9. In contrast to the Q blends, the long period for the AP blends initially increased with time and then reached a plateau value. Similar time dependence was found for other AP blends crystallized at various temperatures. Crystallization isotherms for the AP blends and the pure PCL crystallized at 37 °C are plotted in Figure 4.10. Nearly identical features to those found in the Q blends were observed. The peak scattering intensity at time zero generally increased with increasing PC crystallinity whereas the overall change in the peak scattering intensity, $[I_{max}(\infty) - I_{max}(0)]$, decreased, reflecting a reduction in the PCL crystallinity, with increasing PC concentration. The half crystallization time, $\tau_{1/2}$, as a function of PC composition and crystallization temperature is summarized in Figure 4.11. Similar to the Q blends, the lamellar growth rate decreased with increasing crystallization temperature and generally decreased with the addition of PC. A comparison between Figures 4.7 and 4.11 clearly demonstrates that the lamellar growth rate increased with increasing PC crystallinity for a given blend composition. This finding unequivocally shows that the presence of amorphous PC retards both the overall crystallization rate as measured by DSC and the lamellar growth rate as monitored by synchrotron SAXS.

The composition and crystallization temperature dependence of the long period are shown in Figure 4.12. Similar to the Q blends, a systematic increase in the long period with increasing crystallization temperature was found. The PC long periods (measured at 75 °C) were lower than those obtained for the Q blends. This disparity in the PC lamellar structure might be attributed to the differences in the thermal history imposed on the samples. The long periods for the AP blends (with smaller PC long periods) were smaller than those found in the Q blends and thus reflecting the composite nature of the mixed lamellae. This difference in the interlamellar spacing has provided an additional evidence for supporting the random mixing model for PCL and PC lamellae.

One of the most profound differences between the AP and the Q blends could rest with the time evolution of the long period. In contrast to the Q blends, the long period for the AP blends initially increased with time and then approached a plateau value in the later stage of crystallization. This behavior suggested that the PC lamellae in the AP blends experienced rearrangement resulting in a reduction of the long period upon quenching to the PCL crystallization temperature. In the case of the Q blends, the PC lamellae structure remained virtually intact at the PCL crystallization temperature. Several mechanisms could account for the apparent "collapse" of the PC lamellae observed in the AP blends. It is well known that lamellar flattening can lead to a reduction in the long period as the PC may undergo further (secondary) crystallization. Isothermal thinning resulting from low temperature annealing can also account for the decrease in the long period.

The induction period for the AP blends is shorter than that for the Q blends. A recent SAXS study on poly(ethylene terephthalate)[10] revealed that a growth process that is very similar to the spinodal decomposition type of phase separation process occurred during the induction period. Crystallization commences after a dense domain characterized by a long-range ordered structure grows to a certain size. The changes in the PC long period may be related to the scattering arising from this dense domain. As PCL crystallizes, PCL lamellae form in the amorphous intralamellar phase according to the insertion model as illustrated in Figure 4.13. Subsequently, these PCL lamellae dominate the scattering resulting in an invariant in the long period. In agreement with the Q blends, the final crystalline blend morphology is adequately described by the random mixing model in which PCL and PC lamellae are homogeneously dispersed in the amorphous matrix.

The exact origin of the differences observed in the time evolution of the long period between the Q and the AP blends is highly complex and not well understood. However,

there were several distinct differences between these two types of blends. Due to the higher PC crystallinity, the mobility in the amorphous phase for the AP blends was higher than that for the corresponding Q blends due to the depletion of PC in the mixed amorphous phase resulting from crystallization. On the basis of the overall crystallization rate results and lamellar growth measurements, the AP blends crystallized faster than the corresponding Q blends. As indicated above, the induction period was shorter for the AP blends as compared with that for the Q blends. It remains to be a challenge to derive a satisfactory mechanism based on these differences which can provide a rational explanation for describing the initial time dependence of the long period.

4.4 Conclusions

The isothermal crystallization kinetics of PCL-rich blends containing various amounts of PC crystallinity have been probed with synchrotron SAXS. The effects of PC composition, crystallization temperature and PC crystallinity on the PCL crystallization kinetics have been systematically investigated. As in the DSC measurements, the PCL lamellar growth rate for the AP blends was higher than that for the corresponding Q blends. To a first order of approximation, it was found that the lamellar growth rate was predominantly controlled by the amount of amorphous PC present in the blends. The half crystallization time derived from the temporal change of the peak intensity increased with the crystallization temperature and generally increased with the addition of PC. Similarly, the long period increased with increasing crystallization temperature.

For the Q blends, the long period initially decreased with time and then reached a plateau value at the later stage of crystallization. An insertion model, where the PCL is crystallized in the amorphous intralamellar phase of the existing crystalline PC, can account for the reduction in the long period and the absence of multiple peaks. This type of crystallization mechanism is also consistent with our quantitative SAXS results,

described in Chapter 6, which suggest that random mixing of PCL and PC lamellae occurs in the semicrystalline/semicrystalline state. In the case of the AP blends, the PC lamellae experienced rearrangement as reflected by the reduction in the long period upon quenching to the PCL crystallization temperature. Additionally, the long period initially increased with time and finally approached a plateau value. The origin of this phenomenon is not well understood and remains to be a challenge to derive a universal crystallization mechanism which can explain the differences in the time evolution of the lamellae for both the Q and AP blends.

References

1. Barham, P.J. and Keller, H.H. *J. Polym. Sci., Phys. Ed.* **27**, 1029 (1989).

2. Elsner, G.; Koch, M.J.; Bordas, J. and Zachman, H.G. *Makr. Chem.***182**, 1262 (1981).

3. Elsner, G.; Riekel, C. and Zachmann, H.G. *Adv. Polym. Sci.* **67**, 1029 (1985).

4. Nojima, S.; Tsutsui, H. and Urushihara, A. *Polym. J.* **18**, 451 (1986).

5. Chu, B.; Wu, D.Q. and Howard, R. *Rev. Sci. Instrum.* **60**, 3224 (1989).

6. Song, H.H.; Stein, Stein, R.S.; Wu, D.Q.; Ree, M.; Philips, J.C.; Legrand, A and Chu, B. *Macromolecules* **21**, 1180 (1988).

7. Song, H.H.; Wu, D.Q.; Chu, B.; Satkowski, M.; Ree, M.; Stein, R.S. and Philips, J.C. *Macromolecules* **23**, 2380 (1990).

8. Tashiro, K; Satkowski, M.M.; Stein, R.S.; Li, Y; Chu, B. and Hsu, S.L. *Macromolecules* **25**, 1809 (1992).

9. Glatter, O. and Kratky, O. *Small Angle X-Ray Scattering*; Academic Press; New York, 1982.

10. Imai, M.; Mori, K.; Mizukami, T; Kaji, K. and Kanaya, T. *Polymer* **33(21)** 4457 (1992).

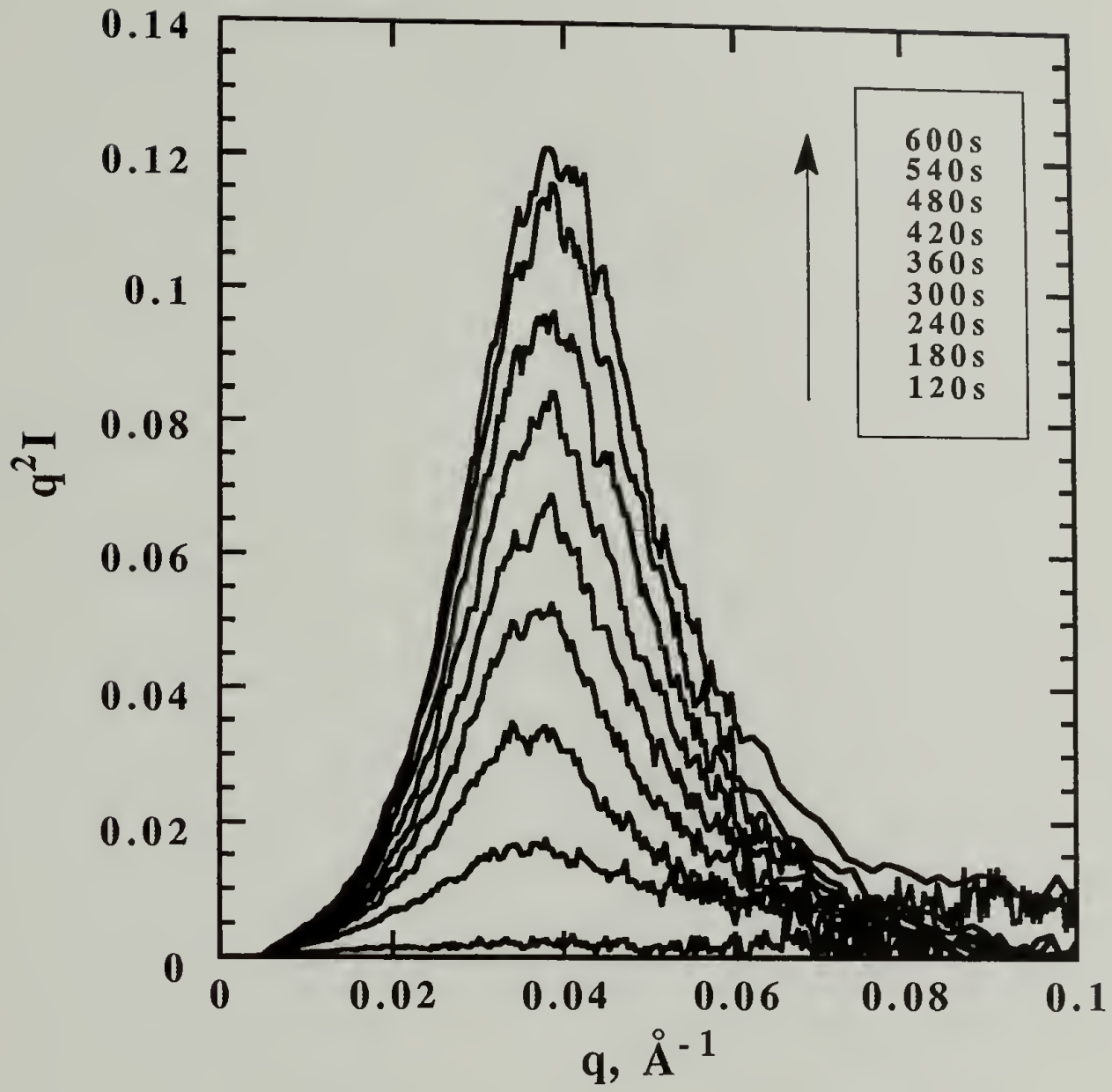

Figure 4.1 Synchrotron SAXS profiles for PCL crystallized at 41 °C Crystallization time measured in second is indicated in the legend. Each SAXS profile was accumulated for 20 sec.

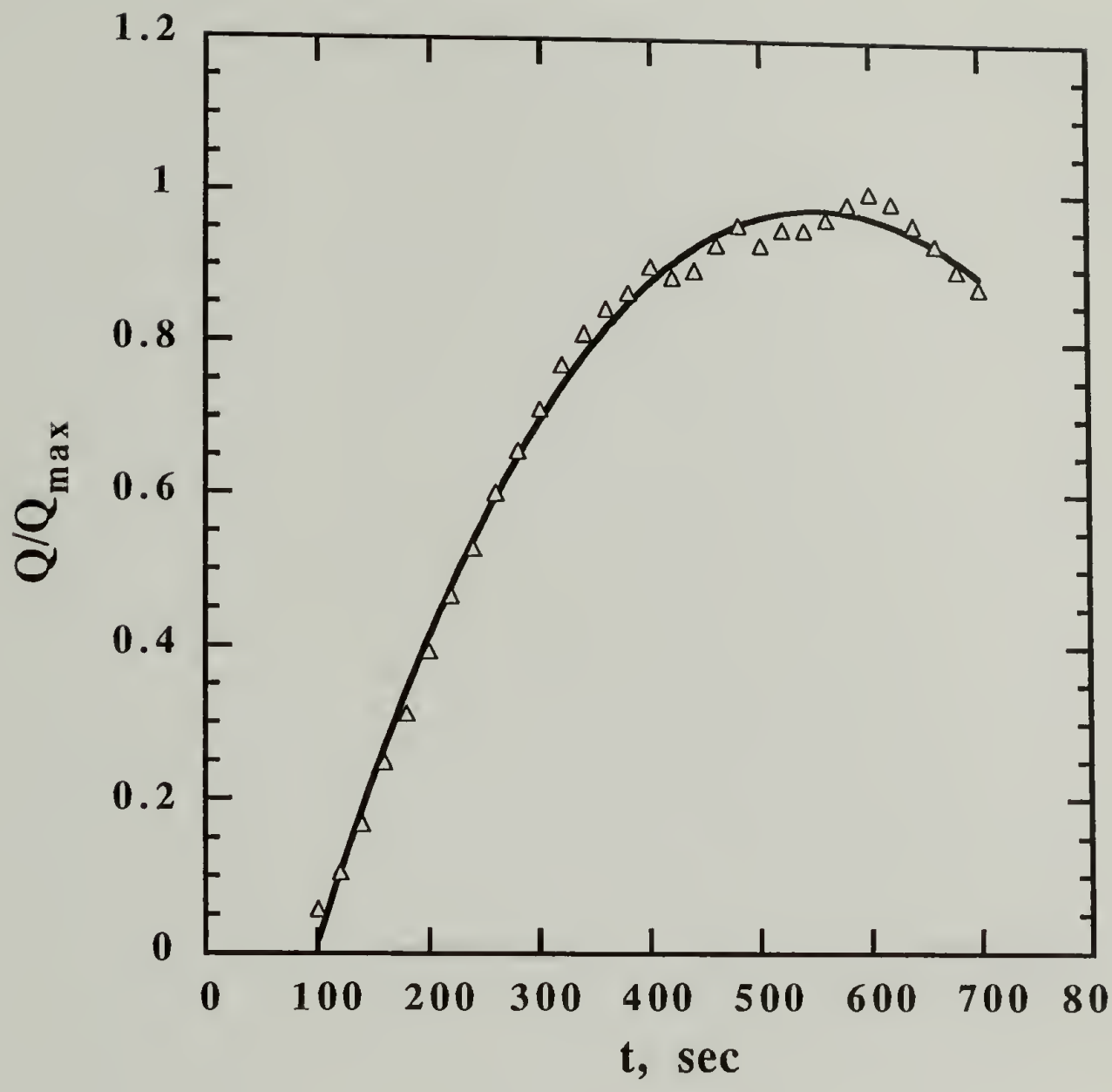

Figure 4.2 Normalized invariant for pure PCL crystallized at 41 °C.

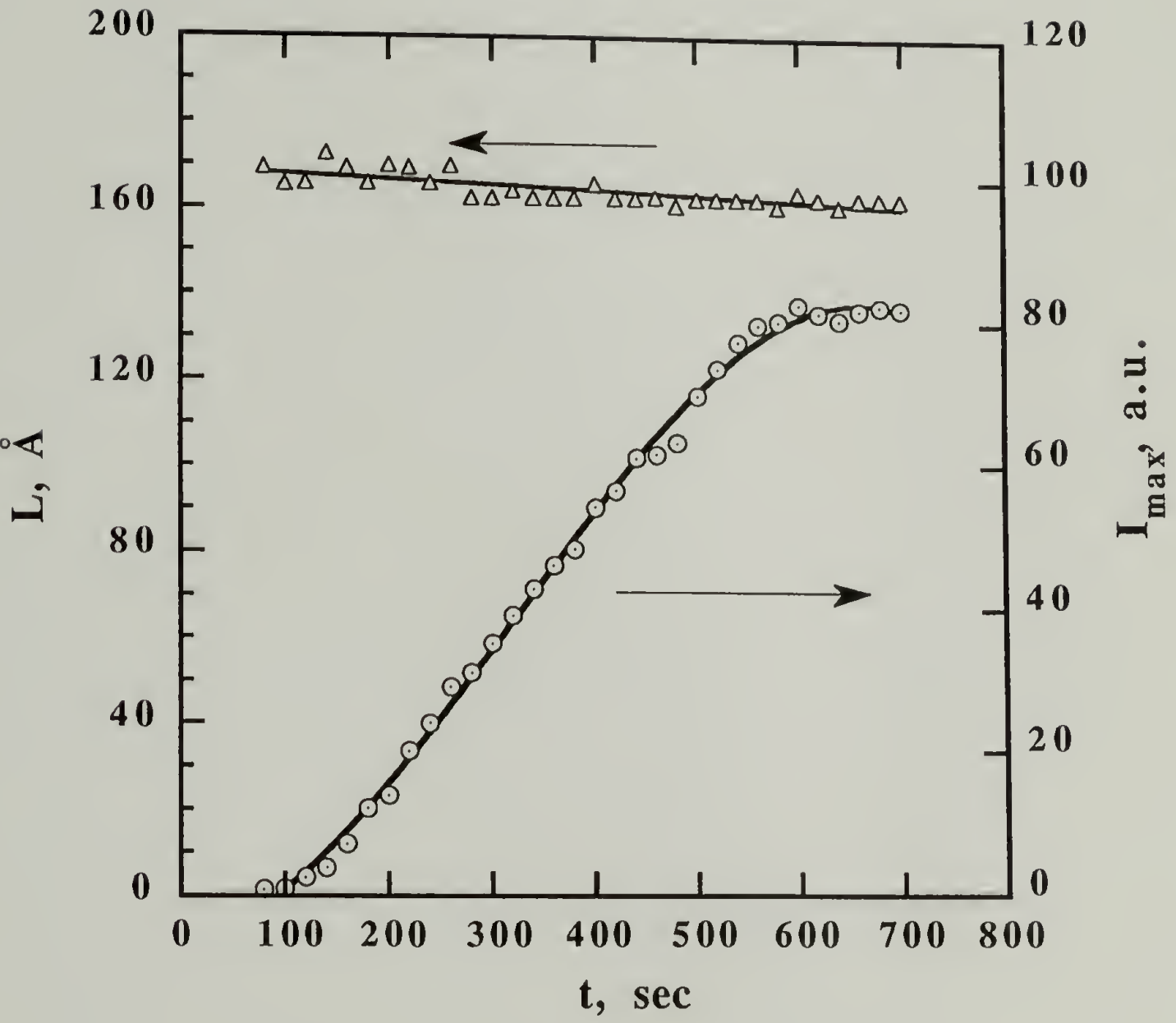

Figure 4.3 Time dependence of the long period, L, and the peak intensity, I_{max}, for pure PCL crystallized at 41 °C. The triangle represents the long period and the circle denotes the I_{max}.

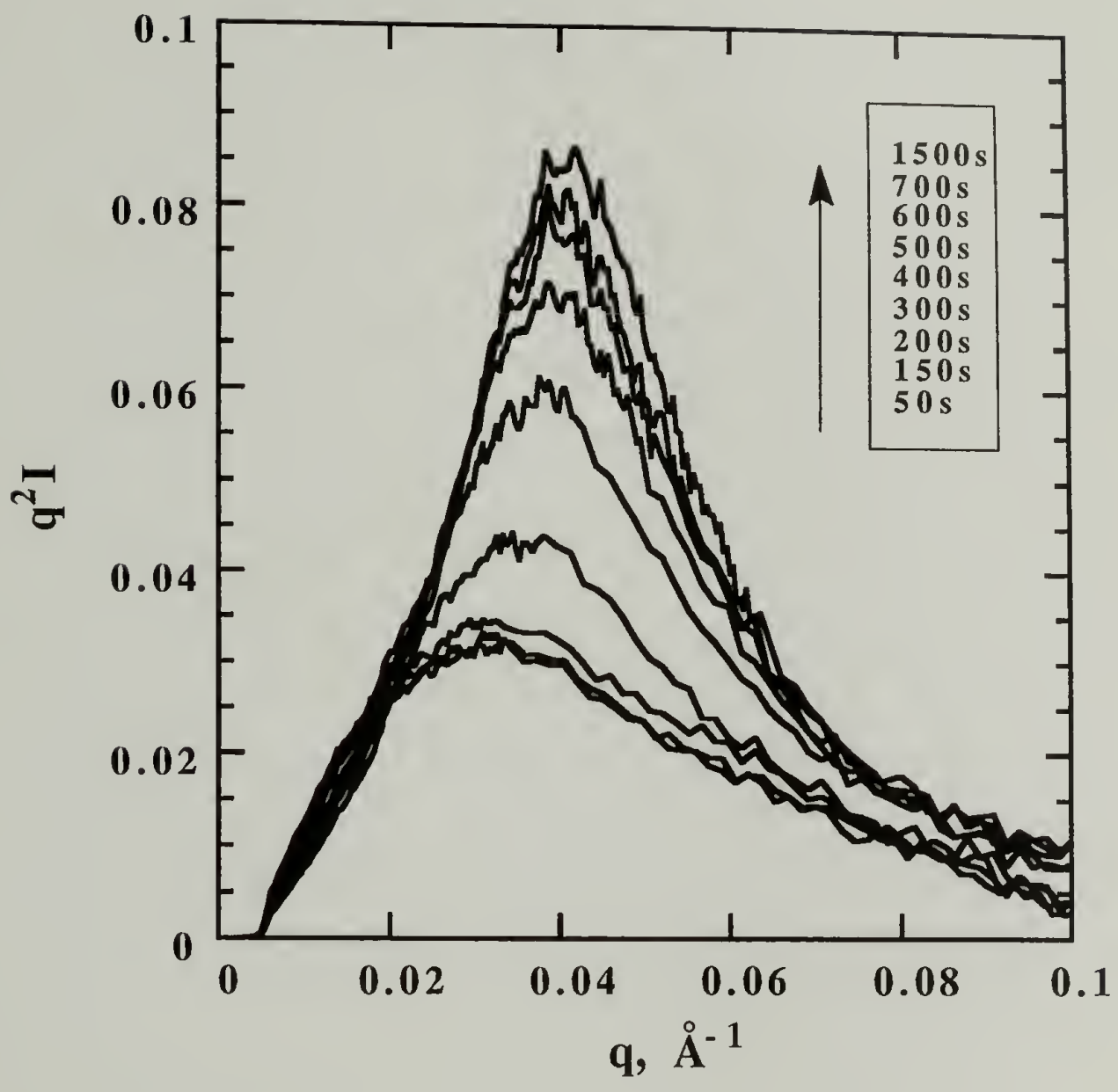

Figure 4.4 Synchrotron SAXS profiles for a 80%PCL/20%PC quenched blend crystallized at 41 °C. Crystallization time measured in second is indicated in the legend. Each SAXS profile was accumulated for 50 sec.

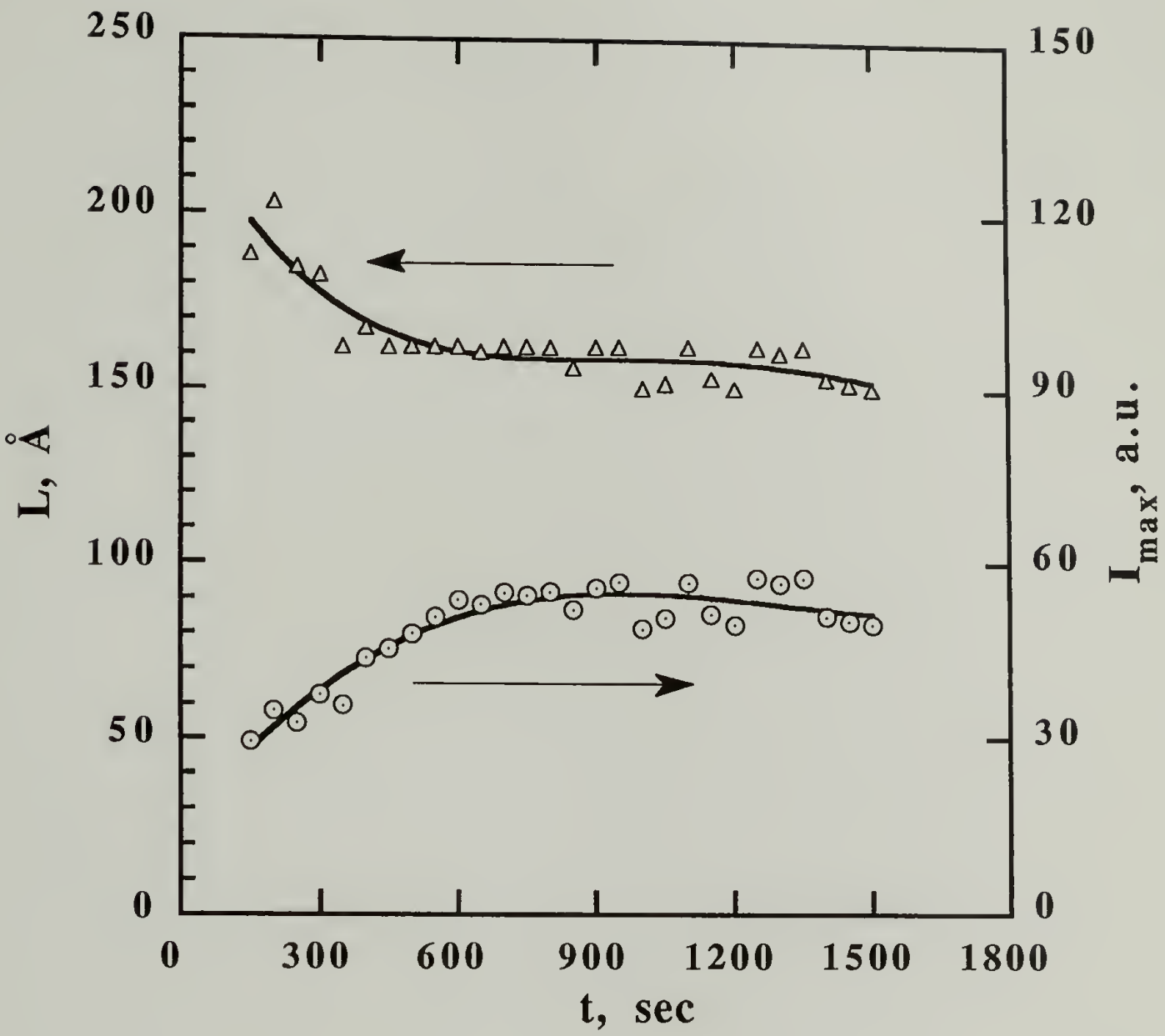

Figure 4.5 Time evolution of the long period, L, and the peak intensity, I_{max}, for a 80%PCL/20%PC quenched blend crystallized at 41 °C. The triangle represents the long period and the circle denotes the I_{max}.

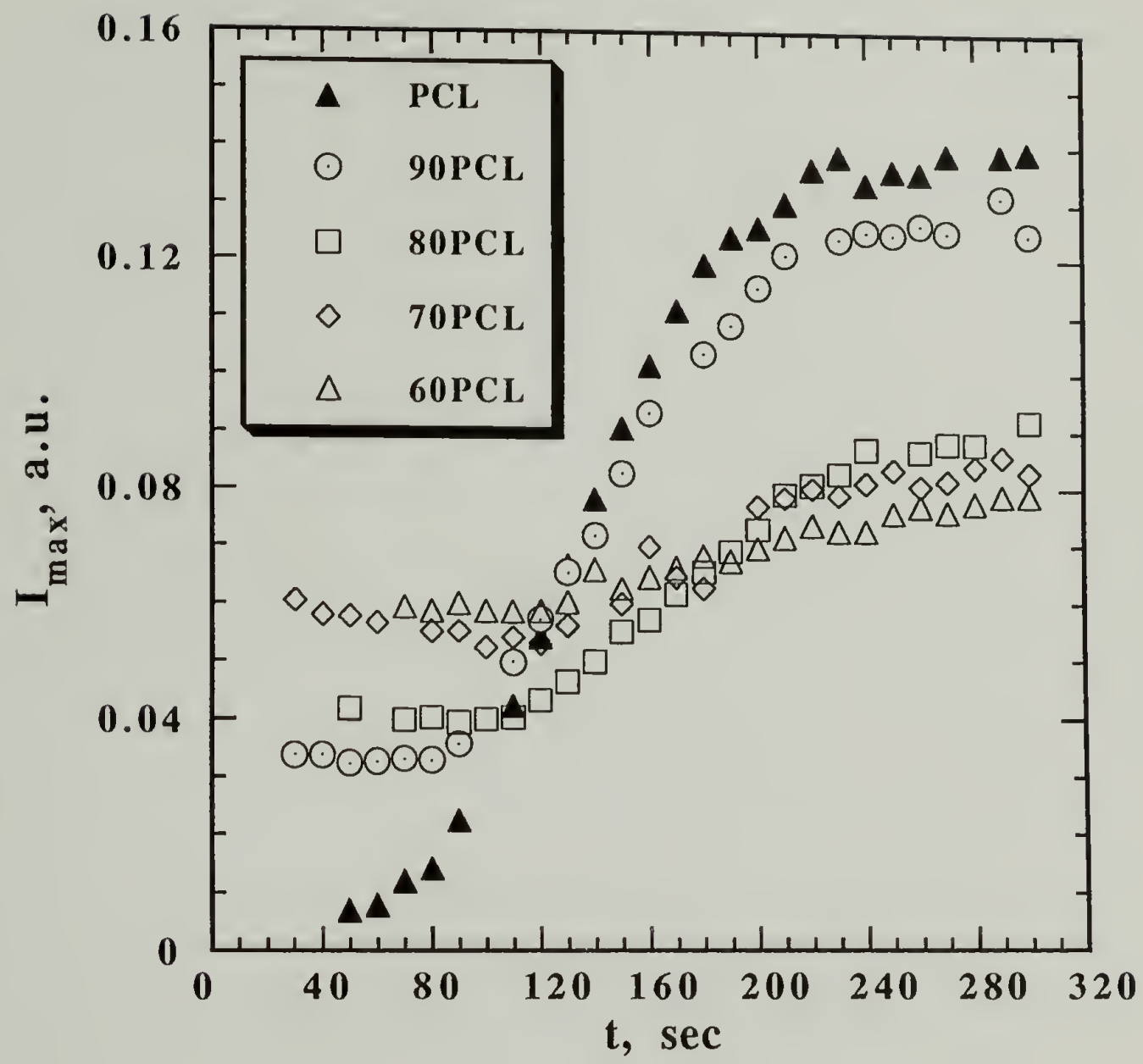

Figure 4.6 Crystallization isotherms for the quenched blends crystallized at 37 °C.

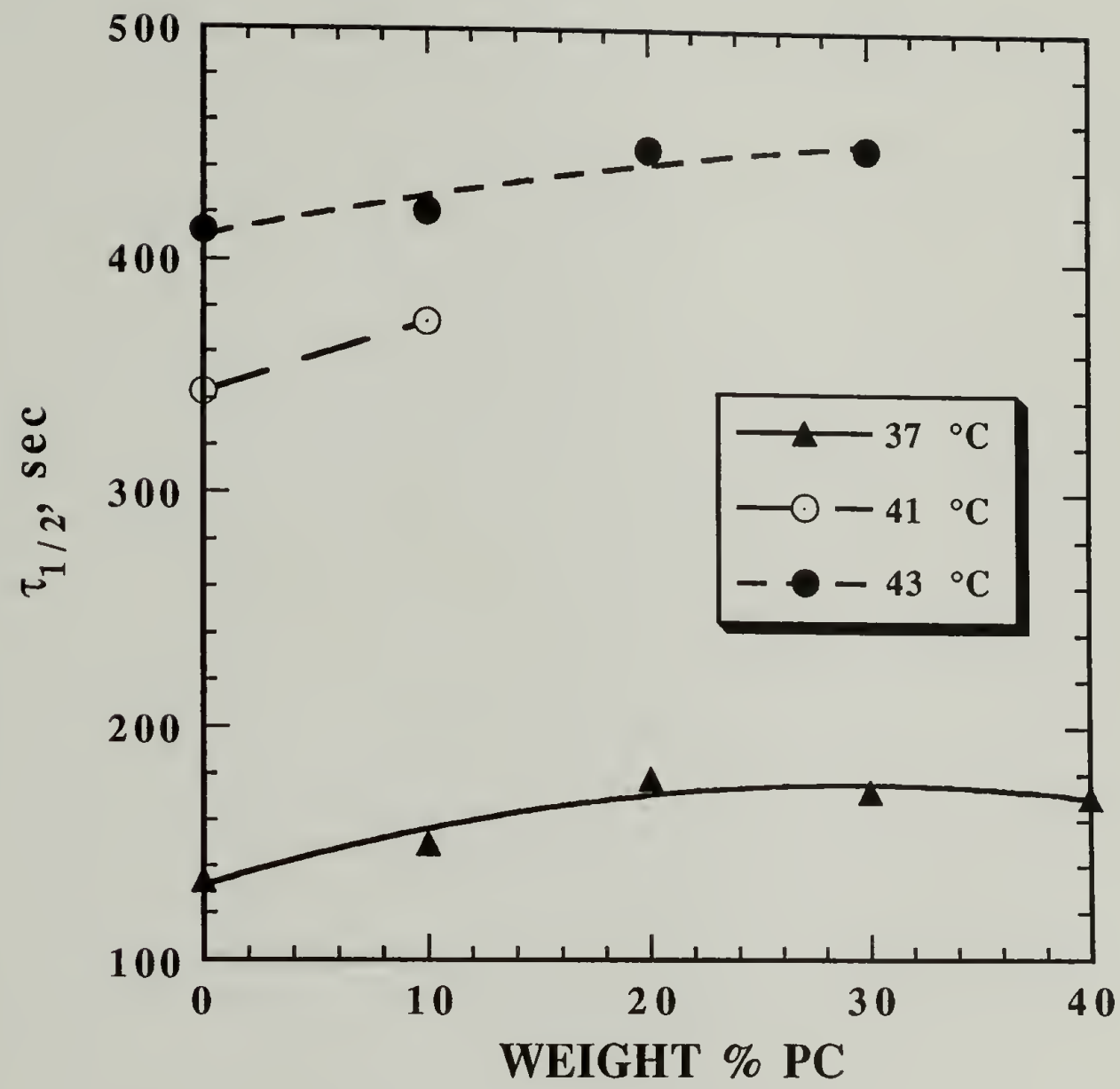

Figure 4.7 Half crystallization times, $\tau_{1/2}$, for the quenched blends.

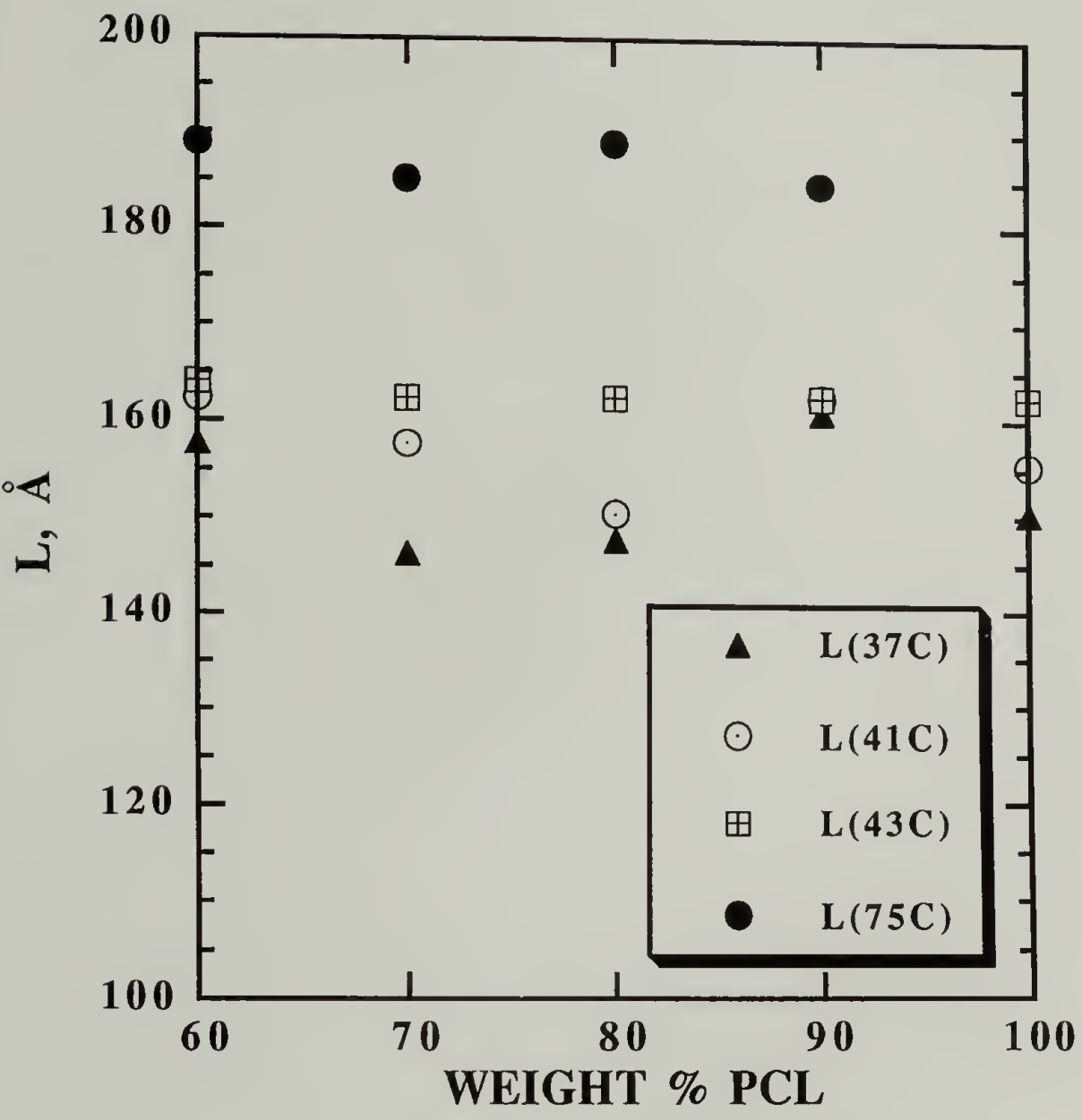

Figure 4.8 Long period as a function of crystallization temperature and composition for the quenched blends.

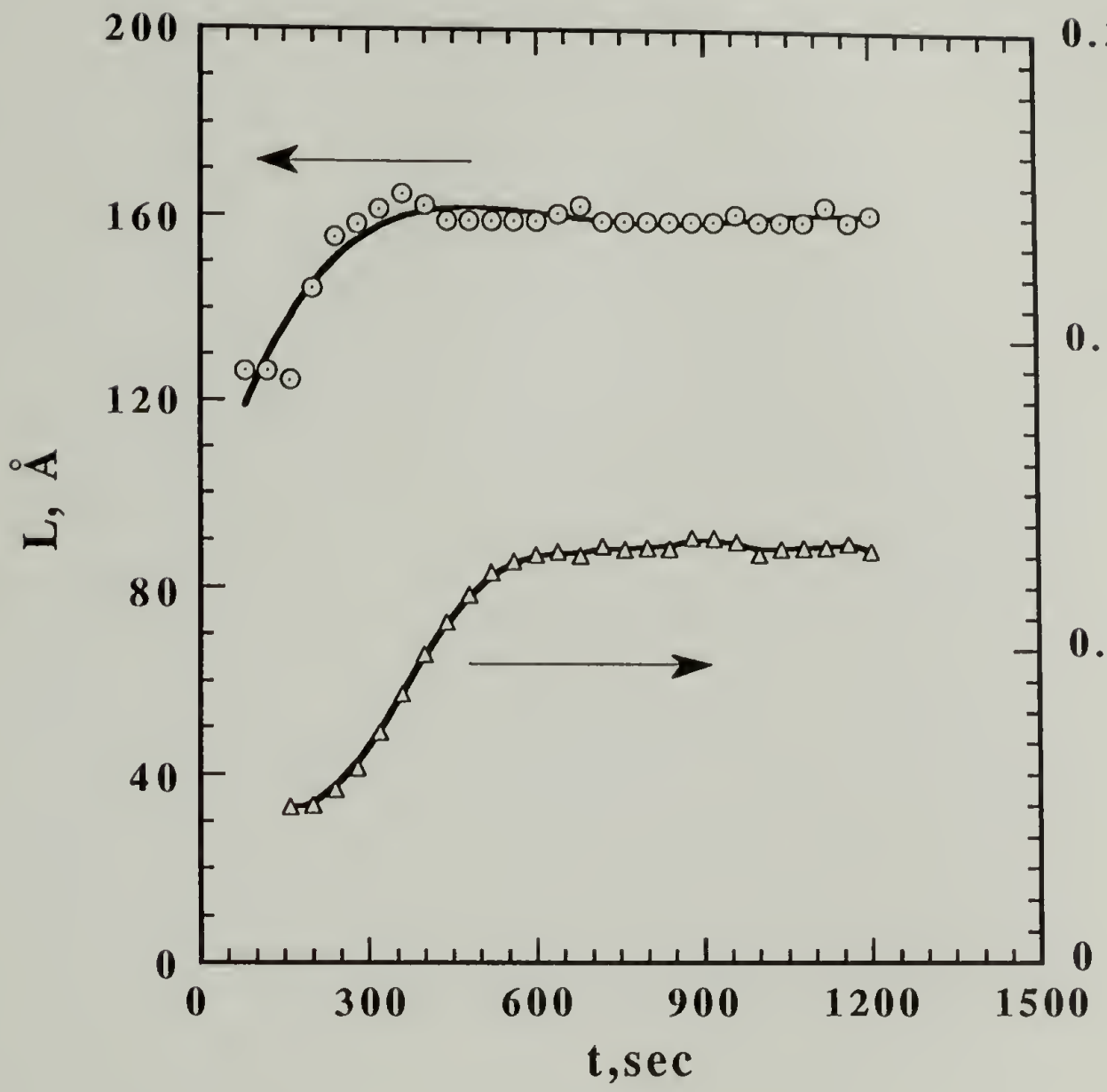

Figure 4.9 Time evolution of the long period, L, and the peak intensity, I_{max}, for a 80%PCL/20%PC as-precipitated blend crystallized at 43 °C.

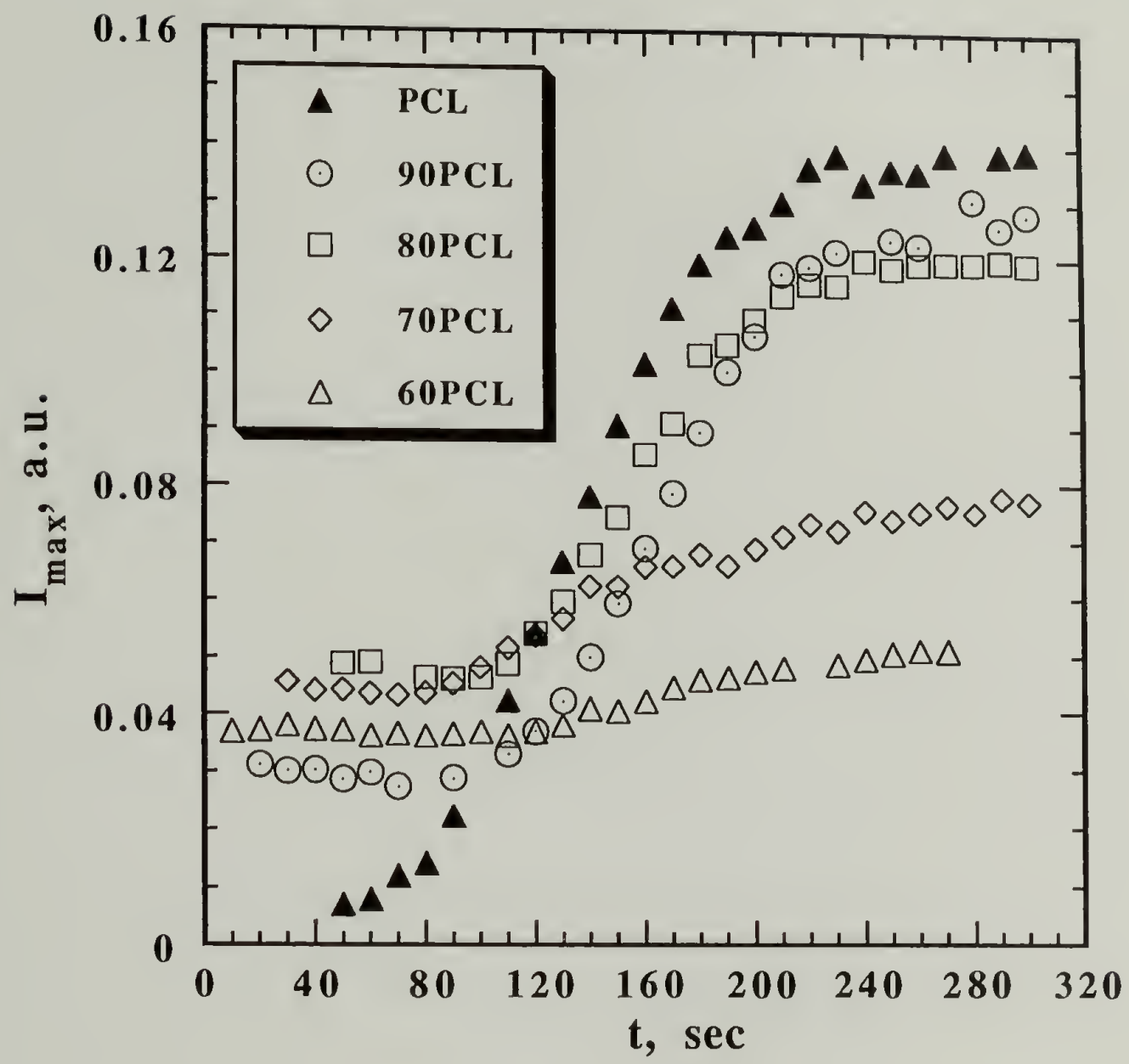

Figure 4.10 Crystallization isotherms for the as-precipitated blends crystallized at 37 °C.

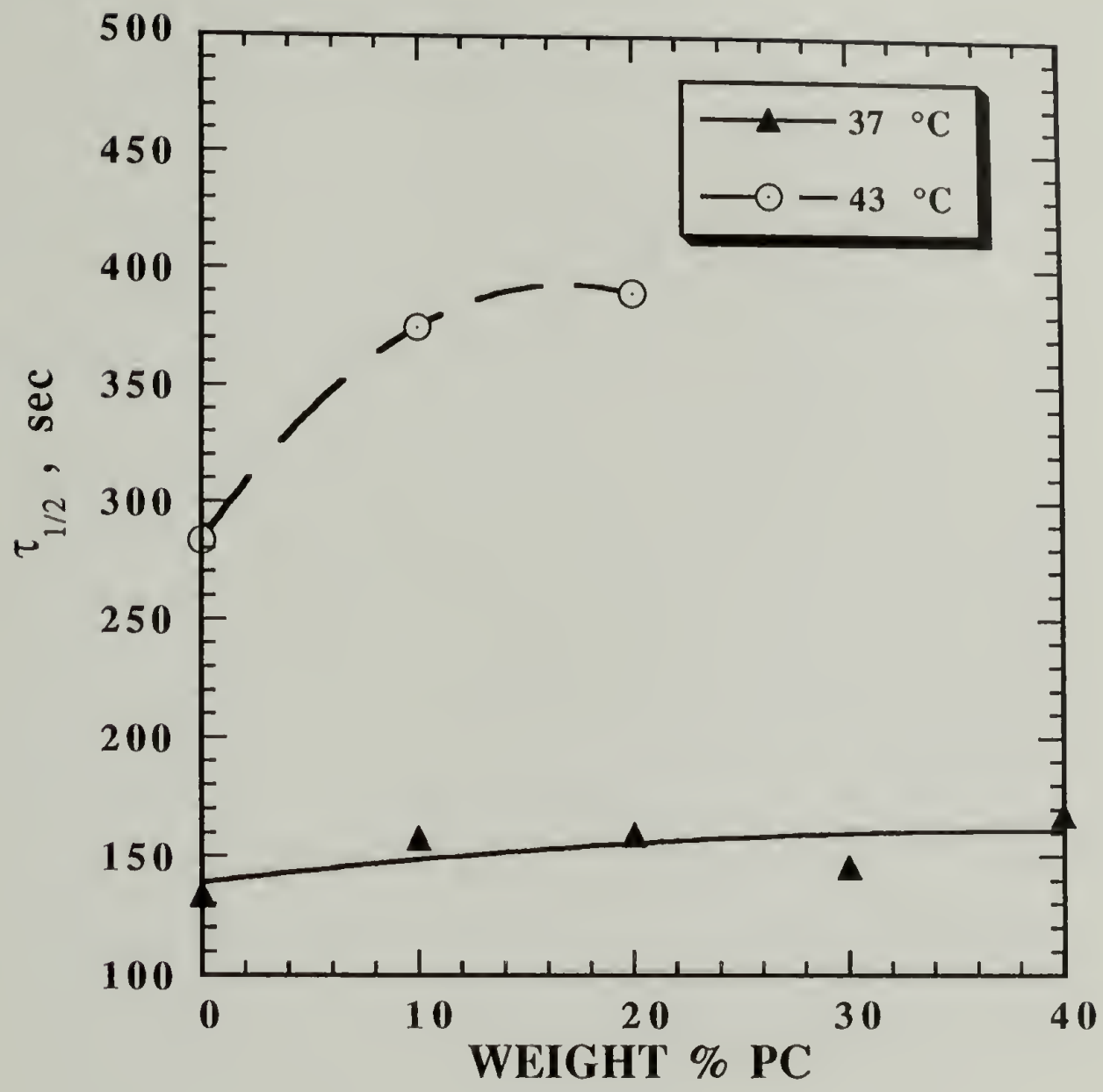

Figure 4.11 Half crystallization times, $\tau_{1/2}$, for the as-precipitated blends.

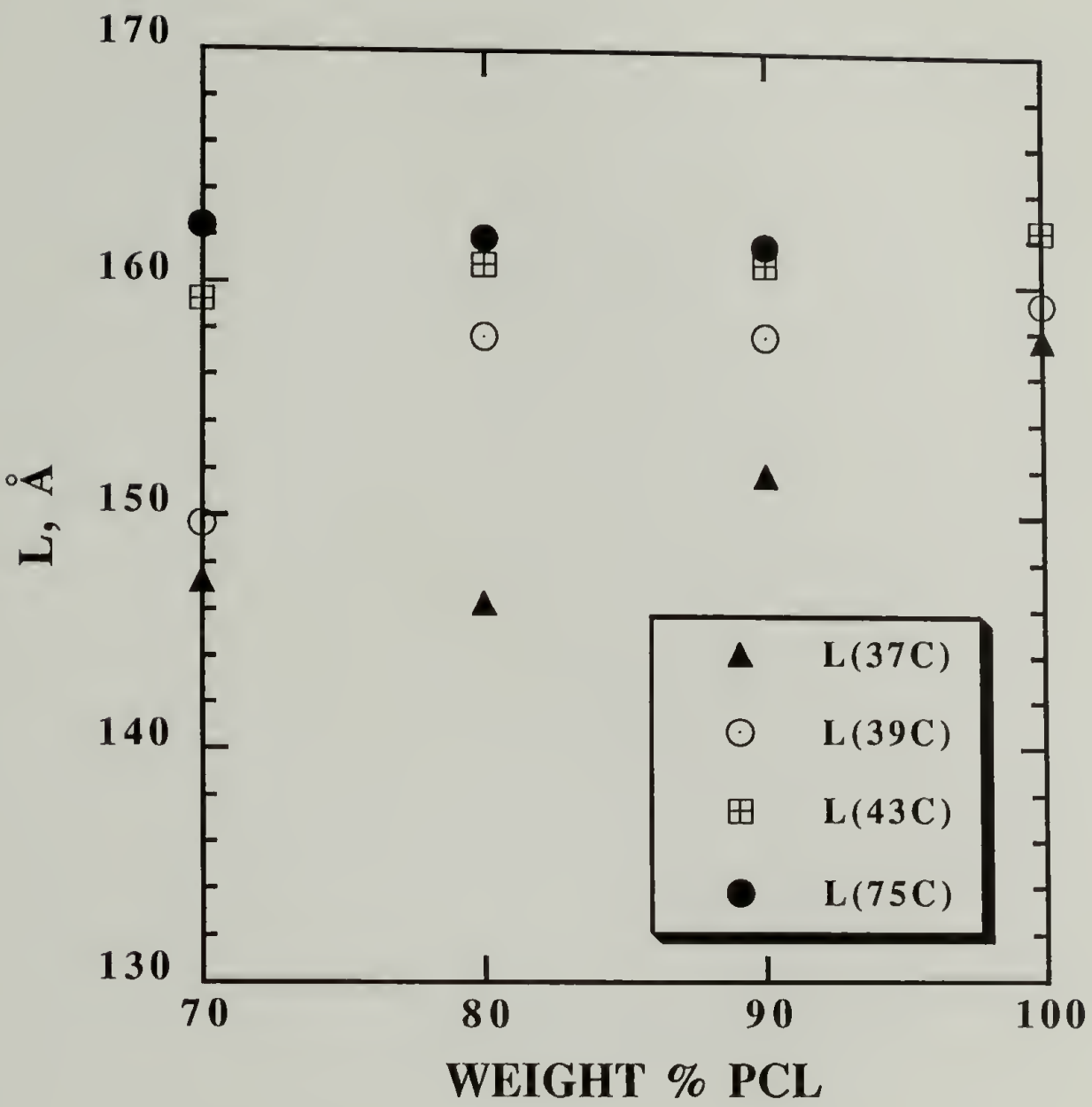

Figure 4.12 Long period as a function of crystallization temperature and composition for the as-precipitated blends.

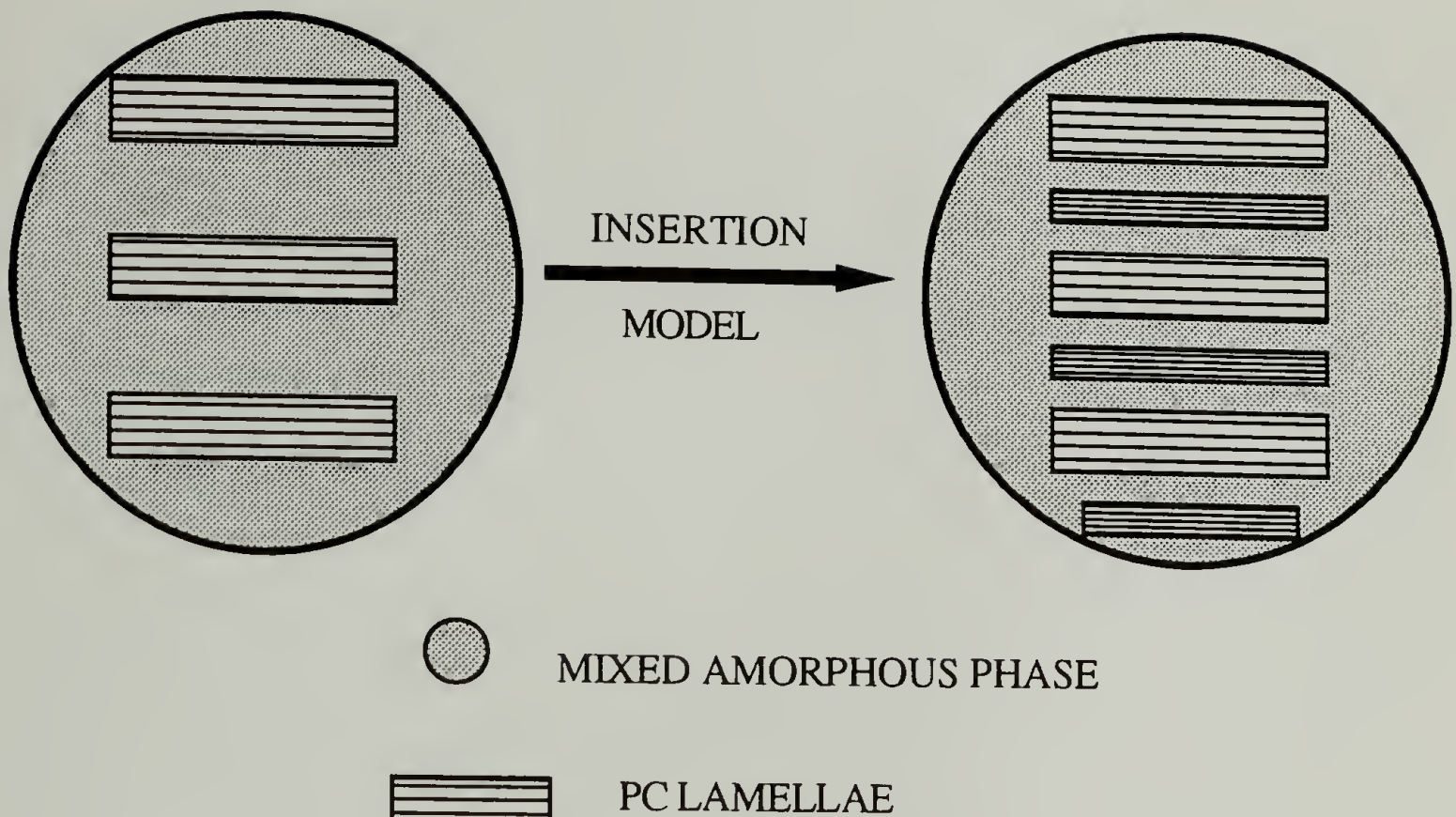

Figure 4.13 Schematic representation of the insertion model showing PCL crystallizing in the intralamellar phase of PC.

CHAPTER 5

SMALL-ANGLE NEUTRON AND X-RAY SCATTERING STUDY OF CRYSTALLINE BLEND MORPHOLOGIES

5.1 Introduction

The focus of this morphological investigation is to examine the structure of the amorphous phase in the semicrystalline/amorphous state and to elucidate the crystalline blend morphologies in both the semicrystalline/amorphous and semicrystalline/semicrystalline states. A detailed presentation of the SAXS and SALS results for both the h-PC/PCL and d-PC/PCL blends including the correlation function analysis and invariant calculation will be discussed in the next chapter. Attention will be directed at a critical analysis of the SANS results of d-PC/PCL blends in the present chapter.

Unique to SANS is the specificity with which the labeled component can be examined. SANS arises from the difference in the scattering length density and directly probes the spatial arrangement between deuterium and hydrogen or d-PC and PCL since PC is completely deuterated. In contrast, SAXS arises from the difference in electron density as found in the crystalline-amorphous region. Combination of both SANS and SAXS can offer invaluable complementary structural information which are specific to the labeled component.

5.2 Experimental

As described in Chapter 2, solution cast blends were prepared in an identical manner as the those used in the amorphous/amorphous blend study. However, the molecular weight of the d-PC is different from that of the one used in the χ measurement as indicated by Table 2.1. Scattering samples were compression molded typically at

T_g+50 °C under vacuum. Samples were then rapidly transferred to a metal surface and quenched to room temperature. Sample disc dimension was about 1 mm in thickness and 15 mm in diameter.

Both SANS and SAXS measurements were performed at Oak Ridge National Laboratory (ORNL) in Tennessee. SANS experiments were conducted on the W.C. Koehler 30m spectrometer. The neutron wavelength was 4.75 Å ($\Delta\lambda/\lambda$ = 5%) and the source (3.5 cm dia.) and sample (1.0 cm dia.) slits were separated by a distance of 7.5 m. The sample-detector distance was 10 m and the data were corrected for instrumental backgrounds and detector efficiency on a cell-by-cell basis, prior to radial averaging to give a q-range of 0.007 to 0.07 $Å^{-1}$. The net intensities were converted to an absolute (±5%) differential cross section per unit sample volume (in units of cm^{-1}) by comparison with pre-calibrated secondary standards.[1] Incoherent scattering backgrounds were estimated from the scattering of the hydrogeneous polymers and were subtracted from the sample scattering.

The transmission of the sample was measured in a separate experiment[2] by collimating the beam with slits (irises) ~ 1 cm in diameter, separated by ~ 7.5 m. A strongly scattering sample, porous carbon, was placed at the sample position to spread the beam over the whole detector, positioned at a sample-detector distance ~ 10 m. The total count summed over the whole detector (> 10^5) was recorded in a time period ~ 1 minute and the sample being measured was placed over the source slit, thus attenuating the beam. The count was repeated over the same time interval and the transmission was given by the ratio of the two counts after minor corrections (< 0.1%) for the beam-blocked background due to electronic noise, cosmic rays, etc.

SAXS measurements were performed on the ORNL 10m spectrometer[3] operating at an accelerating voltage of 40 KeV and a current of 100 mA. The instrument was operated with a sample-detector distance of 5.17 m using $Cu_{k\alpha}$ radiation (λ = 1.54 Å) and a 20X20 cm^2 area detector with cell (element) size ~ 3 mm. Corrections were made for instrumental backgrounds and detector efficiency (via an Fe^{55} standard which emits γ-rays isotropically) on a cell-by-cell basis, prior to radial averaging to yield a q range of 0.005 to 0.1 $Å^{-1}$. As in the SANS experiments, the net scattering intensities were converted to an absolute differential cross section by means of pre-calibrated secondary standards.[4]

5.3 Results and Discussion

5.3.1 Differential Scanning Calorimetry

The phase transitions for the d-PC/PCL blends are summarized in Figure 5.1. Due to solution-induced crystallization and annealing effects, the d-PC was semicrystalline in all the blends. In the case of the PCL-rich blends, both components were semi-crystalline. Both the PCL and d-PC crystallinities (for the solution cast samples), normalized with respect to the composition of each component, as a function of composition are plotted in Figure 5.2. The PCL crystallinity decreased with increasing d-PC concentration, whereas the d-PC crystallinity exhibited a much more complex composition dependence. Additionally, it was found that the PCL crystallinity was higher for the solution cast samples than that obtained for the precipitated (blends recovered from precipitation in methanol) samples where solution-induced crystallization was greatly suppressed.

5.3.2 Contrast Variations

Before embarking on the discussion of the scattering profiles of the blends, the SANS and SAXS profiles of the two homopolymers should be examined. The SAXS

plots for PCL and PC are shown in Figures 5.3 and 5.4, respectively. The SAXS and SANS profiles for PC recorded at RT and elevated temperatures were almost identical. The SAXS clearly showed strong lamellar scattering, whereas the SANS plot was essentially flat and appeared to be dominated by incoherent scattering. In contrast, a peak should emerge in the SANS for a 100% deuterated semicrystalline PC, due to the positive and negative scattering lengths of D^2 and H^1, as such a sample was not available for this study. Similarly, PCL showed the same scattering behavior as the PC where the SANS appeared virtually flat and was predominantly comprised of the incoherent component.

Figure 5.5 shows a typical SANS plot for a 50d-PC/50PCL blend recorded at both RT and 85 °C. The scattering profiles at RT and 85 °C were almost superimposable for all the blends thus indicating that the SANS was invariant with respect to the physical state (amorphous or crystalline) of PCL. Furthermore, the intensity for all the SANS plots decreased monotonically with the scattering vector q. These two findings suggested that the SANS was dominated by the contrast between d-PC and PCL. The neutron scattering length density (SLD), electron density and the mass density for h-PC, d-PC and PCL are shown in Table 5.1. Based on the contrast comparison shown in Table 5.2, the absence or the "smearing" of the PCL and PC lamellar peaks can be easily rationalized from the scattering contrast differences. The neutron SLD contrast between d-PC and PCL was at least two orders of magnitude greater than that between the crystalline and amorphous phase for d-PC or PCL. Similarly, this contrast factor was about 1000 times greater than that between the mixed amorphous phase and the crystalline d-PC phase. Therefore, SANS was dominated by the contrast between deuterium and hydrogen or d-PC and PCL. By comparison, the electron density contrast between the crystalline and amorphous region for PCL and PC was about 160 times and 30 times, respectively, greater than the corresponding neutron SLD. This difference could easily explain the strong lamellar signals observed in SAXS and their absence in SANS.

5.3.3 Small-Angle X-ray Scattering

The Lorentz-corrected SAXS profiles obtained at RT and 75 °C are shown in Figures 5.6 and 5.7, respectively. For blends with more than 50% d-PC, the SAXS profiles at RT and 75 °C were almost identical indicating that the scattering predominantly came from the PC lamellae. This is in agreement with the crystallization kinetics results which revealed that PCL crystallization was strongly suppressed in these materials. In general, the peaks occurred at smaller q (larger long period) for the 75 °C curves as compared to those for the RT curves. These findings are summarized in Figure 5.8. For the PCL-rich blends, the peak observed at RT was a superposition of PCL and d-PC lamellar scattering since these materials were semicrystalline/semicrystalline at temperatures below the melting point of PCL. The long periods measured from these samples represent an average size of the d-PC and PCL lamellae. This observation could suggest that the d-PC and PCL lamellae are randomly mixed as a segregated arrangement will give rise to two peaks in the SAXS. The interpretation of the high temperature SAXS data is more straightforward since PCL was in a completely amorphous state. Figure 5.8 shows that the d-PC long periods in PCL-rich blends were almost identical. In the case of d-PC rich blends, the d-PC long period appeared to increase with increasing PCL. This increase in the long period could be attributed to interlamellar incorporation of PCL in the amorphous region of the PC lamellae for the d-PC rich blends. A more quantitative analysis of the SAXS data will be explored further in the next chapter.

5.3.4 Small-Angle Neutron Scattering

As discussed before, the SANS results recorded at RT and 85 °C are almost superimposable. To simplify the analysis, the high temperature data measured from a truly two phase material, consisting of a d-PC crystalline phase and an amorphous phase, will constitute the focus of the subsequent discussion. Traditionally, the Debye-Bueche

model[5] based on a simple exponential correlation function shown below is commonly applied to a random two-phase system.

$$\gamma(r) = \exp\left(-\frac{r}{a_c}\right) \tag{5.1}$$

By Fourier transforming the exponential correlation function, the intensity distribution is obtained and yields a Lorentzian function with a parameter a_c, defined as the correlation length, which is a measure of the size of heterogeneity.

$$I(q) = \frac{I(0)}{(1 + q^2 a_c^2)^2} \tag{5.2}$$

According to the above equation, a plot of $I^{-1/2}(q)$ versus q^2 should be linear and the [slope/intercept]$^{1/2}$ yields a_c. Figure 5.9 shows a typical Debye-Bueche plot and the deviation from linearity at small q is evident. This simple model fails to fit the SANS data over the entire q space examined in this study.

As is commonly done for a more complex system, the deviation from linearity at smaller angles is corrected for by introducing a second term to the correlation function as shown below.

$$\gamma(r) = f\exp\left(-\frac{r}{a_1}\right) + (1-f)\exp\left(-\frac{r^2}{a_2^2}\right) \tag{5.3}$$

This model is often referred to as the two-correlation length model[6] in which a_1 is termed the short range correlation length and a_2 is the long range correlation length. The parameter **f** is defined as the fractional contribution of the exponential correlation function.

The intensity distribution based on the above correlation function yields a sum of a Lorentzian and a Gaussain function as shown below.

$$\mathbf{I(q) = \frac{A_1}{(1+q^2 a_1^2)^2} + A_2 \exp\left(-\frac{q^2 a_2^2}{4}\right)} \tag{5.4}$$

The parameter **f,** whose value ranges from 0 to 1, is defined in terms of the following equation.

$$\mathbf{f = \frac{A_1}{\left[A_1 + \frac{8}{\sqrt{\pi}}\left(\frac{a_1}{a_2}\right)^3 A_2\right]}} \tag{5.5}$$

where A_1 and A_2 are defined as below.

$$\mathbf{A_1 = 8\pi a_1^3 f \phi (1-\phi)(\rho_1-\rho_2)^2} \tag{5.6}$$

$$\mathbf{A_2 = \pi^{3/2} a_2^3 (1-f)\phi (1-\phi)(\rho_1-\rho_2)^2} \tag{5.7}$$

The term $(\rho_1-\rho_2)^2$ is the square of the difference of the neutron SLD between the two phases. Based on table 5.2, the SLD contrast is dominated by the contrast between d-PC and PCL. Hence, $(\rho_1-\rho_2)$ represents the neutron SLD between these two components. The zero angle scattering is simply equal to

$$\mathbf{I(0) = A_1 + A_2} \tag{5.8}$$

Effectively, this model consists of four fitting parameters including a_1, a_2, A_1 and A_2. However, A_1 and A_2 can be calculated from Equations 5.6 and 5.7. As an internal check for the applicability of this model, the calculated zero angle scattering intensity is usually compared to the measured (curve fitted) value. It is clear that the calculated zero angle scattering depends on the parameter **f** which is in turn determined from the fitted values of A_1 and A_2. Since the calculated I(0) scales linearly with **f**, it is reasonable to assume that the parameter **f** has a minor contribution to the calculated I(0) as compared to the higher order terms like the scattering length density contrast and the two correlation lengths.

The two-correlation length model yielded a very good fit to the SANS data. A typical fit of Equation 5.4 to the data can be found in Figure 5.10. The dependence of the parameter **f**, the fractional contribution of the exponential correlation function, and the d-PC crystallinity with composition is shown in Figure 5.11. Both **f** and d-PC crystallinity do not vary monotonically with composition. However, this complex dependence may be rationalized if a "simple-minded" correlation is made between **f** and d-PC crystallinity. The parameter **f** is a measure of the degree of exponentiality or can be regarded as a measure of "amorphousness" in the blends. This would imply that **f** should vary inversely with crystallinity in the blends. Furthermore, it is implicit in this reasoning that the exponential correlation function represents the amorphous component and the Gaussian correlation function describes the d-PC crystalline component. From Figure 5.11, one can observe that indeed the parameter **f** generally increased as d-PC crystallinity decreased. This relationship corroborates the assumption that the degree of exponentiality as expressed in terms of **f** is an indirect measure of the degree of "amorphousness".

The zero angle scatting intensities derived from the best fit and those calculated from Equations 5.6 and 5.7 are shown in Figure 5.12. The values extrapolated from the

best fit and those calculated from the model agree reasonably well. Invariably, the calculated zero angle scattering intensity was always greater than that derived from the best fit. The short range and long range correlation length as a function of composition are plotted in Figure 5.13. Based on the magnitude and the composition dependence of the correlation length, one can identify the long range correlation length to be the PC crystalline domain and the short range correlation length as the correlation distance between d-PC and PCL in the amorphous phase. The long period of d-PC measured from SAXS is also plotted in this Figure. Both the long range correlation length and the long period exhibit identical composition dependence and thereby further supports the applicability of this two-correlation length model and our interpretation.

The long range correlation length was about two times larger than the long period. This discrepancy may be related to crystallization-induced phase separation where there exists a d-PC rich region, near the crystalline d-PC, within which the PCL is excluded. This picture is also consistent with the entropy consideration where crystalline order has to dissipate over a finite distances. It is highly entropically unfavorable to have a sharp interface between the crystalline d-PC and the amorphous phase. Based on this argument, the long range correlation length may be viewed as a sum of a PC crystalline domain and a PC rich phase possibly resulting from crystallization-induced localized phase separation. However, this interpretation could be one of the few possibilities. It is also important to realize that the long range correlation length does not have to be numerically equal to the long period but the two quantities are related by a proportionality constant. This statement stems directly from the fact that the correlation distance is a statistical measure whose magnitude is dependent on both the geometry and distribution of the heterogeneity.

In the theoretical framework of the Debye-Bueche model, the system is assumed to be phase separated where the size of the heterogeneity is measured by the correlation length. As stated before, the two phases in question are the d-PC and PCL. Based on the SAXS results, the long range correlation length is attributed to the d-PC crystalline domain. By a similar argument, the short range correlation length could be related to the local cluster found in the amorphous phase. This short range order could result from localized phase separation. Figure 5.14 shows a schematic representation of the morphological model suggested by the two-correlation length analysis.

It is well know that crystallization is an ordering process and could be classified as a form of phase separation. As the blend undergoes crystallization, preferential enrichment of the crystallizing component over the other component may occur in the vicinity of the incipient crystal nuclei. These heterogeneities may develop into local clusters rich in the crystallizing component. Since thermal analytical techniques such as DSC and DMA have spatial resolution of about few hundred Angstroms, these local clusters, roughly 30Å in size, will not be detectable and the amorphous phase may still appear as homogeneous based on these thermal measurements.

5.4 Conclusions

The semicrystalline morphologies of d-PC/PCL blends at both room temperature and elevated temperatures (above the T_m of PCL) have been examined by both SAXS and SANS. The long periods measured at RT were smaller than those obtained at elevated temperature. However, quantitative interpretation of the room temperature SAXS results was complicated by the fact that the scattering actually originated from a superposition of both PCL and d-PC lamellar scattering. For the high temperature SAXS results, the interpretation was more straightforward since PCL was completely amorphous. In the case of the semicrystalline/amorphous blends, SAXS results suggested that the d-PC

lamellae remained essentially unperturbed in the PCL-rich blends. For the d-PC rich blends, d-PC long period increased with increasing PCL. This complex phenomenon will be explored further in the next chapter.

The SANS measured at room temperature and at 85°C were virtually identical indicating that the scattering was dominated by the contrast between deuterium and hydrogen or d-PC and PCL . Crystalline scattering arising from PCL was negligible due the fact that crystalline/amorphous contrast was at least two orders of magnitude less than the d-PC and PCL contrast. A two-correlation length model yielded an excellent fit to the SANS data over the entire composition range. This model not only reproduced the shape but also the absolute magnitude of the scattering curves. Based on the magnitude and composition dependence of the two correlation lengths, the long range correlation length was postulated to be the crystalline d-PC domain and the short range correlation length to be the local cluster in the amorphous phase. The long range correlation length was about two times larger than the long period measured from SAXS. This difference may be attributed to crystallization-induced localized phase separation resulting in a preferential enrichment of PC near the PC crystalline domain. In other words, the long range correlation length may be regarded as a sum of a d-PC crystalline domain and a d-PC rich phase whereas the long period represents only the d-PC crystalline domain. By a similar reasoning, the short range correlation length could be attributed to the local cluster formation possibly resulting also from crystallization-induced phase separation. This suggests that the amorphous phase may not be truly homogeneous and exhibits clustering at about 30Å. Since this size scale cannot be resolved by thermal analytical measurements such as DSC and DMA, the blends will still show a single glass transition temperature and the amorphous phase appears homogeneous. Therefore, combination of the SAXS and SANS results suggested a morphological model for the PCL/d-PC blends in the

semicrystalline/amorphous state as composed of a d-PC crystalline phase dispersed in a matrix amorphous phase consisting of local clusters of about 30Å in size.

Table 5.1

Neutron Scattering Length Density (SLD), Electron Density (ρ_e), and Mass Density (d) for PCL, h-PC and d-PC.

Polymer	SLDX10^{-9}, cm^{-2}	ρ_eX10^{-9}, cm^{-2}	d_A, g/cm^3	d_X, g/cm^3
PCL	7.37d	91.72d	1.090	1.185
h-PC	16.75d	88.97d	1.196	1.315
d-PC	51.21d	88.97d	1.196	1.315

d = Mass Density
A = Amorphous
X = Crystalline

Table 5.2

Neutron Scattering Length Density Difference (ΔSLD) and

Electron Density Difference ($\Delta\rho_e$) for Various Components

Component	$(\Delta SLD)^2$ X 10^{-20}, cm^{-4}	$(\Delta\rho_e)^2$ X10^{-20}, cm^{-4}
d-PC_A - PCL_A	28.319	
d-PC_A - PCL_X	27.579	
d-PC_X - PCL_A	35.177	
d-PC_X - (PCL_A+d-PC_A)	0.0375	
d-PC_X - d-PC_A	0.371	
h-PC_X - h-PC_A	0.0397	1.118
PCL_X - PCL_A	0.00490	0.760

A = Amorphous

X = Crystalline

References

1. Wignall, G.D. and Bates, F.S. *J. Appl. Cryst.***20**, 28 (1987).

2. Dubner, W.S.; Schultz, J.M. and Wignall, G.D., *J. Appl. Cryst.* **23**, 469 (1990).

3. Wignall, G.D.; Lin, J.S. and Spooner, S. *J. Appl. Cryst.* **23**, 241 (1990).

4. Russell, T.P.; Lin, J.S. Spooner, S. and Wignall, G.D., J, *Appl. Cryst.* **21**, 629 (1988).

5. Debye, P.; Anderson, H.R. and Brumberger, H. *J. Appl. Phys.* **28**, 6 (1957).

6. Moritani, M.; Inoue, T. and Kawai, H. *Macromolecules* **3(4)**, 433 (1970).

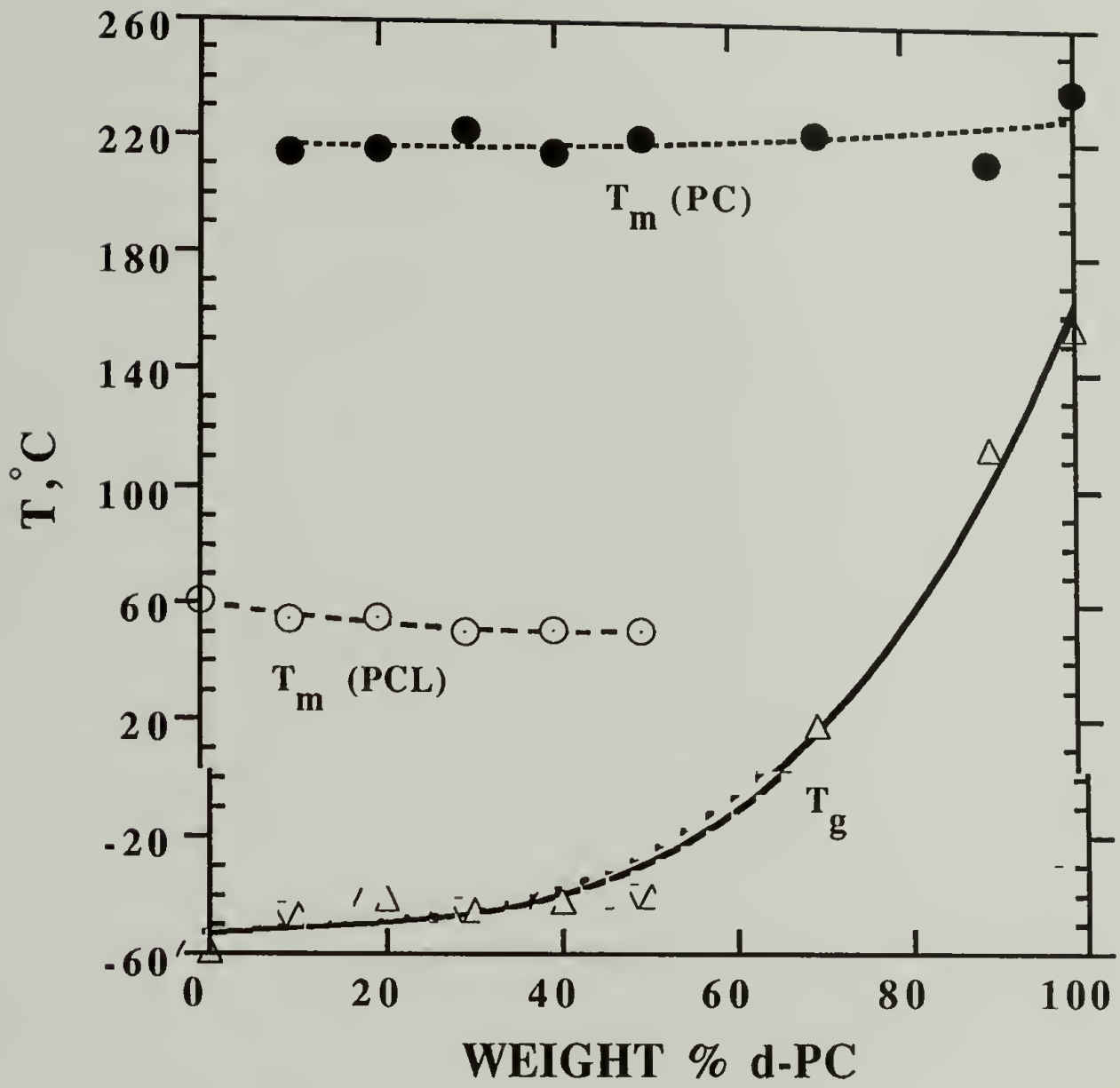

Figure 5.1 Thermal transitions for d-PC/PCL blends.

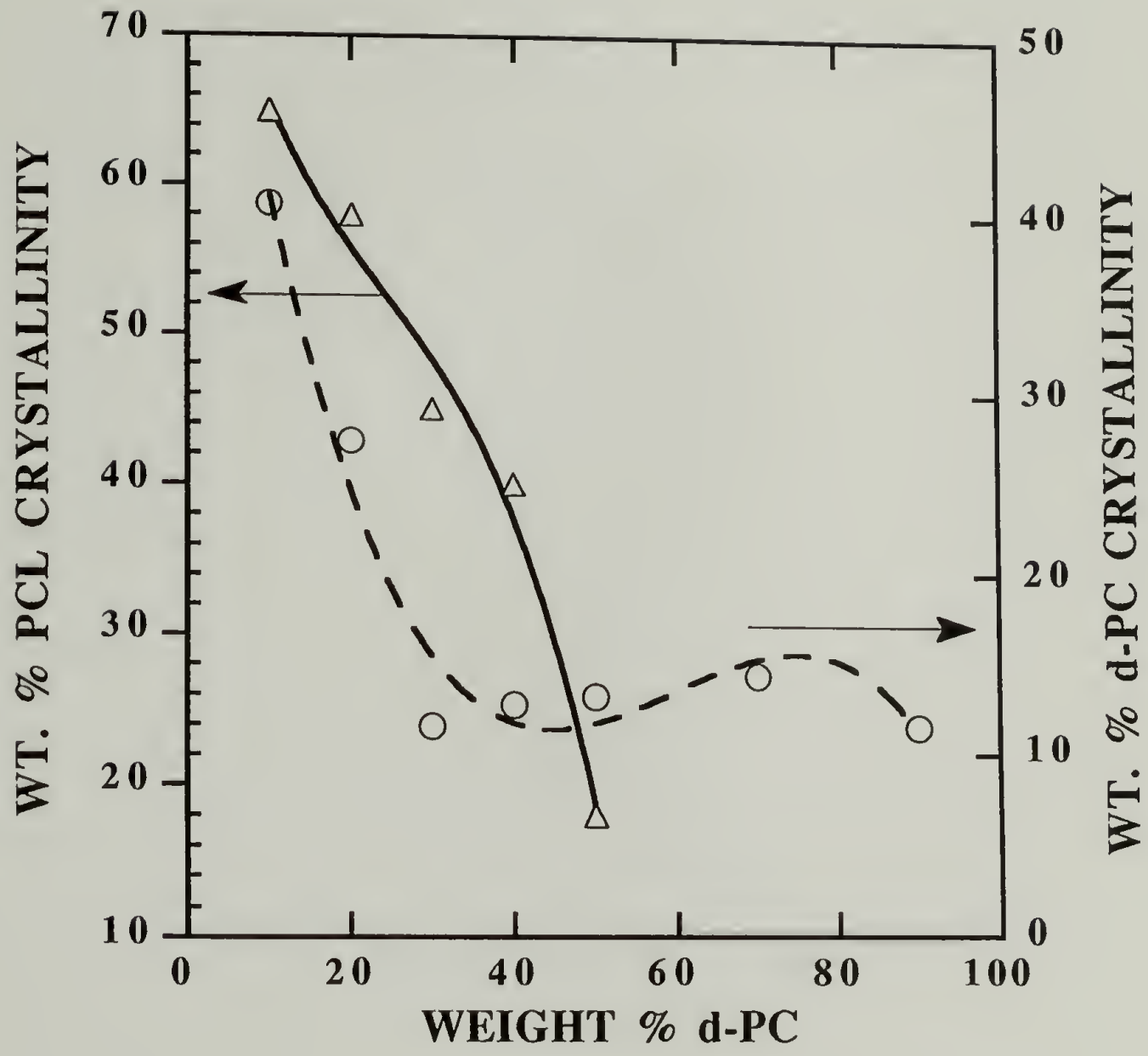

Figure 5.2 Normalized PCL and d-PC crystallinities (for solution cast samples) for d-PC/PCL blends.

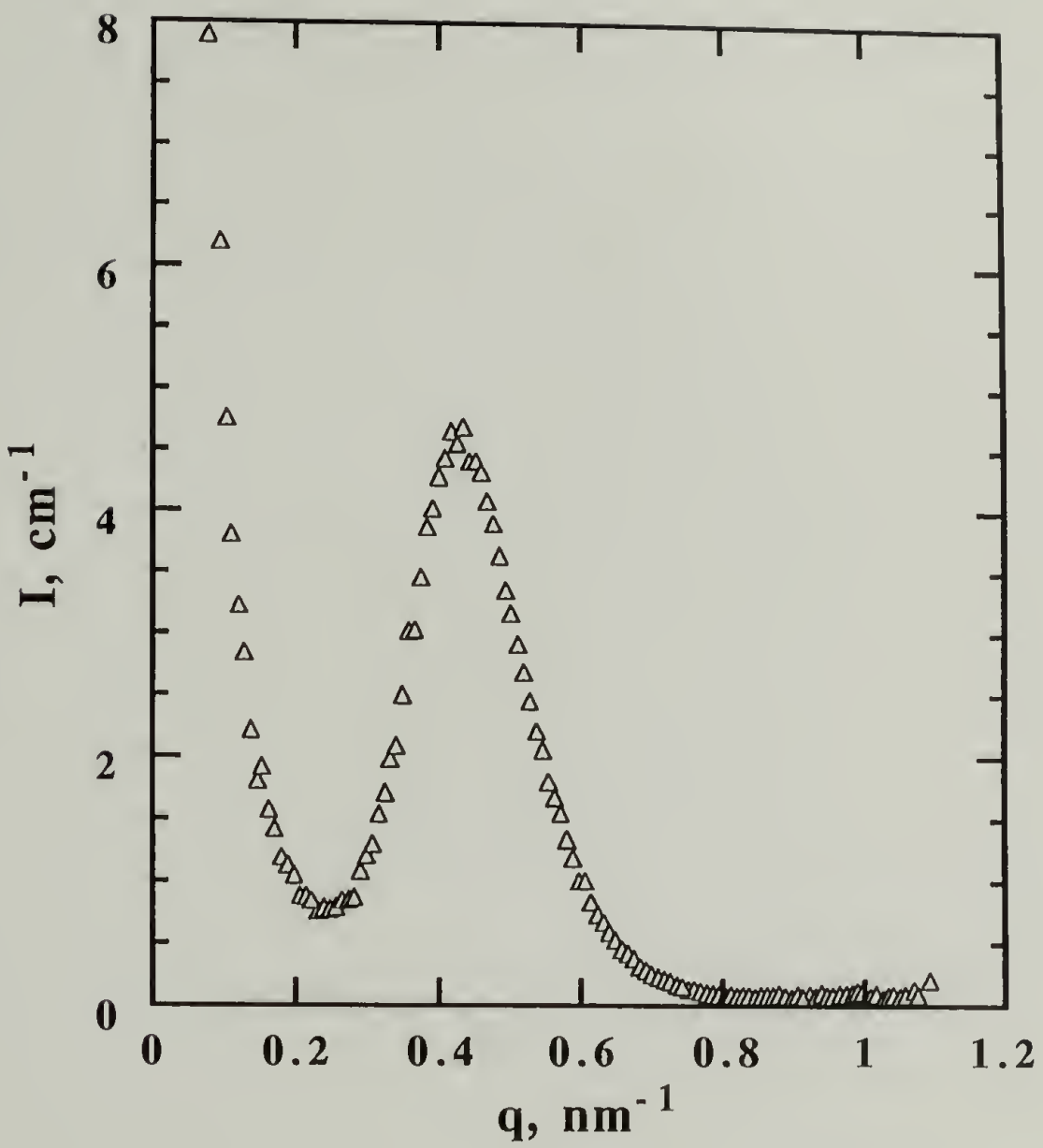

Figure 5.3 SAXS for PCL recorded at room temperature.

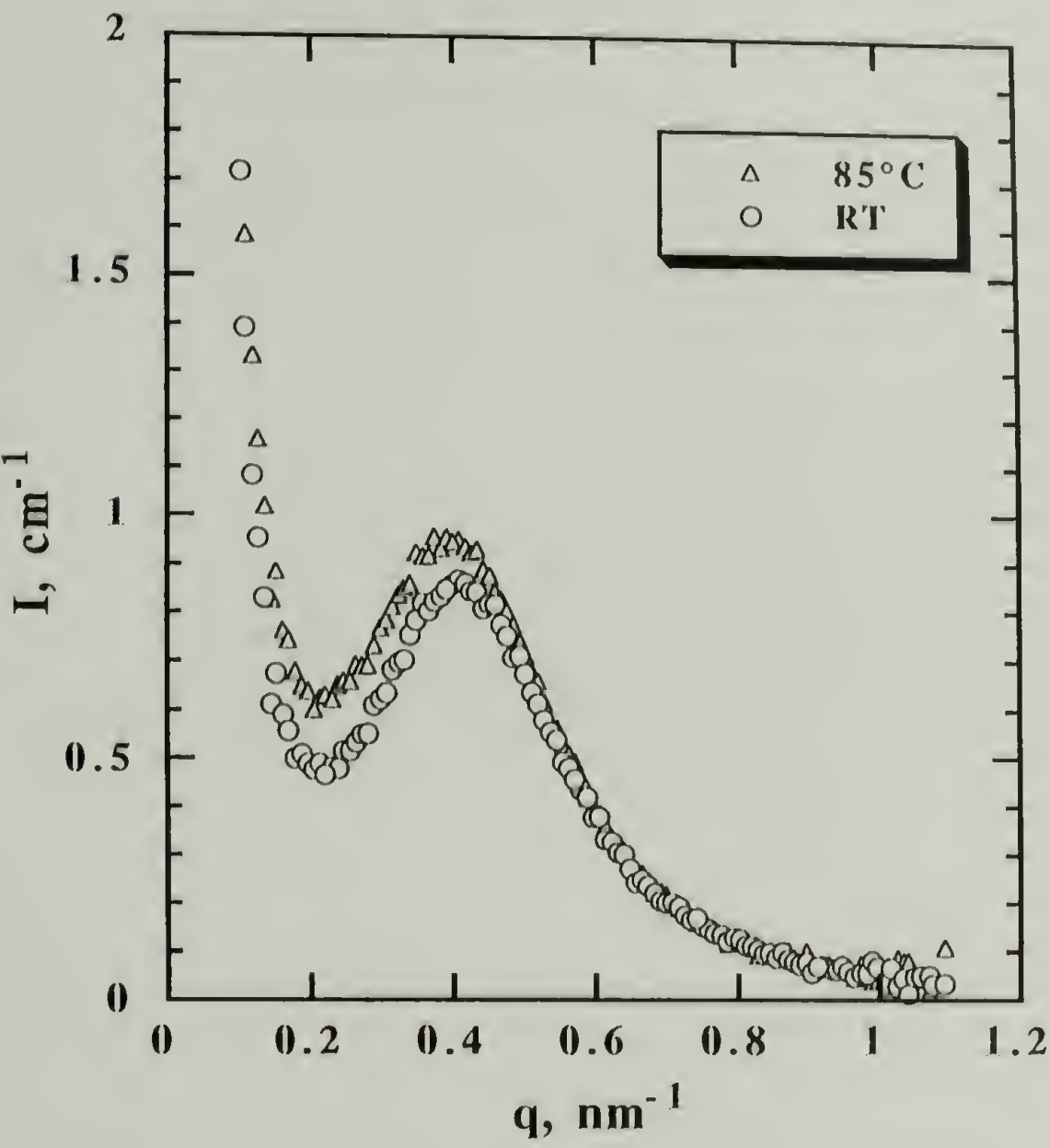

Figure 5.4 SAXS for hydrogeneous (solution-cast) PC.

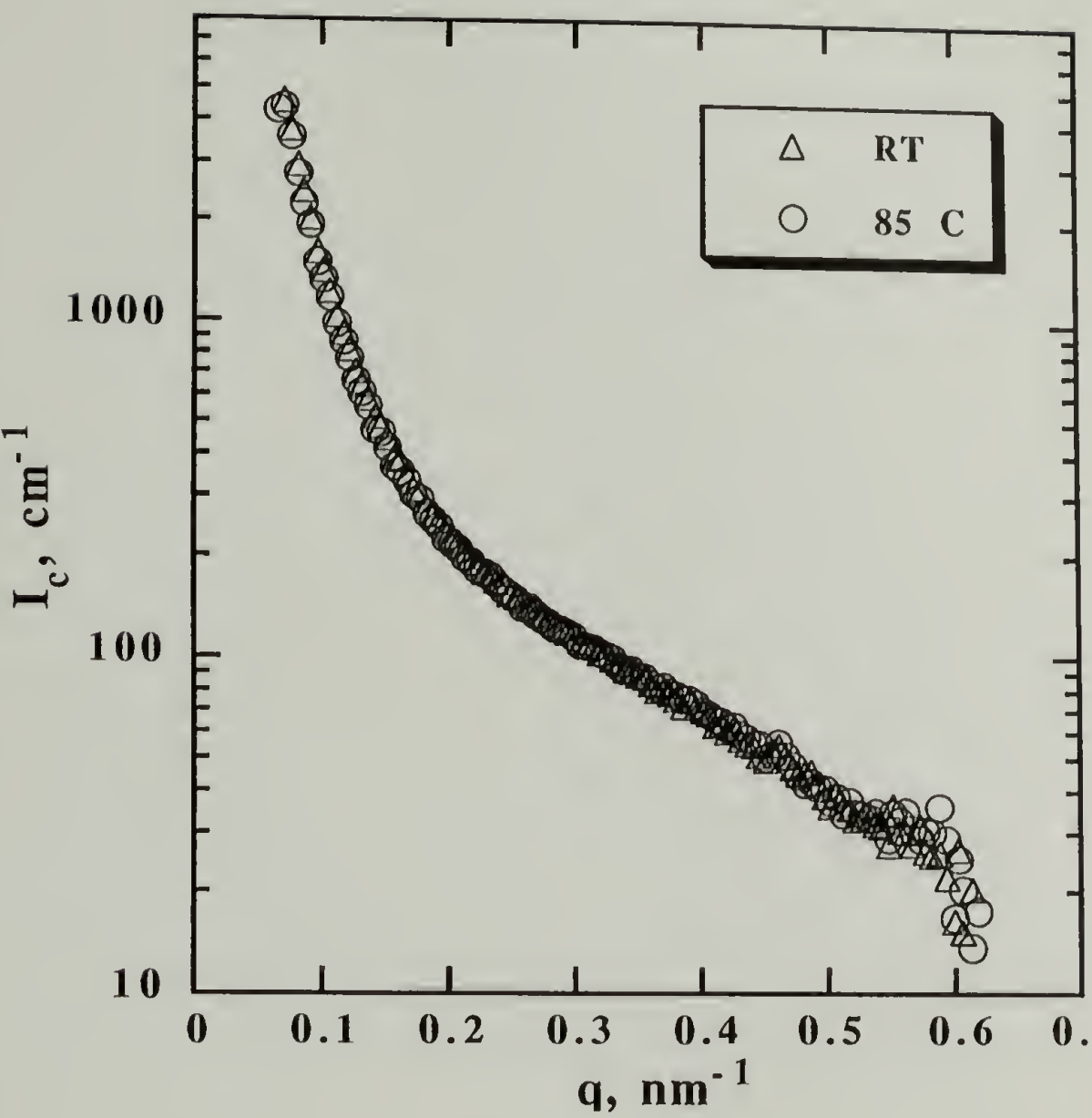

Figure 5.5 SANS for a 50%d-PC/50%PCL blend.

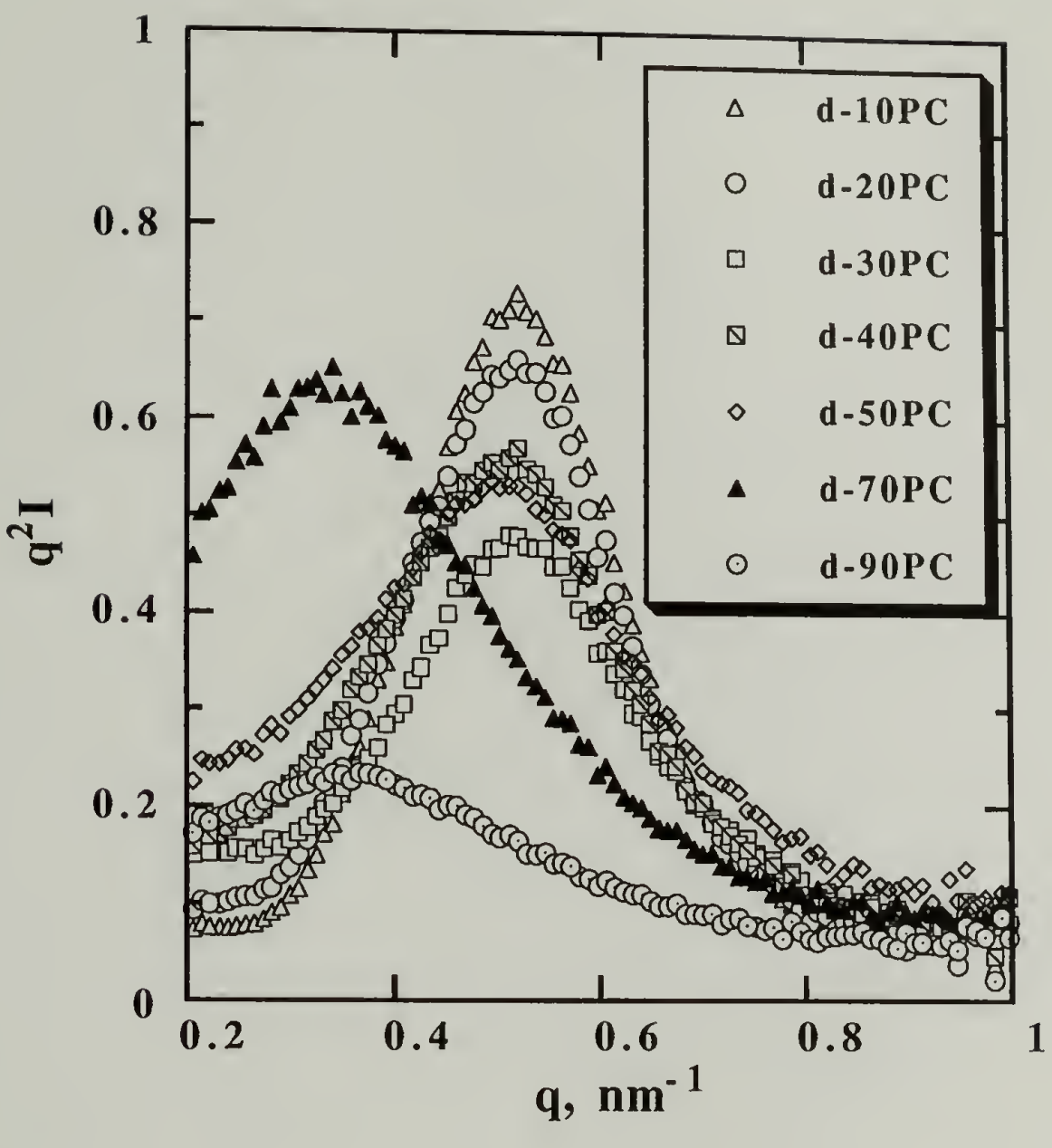

Figure 5.6 Lorentz-corrected SAXS for d-PC/PCL blends measured at room temperature.

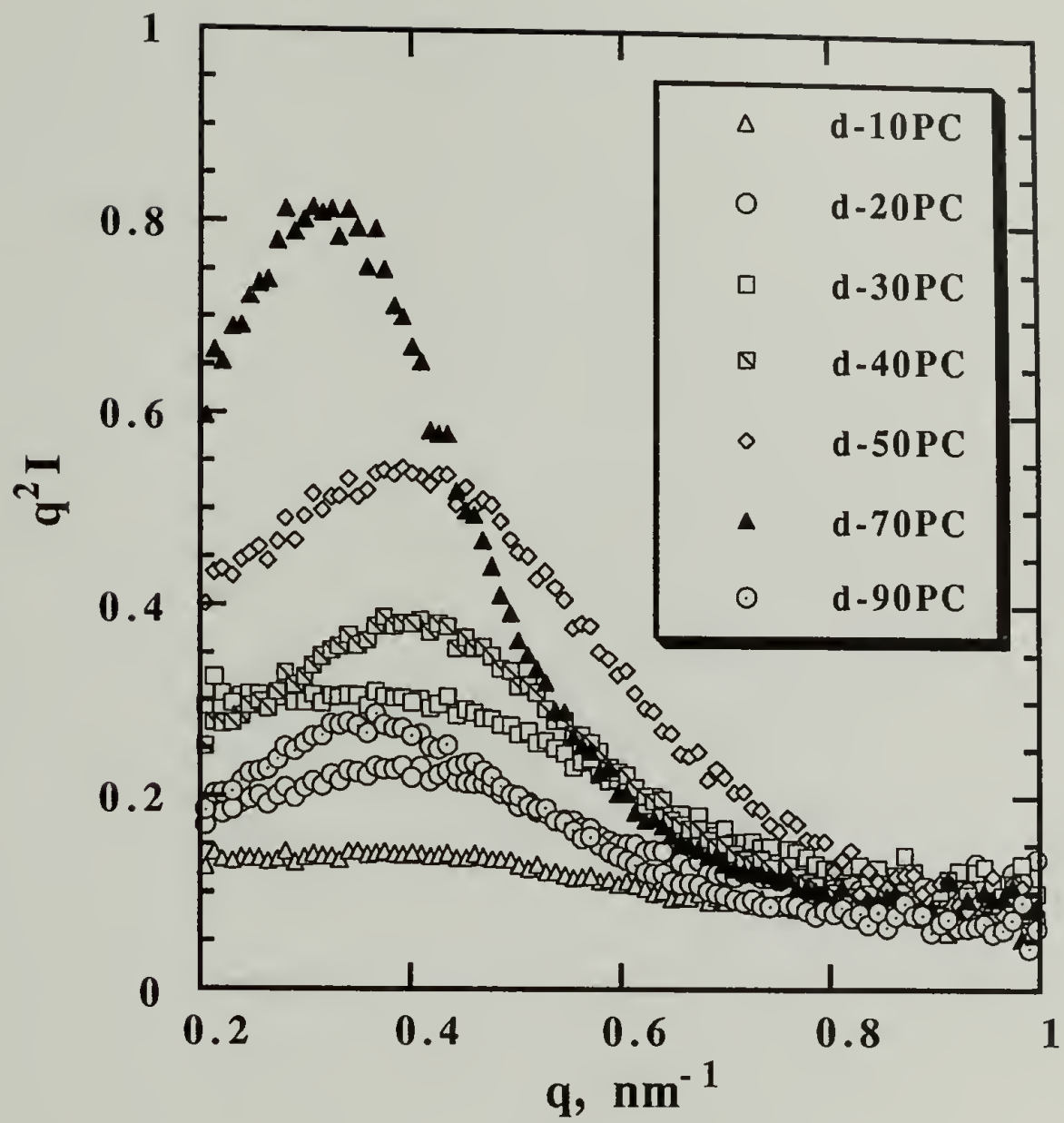

Figure 5.7 Lorentz-corrected SAXS for d-PC/PCL blends measured at 75 °C.

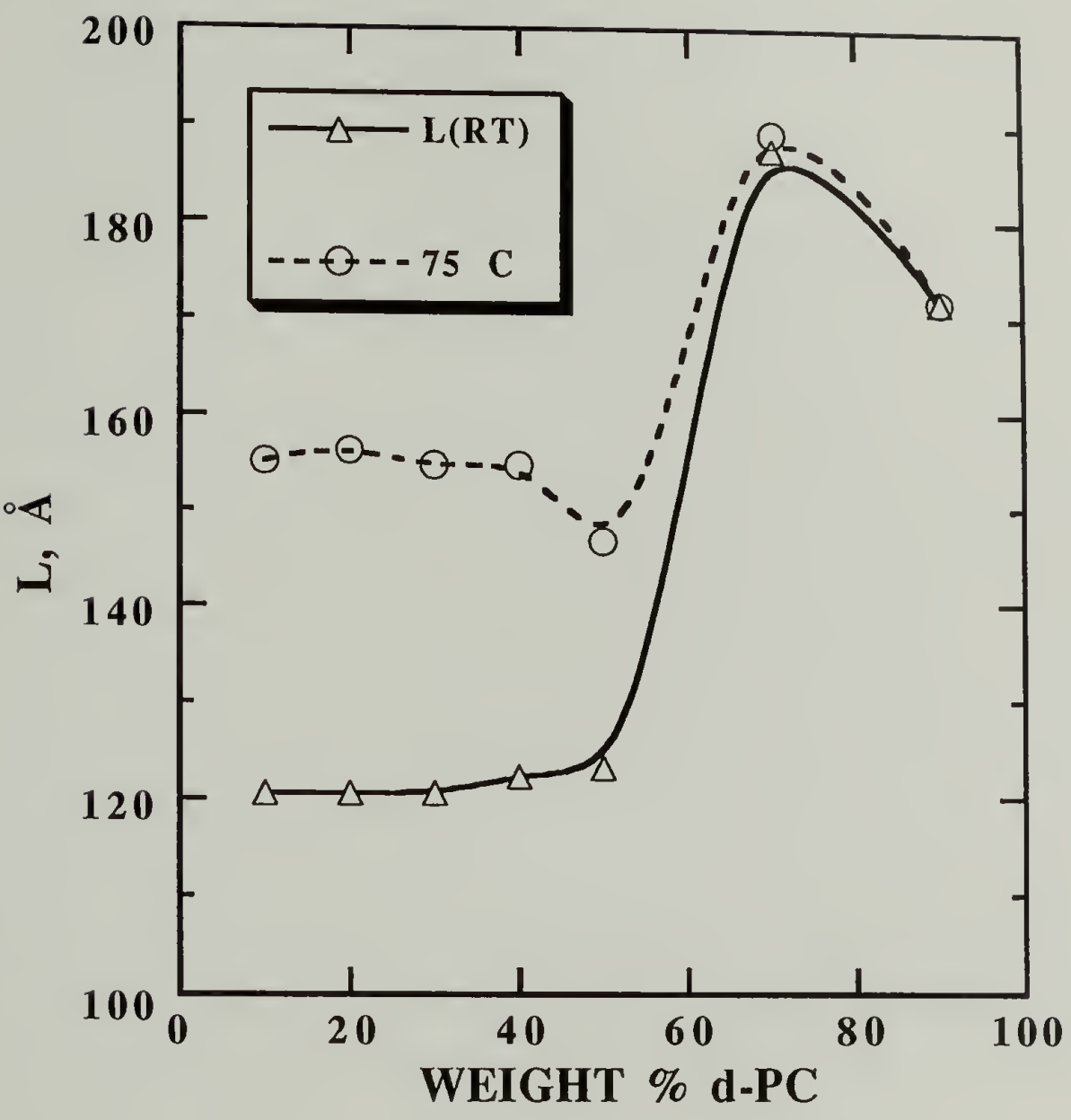

Figure 5.8 Long period for the d-PC/PCL blends.

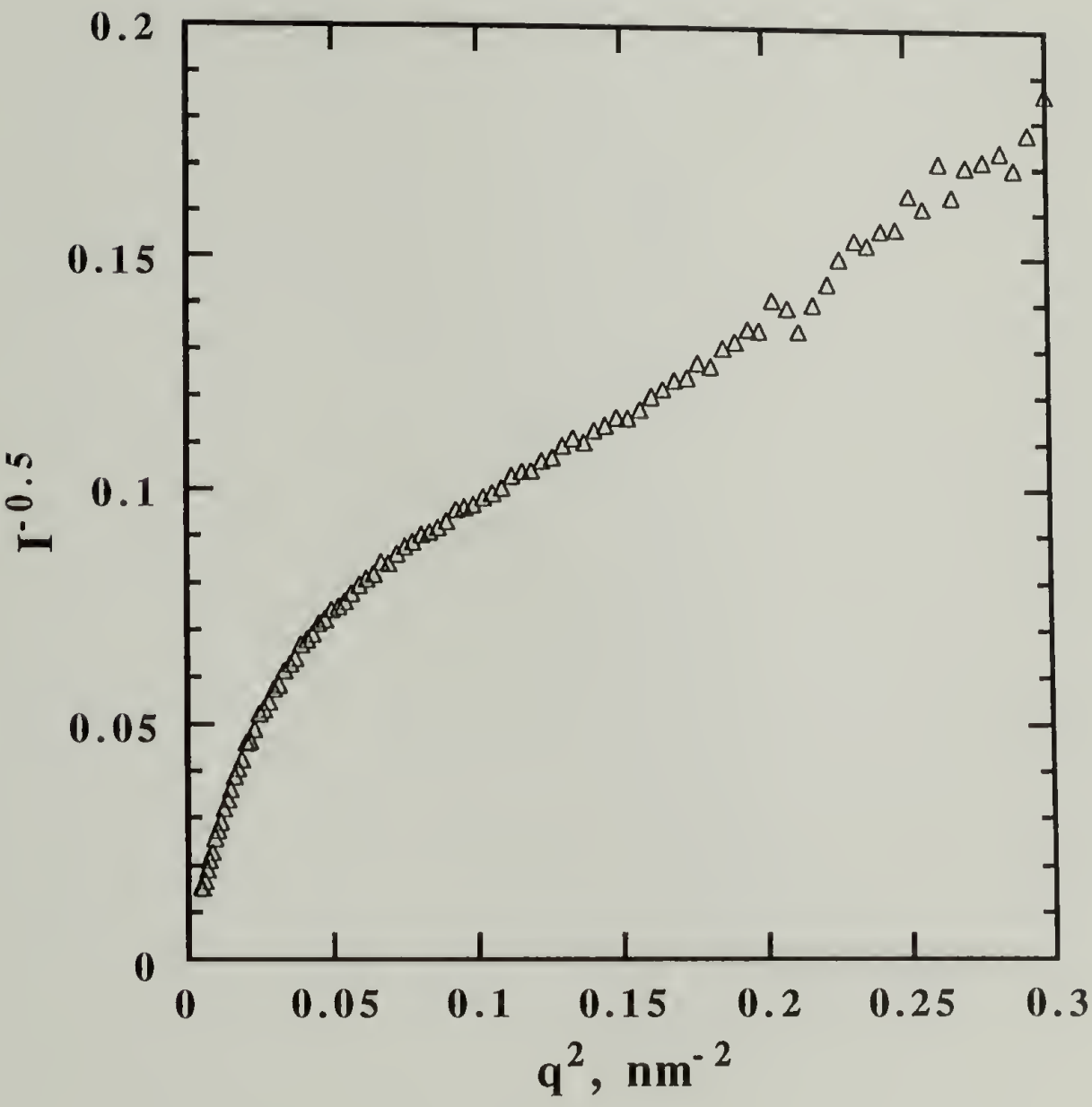

Figure 5.9 Debye-Bueche plot for a 50%d-PC/50%PCL blend.

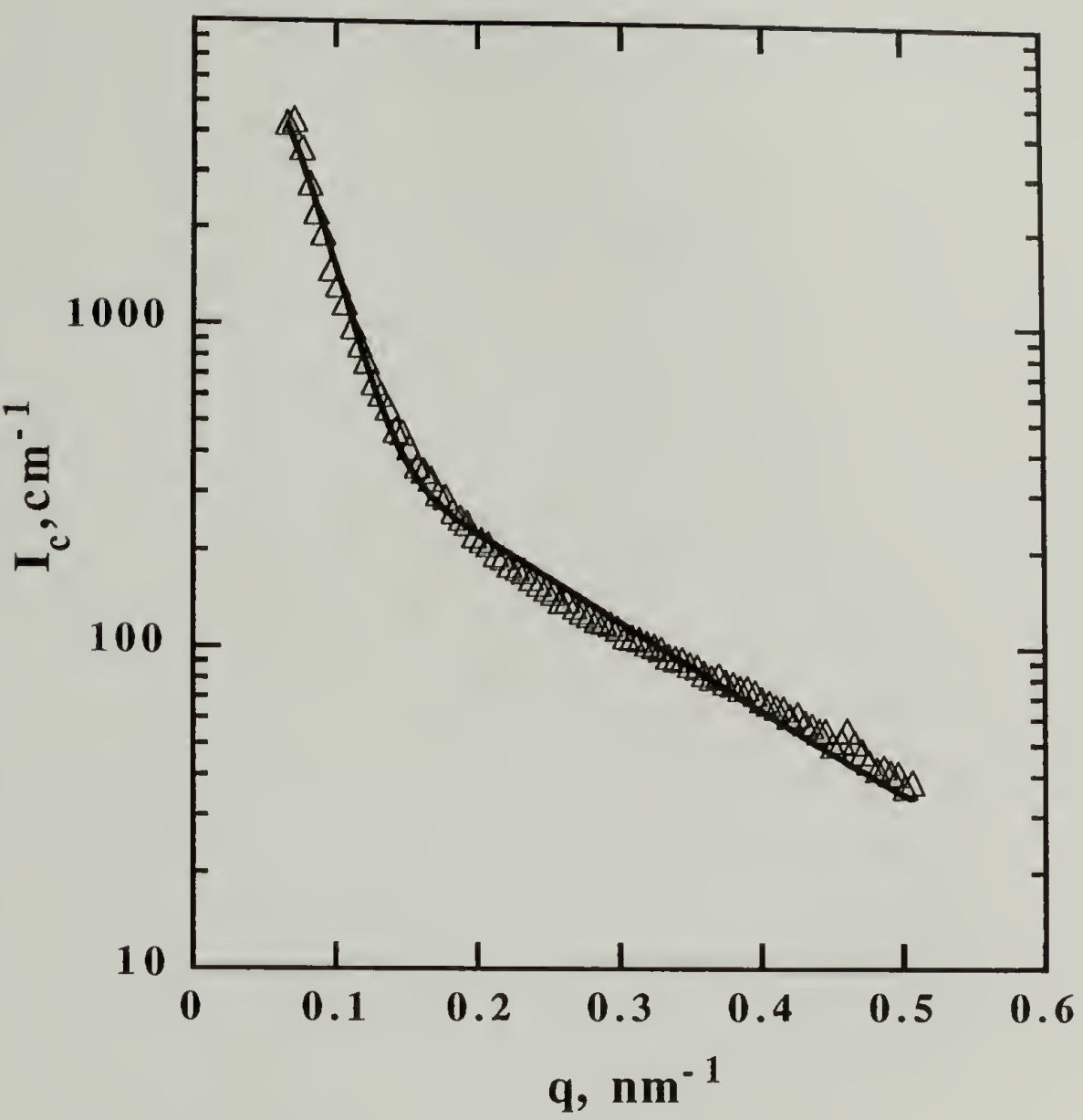

Figure 5.10 A two-correlation length model fit for a 50%d-PC/ 50%PCL blend.

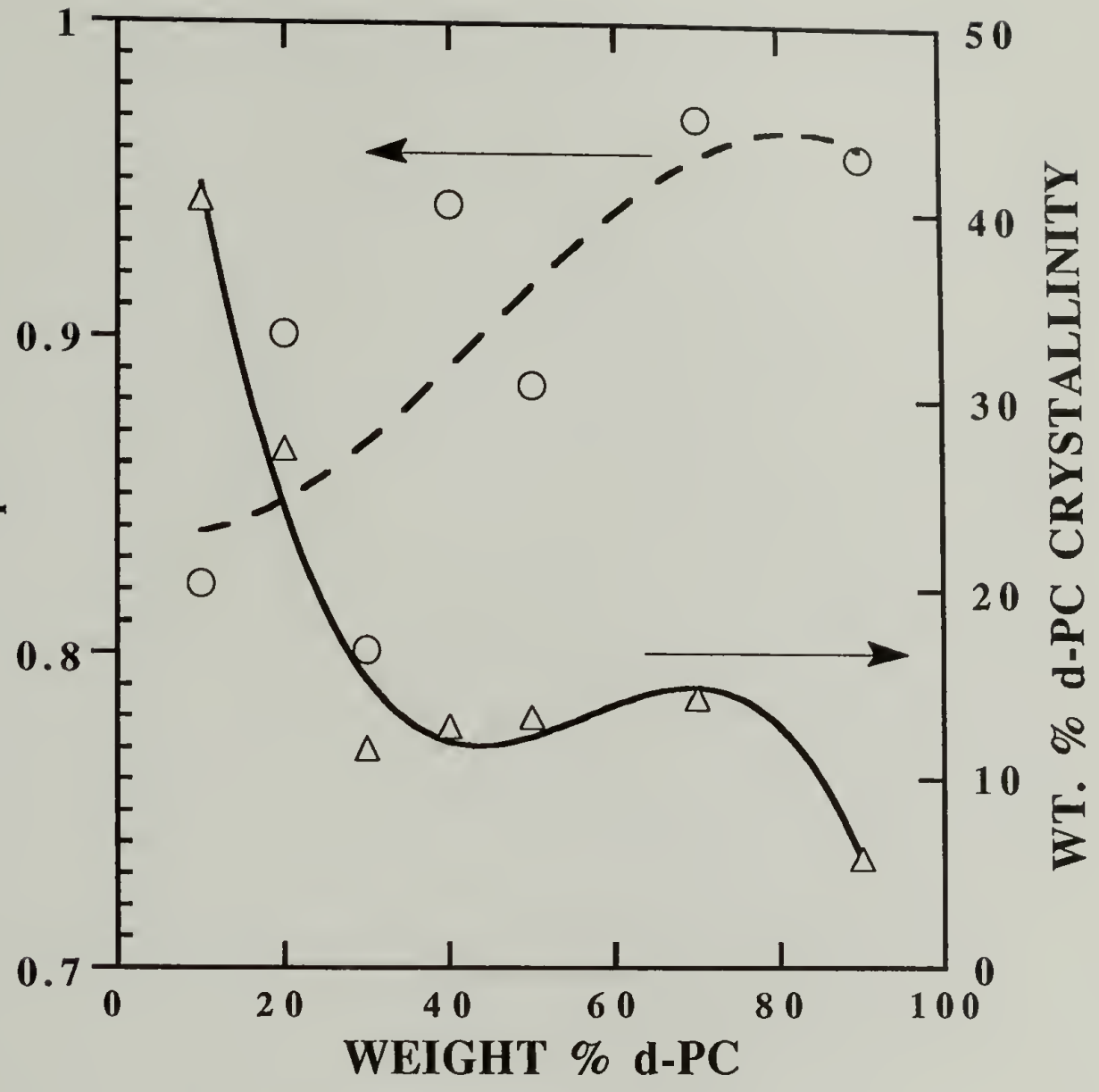

Figure 5.11 Normalized d-PC crystallinity and **f**, fractional contribution of exponential correlation function, for the d-PC/ PCL blends.

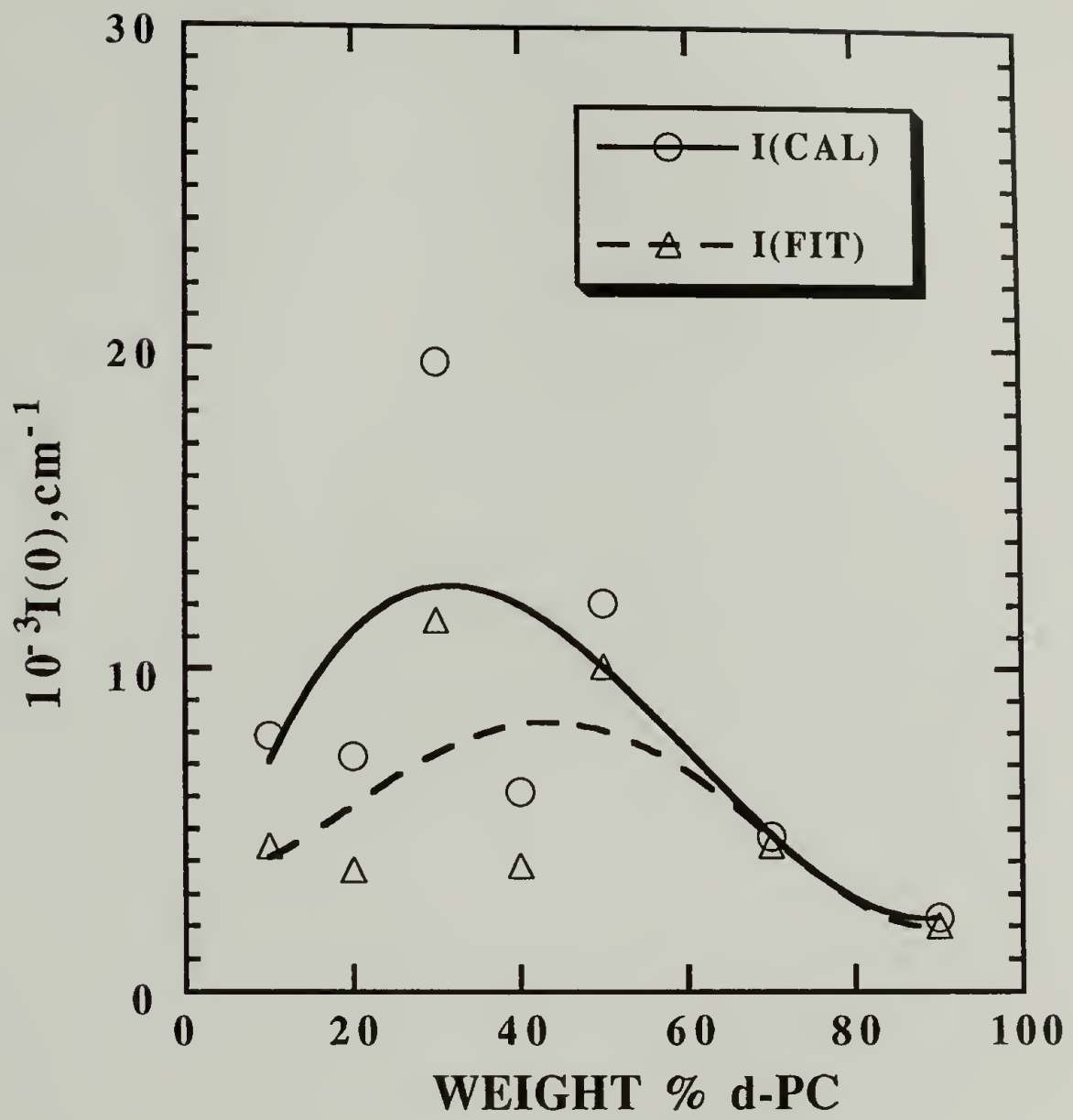

Figure 5.12 Zero angle scattering intensities for d-PC/PCL blends.

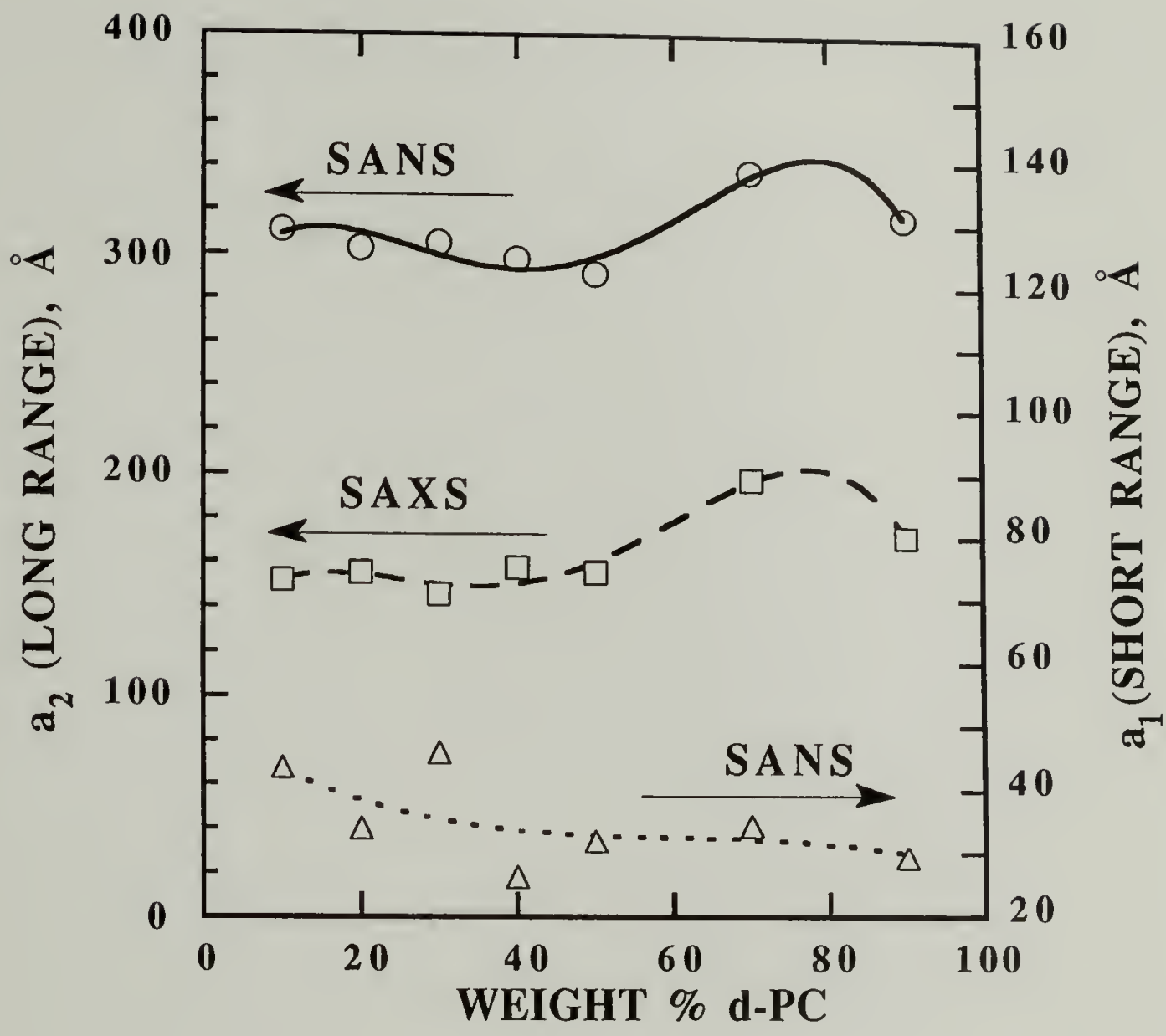

Figure 5.13 Long range and short range correlation length derived from SANS, and the long period measured from SAXS for the d-PC/PCL blends.

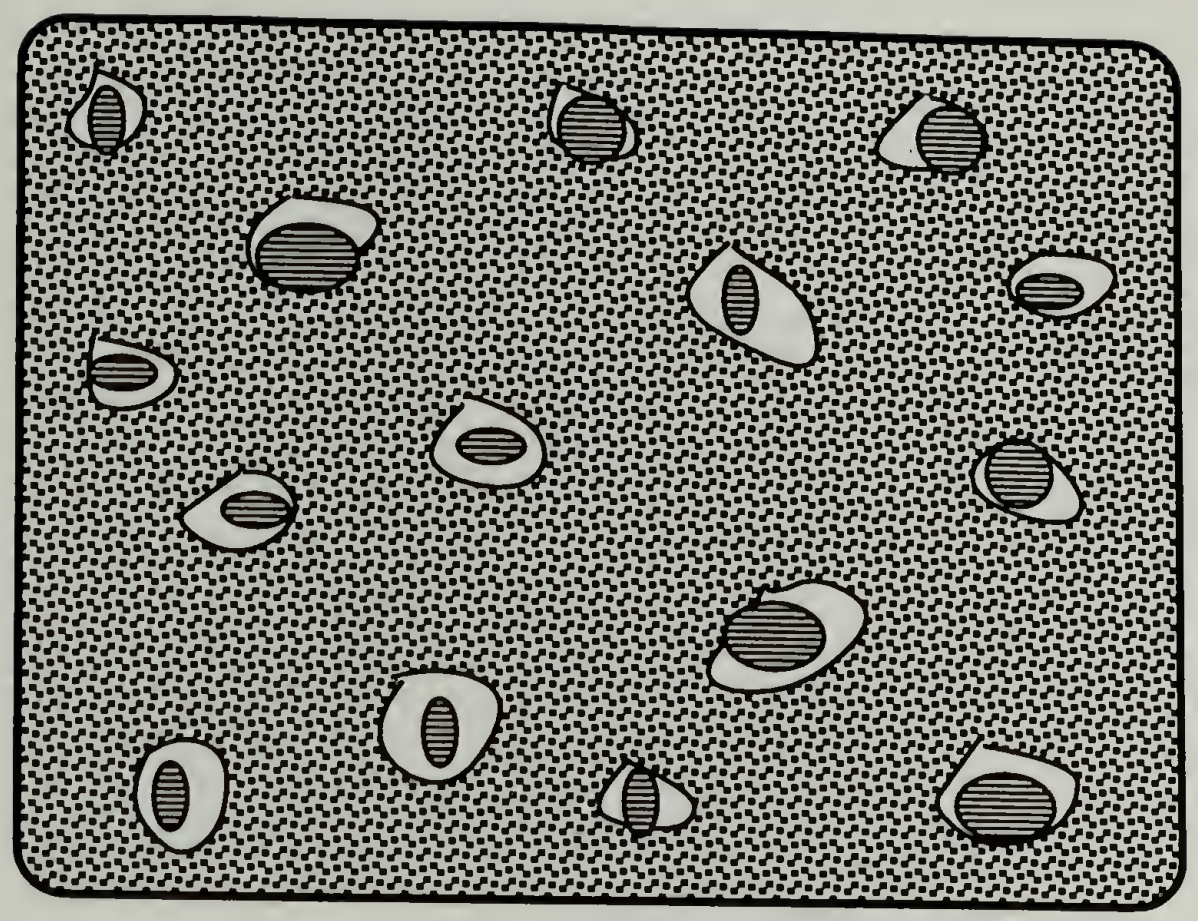

Figure 5.14 Schematic summary of the SANS and SAXS results. The PC crystals are surrounded by a PC-rich amorphous phase. The"mixed" amorphous phase shows clustering at a size scale of about 30 Å.

CHAPTER 6

SMALL-ANGLE X-RAY AND LIGHT SCATTERING STUDY OF SEMICRYSTALLINE/SEMICRYSTALLINE AND SEMICRYSTALLINE/AMORPHOUS BLEND MORPHOLOGIES

6.1 Introduction

Elucidation of the blend morphologies is of paramount importance in understanding the extent of polymer-polymer interaction and the physical properties. The interplay between kinetics and thermodynamics invariably determines the blend morphologies. In this chapter focus will be directed at elucidating the complex crystalline blend morphologies in both the semicrystalline/semicrystalline and semicrystalline/amorphous states as principally studied by small-angle X-ray scattering (SAXS). Results derived from the SALS study will also be reviewed.

The semicrystalline/amorphous state of PCL/d-PC blends as revealed by small-angle neutron scattering (SANS) was discussed in the last chapter. Based on the two-correlation length model analysis, the morphology of the PCL/d-PC blends may be described by a model composed of a d-PC crystalline phase dispersed in a matrix amorphous phase consisting of local clusters of about 30Å in size. A more detailed analysis of the SAXS results will be explored in the present chapter. The main focus of the subsequent discussion is to examine the blend morphologies, at both the lamellar and spherulitic level, in both the semicrystalline/semicrystalline and semicrystalline/amorphous states. SAXS is employed to unravel the lamellar organization of both PCL and PC. Correlation function analysis, absolute invariant calculation and Porod analysis will be used to determine the characteristic morphological parameters including the crystal- and amorphous-phase thickness and the transition layer thickness. Small-angle light

scattering (SALS) coupled with polarized optical microscopy will be used to probe the spherulitic structure.

According to Keith and Padden,[1] the spherulitic organization is predominantly controlled by the length parameter $\delta = D/G$, where D is the diffusion coefficient of the amorphous component and G is the linear growth rate of the crystals. The "δ" parameter is effectively a measure of the degree of "impurity" segregation from the growth front. Since both components in the present system can undergo crystallization, the "impurity" could be either PCL or PC. In the case of the PCL-rich blends, PCL is highly mobile at the crystallization temperatures of PC and hence "δ" is expected to be fairly large. Substantial migration of PCL from the PC crystal front will occur. In contrast, PC is already in a semicrystalline and highly immobile state at the PCL crystallization temperatures and hence "δ" is expected to be very small. Optical microscopy coupled with SALS will be used to identify both the PCL and PC spherulitic structure in the PCL-rich blends

Depending on the polymer-polymer specific interactions and the cooperative diffusion coefficient, a wide spectrum of morphologies may be found in semicrystalline/ amorphous blends. The amorphous component in such a blend system can either reside between the crystalline lamellae (interlamellar), or can be incorporated within the spherulites (interfibrillar), or even be rejected from the spherulites (interspherulitic). The interlamellar case has been observed in blends of PCL/poly(vinyl chloride), (PVC),[2] poly(vinylidiene fluoride), (PVF_2) with poly(methyl methacrylate), (PMMA),[3] and poly(ethylene oxide), (PEO) with PMMA.[4] The interfibrillar case is found in blends of isotactic polystyrene and atactic polystyrene.[5] The last mode of incorporation has been demonstrated in blends of high and low molecular weight PEO.[6]

In the case of semicrystalline/semicrystalline blends, there can exist even more possible structures and much more complex morphologies. Blends of random copolymers of vinylidene fluoride/trifluoroethylene (VF_2/FE_3) of different compositions were found to undergo cocrystallization.[7] More recently, blends of linear low density polyethylene (LLDPE) and high density polyethylene (HDPE) were also observed to crystallize within a single crystal lattice.[8] Since both PCL and PC can crystallize in the PCL-rich blends, the PCL/PC system may be classified as a semicrystalline/semicrystalline blend. The necessary conditions for cocrystallization are based on 1) miscibility in the melt, 2) similarity in the crystalline structure of the individual polymers, 3) nearly identical crystallization window. As mentioned before, no cocrystallization can occur between PCL and PC as the crystal lattice parameters for the two polymers are very different.[9-10] In the semicrystalline/semicrystalline state, the PCL and PC lamellae may either order in blocks rich in one population of lamellae (segregated arrangement) or mix in a random fashion where the two different types of lamellae are homogeneously dispersed in the amorphous phase. Efforts will be made to discriminate these two modes of lamellar arrangement.

In addition to the composition and temperature, the effects of blend preparation and thermal history on the morphology will be examined. Blends are normally prepared by melt blending, solution casting from a common solvent, or solution blending followed by precipitation where the blend is recovered by precipitating the solution in a non-solvent. Three different types of samples will be discussed: 1) as precipitated (AP) blends, 2) quenched (Q) blends prepared by first heating the AP blends to a temperature above the melting point of PC and then quenching the samples to room temperature, 3) solution cast (SC) blends. Both the PCL and PC crystallinity are strongly dependent on the preparation procedure and consequently the lamellar arrangements may be different. Attempts will be

made to decouple the effects of the amorphous and crystalline component on the lamellar and spherulitic organizations.

6.2 Experimental

SAXS experiments were conducted at the Oak Ridge National Laboratory (ORNL) in Tennessee. Measurements were performed on the ORNL 10m spectrometer[11] operating at an accelerating voltage of 40 KV and a current of 100 mA at both room temperature and 75 °C. The instrument was operated with a sample-detector distance of 5.13 m using $Cu_{k\alpha}$ radiation (λ = 1.54 Å) and a 20X20 cm^2 area detector with cell (element) size ~ 3 mm. Corrections were made for instrumental backgrounds and detector efficiency (via an Fe^{55} standard which emits γ-rays isotropically) on a cell-by-cell basis, prior to radial averaging to yield a q range of 0.005 to 0.1 $Å^{-1}$, where $q = (4\pi/\lambda)\sin(\theta/2)$, λ is the X-ray wave-length, θ is the scattering angle. The scattering profiles were corrected for sample absorption and incident X-ray fluctuations. The net intensities were converted to an absolute differential cross section per unit sample volume (in units of cm^{-1}) by comparison with pre-calibrated secondary standards.[12] Thermal density fluctuation scattering[4] was estimated by measuring the SAXS at high scattering vectors, $0.019 < q < 0.47$ $Å^{-1}$, and eliminated by evaluating the slope of Iq^4 versus q^4 plot.

The small-angle light scattering (SALS) patterns were recorded either by a film or an optical multichannel analyzer with a laser light source of 6328 Å wavelength under horizontal-vertical (H_v) polarization condition. An Zeiss optical microscope equipped with a cross polarizer was used to image the spherulites directly and to complement the SALS observations.

6.3 Results and Discussion

6.3.1 Small-Angle X-Ray Scattering

SAXS is a very powerful morphological tool for studying the detailed lamellar organization of semicrystalline polymers. It is well known that the contrast mechanism for SAXS is based on the electron density difference between the crystalline and amorphous region. The mass density, the electron density for PC and PCL, and the electron density difference between the crystalline and the amorphous region for PCL and PC are displayed in Table 6.1. It can be seen that the contrast for PC is about 1.5 times greater than that for PCL. This fact is critical to the analysis of the absolute scattering cross section of the blends to be described later.

6.3.1.1 SAXS Analysis

Traditionally, three approaches are often used to analyze the SAXS profiles: 1) calculation of the long period or the interlamellar spacing directly from the scattering curve, 2) computation of the electron density correlation function[13-15] from which the amorphous- and crystal-phase thickness may be obtained, 3) fitting of the scattering profiles to morphological models.[16-18] The first two methods will be used to evaluate the various morphological parameters. The long period is calculated from the equation $L=2\pi/q^*$, where q^* is the peak value found in the Lorentz-corrected $q^2I(q)$ versus q plot. The normalized one-dimensional correlation can be evaluated from the scattered intensity I(q) by the following equation[14]

$$\gamma(z) = \frac{1}{\gamma(0)} \int_0^\infty q^2 I(q) \cos(qz) dq \qquad (6.1)$$

where z is along the direction from which the electron density distribution is measured. Since the experimentally accessible q-range is finite, it is necessary to extend the data to

both lower and higher q-values. Linear extrapolation is used to extend the data from the smallest measured q value to zero. Large q values could be damped to infinite q value by using a Porod-type (q^{-4} decay) model.[14] A schematic depiction of a correlation function is shown in Figure 6.1.

Peak width measured at half height of the Lorentz-corrected SAXS profiles will be used to assess the heterogeneity of the lamellar distribution. Porod analysis will be performed to determine the transition zone width between regions of different electron densities. In addition to the other corrections, the thermal density fluctuations must be subtracted from the background scattering. Based on the Porod law,[19-21] the thermal fluctuations and the interface thickness can be expressed as

$$q^4 I(q) = K_p H^2(q) + I_{fl} q^4 \tag{5.2}$$

where $H^2(q) = \exp(-\sigma^2 q^2)$ is a Gaussian smoothing function, which accounts for the negative deviations from the Porod law due to the presence of an interface, with σ as the standard deviation. The interfacial thickness E is related to σ by the equation $E=(12)^{1/2}\sigma$. I_{fl} is the background scattering due to the thermal density fluctuations and can be estimated from the slope of a plot of $q^4I(q)$ versus q^4 at large scattering vectors.[4] Similarly the interfacial thickness can be estimated from the slope of a plot of $\ln\{[I(q)-I_{fl}]q^4\}$ versus q^2. Finally, the total integrated intensity or the invariant Q, defined below,

$$Q = \frac{1}{2\pi^2} \int_0^\infty I(q)\, q^2\, dq \tag{5.3}$$

measured experimentally will be compared to the model calculation. For an ideal two phase system, the invariant is given by

$$Q = 2\pi^2 \phi_1\phi_2 (\rho_1-\rho_2)^2 \tag{5.4}$$

where ϕ is the volume fraction and ρ is the electron density. This definition may be generalized to a system containing an arbitrary number of phases as the following[22]

$$Q = 2\pi^2 \sum_{i\neq j} \phi_i\phi_j (\rho_i-\rho_j)^2 \tag{5.5}$$

6.3.1.2 Homopolymers

Before embarking on the discussion of the blends, the SAXS profiles of the two homopolymers should be examined. The SAXS absolute scattering cross section for PCL and PC is shown in Figure 6.2. It is well known that PC can undergo crystallization either by prolonged annealing at elevated temperatures (with an optimum crystallization temperature at about 190 °C) or by solution-induced crystallization. The sample shown in Figure 6.2 was prepared by means of solution casting from methylene chloride and had about 35% crystallinity. The PC SAXS pattern remained virtually unaltered at 70 °C as PC was still highly immobile at this temperature. The long periods of the two polymers were similar. Due to the higher electron density difference for PC as indicated by Table 6.1, the integrated scattered intensity for PC will be higher than that for PCL for a given amount of crystallinity. However, the scattered intensity for PCL appeared to be higher than that for PC as this PCL sample had a higher degree of crystallinity. According to Equation 6.4, the scattered intensity is proportional to both the contrast and the volume fraction of the phases.

6.3.1.3 Structure of Semicrystalline/Semicrystalline Blends

As described before, the PCL-rich blends at room temperature contained both PCL and PC crystals as evidenced by DSC and wide angle X-ray scattering. A series of Lorentz-corrected SAXS profiles for the PCL-rich AP and Q blends are shown in Figures 6.3 and 6.4, respectively. From Figure 3.1, it can be seen that the AP samples have higher PC crystallinity than the Q samples. The SAXS profiles clearly indicated that the peak intensity and the total scattered intensity for the AP blends were higher than those for the Q blends due to the larger electron density difference for PC and the higher PC crystallinities found in the AP samples. From the peak position, the long period L or the interlamellar spacing can be obtained. Figure 6.5 shows a plot of the long period as function of composition for both AP and Q blends. A cursory examination of this plot indicates that the long period for the blends was always smaller than that for the pure PCL. For the AP blends, the long period is almost independent of composition. In the case of the Q blends, L decreased with the addition of PC. Effectively, the long period was not only dependent on the PC composition but also on the PC crystallinity.

Since these blends were semicrystalline/semicrystalline, the long period measured is assumed to be the average interlamellar spacing between the PCL and PC lamellae. The observation that the SAXS profiles for all the blends exhibited a single peak could suggest random mixing between the PC and PCL lamellae as a segregated arrangement should give rise to two peaks or at least a shoulder in the SAXS. This hypothesis is further supported by the finding that the PC long periods measured at 75 °C (above the melting point of PCL) shown in Figure 6.6 were different from and larger than those obtained at room temperature (RT). Random mixing of the smaller PCL lamellae with the larger PC lamellae resulted in a depression of the observed long period found in the semi-crystalline/semicrystalline state relative to that measured in the semicrystalline/amorphous

state. This random mixing model can also explain the differences in the composition dependence between the AP and Q blends. The relative invariant of the long period with composition for the AP blends reflected the large contribution of the PC lamellae scattering, due to the higher PC crystallinity, to the SAXS pattern as the PC long period (measured in the semicrystalline/amorphous state) was fairly independent of composition as shown in Figure 6.6. The PCL long period in the PCL-rich blends cannot be isolated as the SAXS measured at RT was a superposition of both PCL and PC lamellar scattering. Therefore, the SAXS profiles recorded at RT could be interpreted as resulted from the scattering of entities consisting of both PCL and PC lamellae.

Peak width, β, measured at half height of the Lorentz-corrected SAXS profiles can be used as a measure of the homogeneity of the lamellae distribution. Figure 6.7 shows a plot of the peak width as a function of compostion for the AP blends. It is observed that β increased with the addition of PC in the semicrystalline/semicrystalline state. In contrast, β decreased with increasing PC in the semicrystalline/amorphous state. Furthermore, β measured in the semicrystalline/semicrystalline state was consistently larger than that obtained in the semicrystalline/amorphous state. In other words, the lamellae distribution was narrower in the semicrystalline/amorphous state as the PCL lamellae were destroyed and did not contribute to the overall SAXS pattern. The larger lamellae heterogeneity found in the semicrystalline/semicrystalline blends further supports the random mixing model. The lamellar peak broadening reflects an increase in the heterogeneity of the lamellae distribution which results from the random mixing of the PCL and PC lamellae.

Porod analysis is commonly used to estimate the width of the transition zone. The slope of a plot of $\ln\{[I(q)-I_{fl}]q^4\}$ versus q^2 is proportional to the width of the interfacial thickness as described earlier. A series of Porod plots for the quenched blends are shown

in Figure 6.8 and the corresponding interfacial thickness as a function of composition for Q and AP blends is plotted in Figure 6.9. Due to the statistical scatter in the intensity data and the difficulty of separating the effects of density fluctuations within the phases, the errors associated with the absolute value of the interfacial thickness could be significant.[23] A monotonic decrease in the interfacial width was found with increasing PC. Similar trends were also found in the solution cast blends. Interestingly, the interfacial width of the blends was intermediate of the two homopolymers. This finding is also consistent with the random mixing model in which both PCL and PC lamellae scatter as a single entity. The PC character of the blends becomes more prominent as the interfacial width approaches that of the pure PC with increasing PC composition and increasing PC crystallinity in the blends.

The total integrated scattered intensity or the invariant is directly related to the mean square fluctuation of electron density and can be calculated according to Equation (5.5). At room temperature the PCL-rich blends consisted of a PCL crystalline phase, a PC crystalline phase and an amorphous phase. To a first order of approximation, the invariant may be calculated from the following "pseudo two-phase model" based on the assumption that all the lamellae contibute to the SAXS intensity

$$\begin{aligned} Q = 2\pi^2 [\, & \phi_1\phi_2(\rho_1-\rho_2)^2 + \phi_1\phi_3(\rho_1-\rho_3)^2 + \phi_1\phi_4(\rho_1-\rho_4)^2 + \\ & \phi_2\phi_3(\rho_2-\rho_3)^2 + \phi_2\phi_4(\rho_2-\rho_4)^2 + \\ & \phi_3\phi_4(\rho_3-\rho_4)^2 \,] \end{aligned} \qquad (5.6)$$

where ϕ is the volume fraction and ρ is the electron density and 1- denotes crystalline PCL, 2- is amorphous PCL, 3- crystalline PC and 4- amorphous PC phase. The values for the volume fraction for the various phases are derived from the DSC measurements

and the overall blend composition. Figure 6.10 shows a comparison between the experimentally measured invariants to the calculated values for the solution cast (d-PC/ PCL) blends. The model calculation exhibited identical composition dependence as the experimental invariant. Moreover, the calculated values differed from the experimental values by no more than a factor of two. Invariably the calculated invariant was greater than the measured invariant. The discrepancy between the measured and the calculated invariant may be attributed to 1) inadequacy of the model, 2) limited experimentally accessible q-range, and 3) the existence of the transition zone which would reduce the electron density difference between the phases and thus decrease the scattering contrast. The simple model used in the calculation neglects the presence of the crystal-amorphous interface.[24] Uncertainties associated with the crystallinity measurement and the presence of micro-voids also could affect the scattering intensity and consequently the invariant. Additionally, the measured invariant represented an integration of the scattered intensity over a finite q-range which could easily led to a lower value compared to the calculation. Extrapolations to both lower and higher q-ranges similar to those used in the correlation function evaluation indicated that the extrapolated regions only contribute less than 10% of the total invariant. In spite of these complications and the inherent complex morphology, the "pseudo two-phase" model with no adjustable parameter nicely reproduced the composition dependence and fairly predicted the absolute magnitude of the invariant.

Figure 6.11 shows a series of correlation function for the AP blends. Direct quantitative interpretation of the correlation function results was complicated by the presence of PCL and PC lamellae. However, it is still instructive to examine the detailed morphological features of the composite lamellae. The long period calculated directly from SAXS and that derived from the correlation function were in good agreement as shown in Figure 6.12. This correlation analysis indicated that both the crystal- and amorphous-phase thickness were almost independent of the PC composition. This

finding could suggest that the PCL lamellae were not significantly perturbed by the addition of PC assuming that the lamellar scattering observed in the semicrystalline/semicrystalline state predominantly came from the PCL lamellae. This approximation is only valid for samples with low PC crystallinties.

6.3.1.4 Structure of Semicrystalline/Amorphous Blends

Measurements were also performed at 75 °C to render the PCL amorphous. Since the SAXS patterns can be assumed to come from PC lamellar scattering, the interpretation was more straightforward. Focus can be directed at a more critical examination of the PC lamellar organization in the semicrystalline/amorphous state. Figure 6.6 shows the long period as a function of PC composition for both AP and Q blends. Due to annealing effects, the PC long periods for the AP blends were always larger than those for the Q blends. The PC long period for the blends was fairly independent of composition and was larger than the pure PC. This difference may be related to the disparity in the thermodynamic driving force for crystallization between the blends and the pure PC. Due to the plasticization of PC by PCL, the T_g of the blend was much lower than that of the pure PC as discussed before.

Similarly, the peak width for the AP blends was smaller than that for the Q blends reflecting a more homogeneous lamellar distribution resulting from annealing. Broadening of the lamellar peak increased with increasing PCL as shown in Figure 6.7. As more PCL was incorporated in the blends, heterogeneity in the PC lamellae distribution increased leading to a widening of the lamellar peak. Moreover, Porod analysis indicated that the interfacial thickness was smaller than that found in the semicrystalline/semicrystalline state and increased with increasing PC. Incorporation of PCL in the blends resulted in a reduction of the interfacial thickness relative to the pure PC as shown in Figure 6.13. Combination of the Porod results derived from the two states demonstrated that the inter-

facial thickness was strongly affected by both the physical state and the composition of the respective components.

As in the semicrystalline/semicrystalline case, the invariant was calculated by

$$Q = 2\pi^2 [\, \phi_1\phi_2(\rho_1-\rho_2)^2 + \phi_1\phi_3(\rho_1-\rho_3)^2 + \phi_2\phi_3(\rho_2-\rho_3)^2] \qquad (6.7)$$

where 1- denotes crystalline PC, 2- amorphous PC, 3- amorphous PCL phase. The measured invariant and the calculated value are plotted in Figure 6.14. In spite of the simplicity of this model, the calculation accurately reproduced the composition dependence of the experimentally obtained invariant. As in the case of the semicrystalline/semicrystalline blends, the calculated values were roughly 50% larger than the measured values. This disparity may be attributed to reasons described before.

As discussed earlier, correlation function analysis provides very localized morphological information regarding the organization of the lamellae. The interlamellar spacing, crystal- and amorphous-phase thickness for the solution cast (d-PC/PCL) blends are shown in Figure 6.15. For the PCL-rich blends, the long period and the associated morphological parameters were almost independent of composition. The invariance of the amorphous-phase thickness with composition indicated that PCL was rejected from the interlamellar region. In contrast, the amorphous-phase thickness for the PC-rich blends increased with increasing PC whereas the crystal-phase thickness remained fairly constant. This phenomenon suggests that PCL was incorporated or trapped within the interlamellar region resulting in an increase in the amorphous-phase thickness.

The transition between interlamellar exclusion and interlamellar inclusion of PCL in the PC lamellae may be related to the glass transition temperatures of the blends. For the

PCL-rich blends, the T_g was below room temperature and therefore the polymer chains were highly mobile at the crystallization temperatures of PC. Under these conditions, PCL can readily diffuse away from the growing crystal front and consequently was excluded from the interlamellar region of the PC lamellae. In the case of PC-rich blends, the T_g was above room temperature and the PCL mobility was highly hindered at RT and even at the drying temperature (90 °C). Therefore, the mode of incorporation or exclusion was controlled by a competition between entropy and mobility or diffusion. As evidenced by the SAXS results, PCL was trapped within the interlamellar region of the PC lamellae which led to a corresponding increase in the long period. This increase was attributed to the incorporation of PCL in the amorphous region of the d-PC lamellae.

Interlamellar exclusion is always entropically favorable provided the amorphous component has sufficient mobility to diffuse away from the crystalline lamellae. However, interlamellar inclusion occurs when either the amorphous component is highly immobile or the specific interactions are so favorable that the enthalpic term dominates the entropy contribution. From the correlation function results, it was observed that the driving force governing the transition from interlamellar exclusion to interlamellar inclusion was controlled by entropy and mobility. The competition between these two forces, depicted in Figure 6.16, provides a rational explanation for the composition dependence of the lamellar arrangement.

6.3.2 Small-Angle Light Scattering

SALS and optical microscopy are most suitable for probing the spherulitic structure of semicrystalline polymers. The SALS H_v patterns for the PCL-rich blends recorded at RT are shown in Figure 6.17. The scattering patterns became larger with increasing PC incorporation. This simply indicated that the PCL spherulitic size decreased with increasing PC due to the inverse relationship between the reciprocal space observed with SALS

and the real space.[25] In agreement with the crystallization kinetics results, PC was found to be a very effective nucleating agent for PCL crystallization. This nucleating effect resulted in an acceleration of the PCL crystallization kinetics and a reduction in the PCL spherulitic size with the addition of PC. At temperatures above the melting point of PCL, the sample appeared nearly dark under cross-polarization condition suggesting that the PC crystals and crystallinity were too small to be imaged either by SALS or microscopy. Complementary information may be obtained from V_v scattering as the intensity is proportional to both the refractive index difference between the tangential and radial component of the spherulite and the surrounding medium.

6.4 Conclusions

The lamellar organization of the semicrystalline/semicrystalline and semicrystalline/amorphous blends was investigated with SAXS. Quantitative SAXS analysis was performed to obtain morphological parameters including the interlamellar spacing, peak width at half height, amorphous- and crystal-phase thickness, interfacial width and the invariant. In the semicrystalline/semicrystalline state a model based on the random mixing of PCL and PC lamellae provides a rational explanation for the composition dependence of the long period and the half height peak width. The SAXS profiles were interpreted in terms of scattering from entities composed of a random mixture of PCL and PC lamellae.

In the semicrystalline/amorphous state (above T_m of PCL) two distinct regions of incorporation were observed. In the case of PCL-rich blends, PCL was rejected from the interlamellar region of the PC lamellae as indicated by the invariant of the long period and the amorphous-phase thickness. In the case of PC-rich blends, PCL was incorporated between the crystalline PC lamellae as supported by the increases in the amorphous-phase thickness with the addition of PCL. This transition from interlamellar exclusion to interlamellar inclusion was postulated to be related to the glass transition temperatures or the

mobility of the blends. Hence, it is seen that the mode of incorporation or exclusion is governed by the competition between entropy and diffusion or mobility. Interlamellar exclusion is always entropically favorable provided the amorphous component has sufficient mobility to diffuse away from the crystalline lamellae. It was observed that interlamellar exclusion found in the PCL-rich blends was entropy-controlled whereas interlamellar inclusion found in the PC-rich blends was mobility-controlled. SALS coupled with optical microscopy indicated that the PCL spherulitic size decreased with the addition of PC. In agreement with the crystallization kinetics results, PC was found to be an effective nucleating agent for PCL crystallization.

Table 6.1

Electron Density (ρ_e), Mass Density (d) and Electron Density Difference ($\Delta\rho_e$) for PCL and PC

Polymer	$\rho_e X10^{-9}$, cm^{-2}	d_A, g/cm^3	d_X, g/cm^3	$(\Delta\rho_e)^2$ $X10^{-20}$, cm^{-4}
PCL	91.72d	1.090	1.185	1.118
PC	88.97d	1.196	1.315	0.760

A = Amorphous

X = Crystalline

d = Mass Density

$(\Delta\rho_e) = (\rho_{eA} - \rho_{eX})$

References

1. Keith, H.D. and Padden, F.J. *J. Appl. Phys.* **24**, 2490 (1963).

2. Russell, T.P. and Stein, R.S. *J. Polym. Sci., Polym. Phys. Ed.* **21**, 999 (1983).

3. Morra, B.S., *Ph.D. Thesis*, University of Massachusetts, Amherst, 1980.

4. Russell, T.P.; Ito, H. and Wignall, G.D. *Macromolecules* **21**, 1703 (1988).

5. Warner, F.P.; Stein, R.S. and Macknight, W.J. *J. Polym. Sci., Polym. Phys. Ed.***15**, 2113 (1977).

6. Keith, H.D. and Padden , F.J. *J. Appl. Phys.* **35**, 1270, 1286. (1964)

7. Tanaka, H. and Lovinger, A.J. *Macromolecules* **1987**, 20, 2683.

8. Tashiro, K.; Satkowski, M.M.; Stein, R.S.; Li, Y.; Chu, B. and Hsu, S.L. *Macromolecules* **25**, 1809 (1992).

9. Bittiger, H. and Marchessault, R.H. *Acta. Cryst.* **B26**, 1923 (1970).

10. Bonart, V.A. *Die Makromolekulare* **92**, 146 (1966).

11. Wignall, G.D.; Lin, J.S. and Spooner, S.J. *J. Appl. Cryst.* **23**, 241 (1990).

12. Russell, T.P.; Lin, J.S.; Spooner, S. and Wignall, G.D. *J. Appl. Cryst.* **21**, 629 (1988).

13. Vonk, C.G. and Kortleve, G. *Kolloid Z. Z. Polym.* **19**, 220, (1967).

14 Strobl, G.R. and Schneider, M. *J. Polym. Sci., Polym. Phys. Ed.*18, 1343 (1980).

15. Balta-Calleja, F.J. and Vonk, C.G. *X-Ray Scattering of Synthetic Polymers*; Elsevier, Amsterdam, 1989.

16. Blundell, D.J. *Acta Crystallogr.* Sect. **A26**, 472, 476 (1970).

17. Gerasimov, V.I. and Tsvankin, D.Y. *J. Polym. Sci., Polym. Phys. Ed.* **12**, 2035 (1974).

18. Hosemann, R. and Bagchi, S.N. *Direct Analysis of Diffraction by Matter;* North-Holland, Amsterdam, 1962.

19. Porod, G. *Kolloid-Z* **124(2)**, 83 (1951).

20. Porod, G. *Kolloid-Z* **125(2)**, 108 (1952).

21. Korberstein, J.T.; Morra, B. and Stein, R.S. *J. Appl. Cryst.* **13**, 34 (1980).

22. Glatter, O. and Kratky, O. *Small Angle X-Ray Scattering; Academic Press*; New York, 1982.

23. Roe, R.J. *J. Appl. Cryst.* **15**, 182 (1982).

24. Hahn, B.R.; Herrmann, S. and Wendorff, J.H. *Polymer* **28**, 201 (1987).

25. Stein, R.S. and Rhodes, M.B. *J. Appl. Phys.* **26**, 3072 (1965).

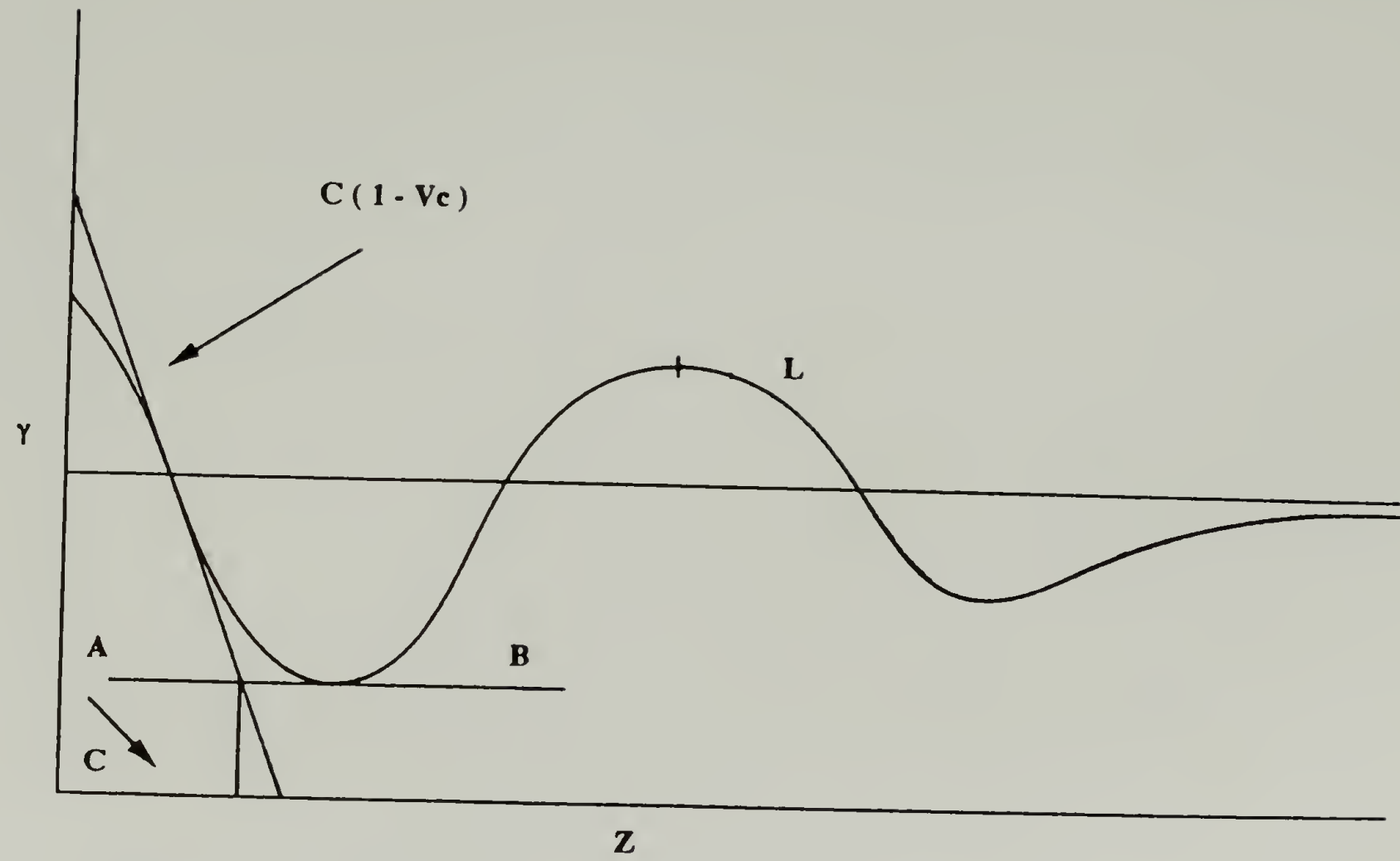

Figure 6.1 A schematic drawing of a correlation function with L = long period, C is the crystalline-phase thickness, V_c = the volume crystallinity. The x-intercept yields C (1-V_c) and the amorphous-phase thickness A = L - C.

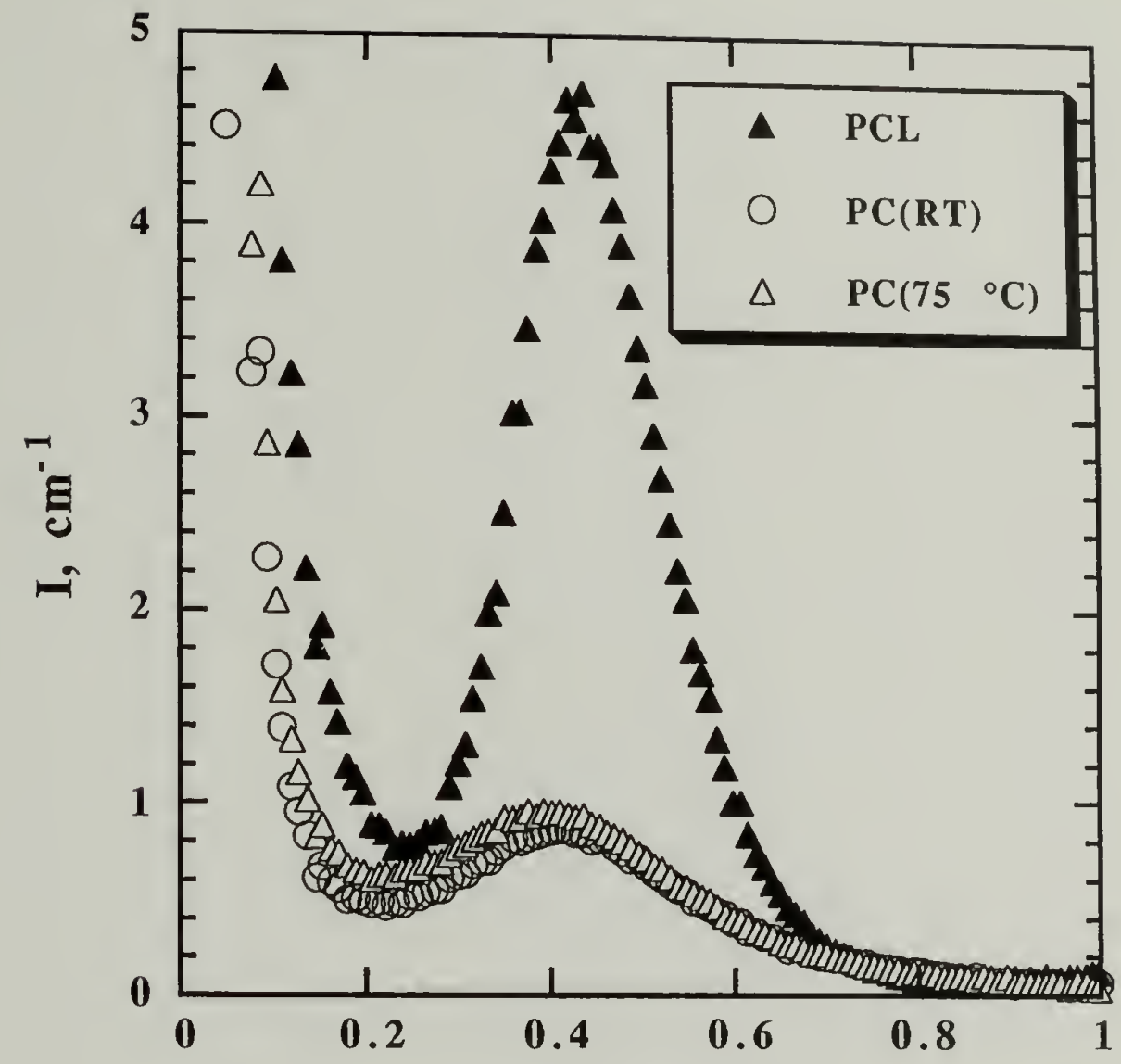

Figure 6.2 SAXS profiles for PCL measured at RT, PC at RT, and PC at 75 °C.

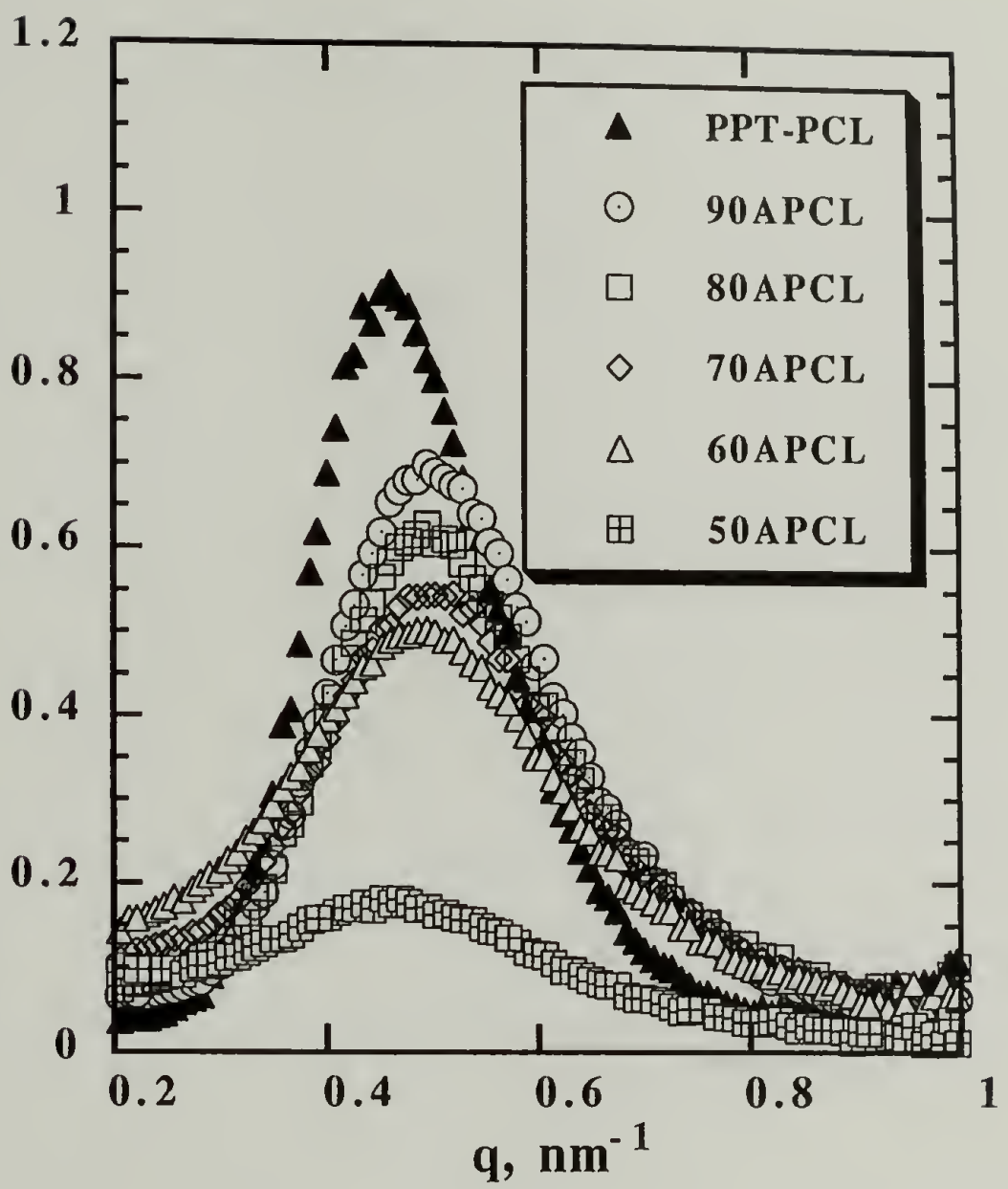

Figure 6.3 Lorentz-corrected SAXS curves recorded at RT for as precipitated PCL-rich blends.

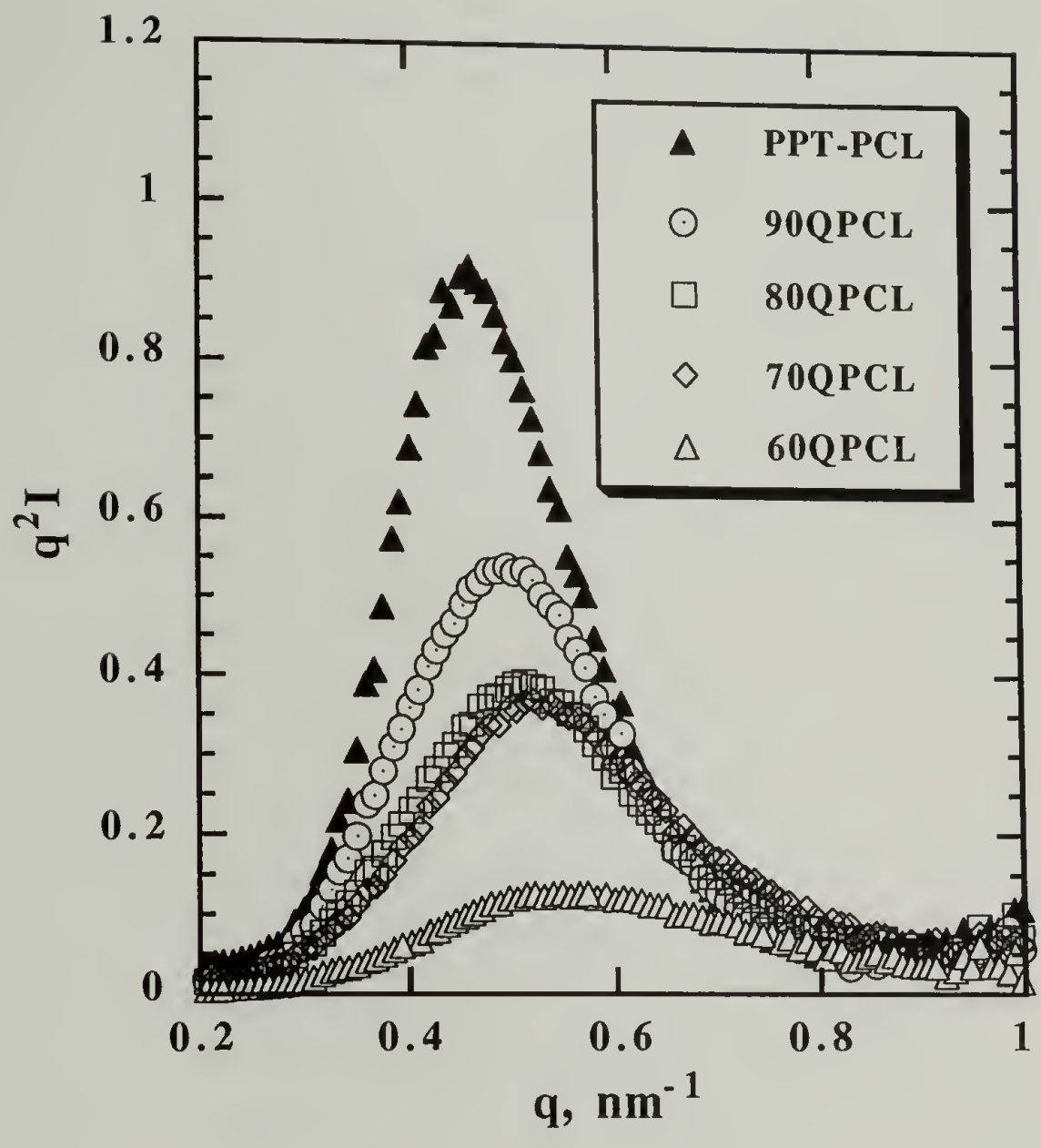

Figure 6.4 Lorentz-corrected SAXS profiles recorded at RT for quenched PCL-rich blends.

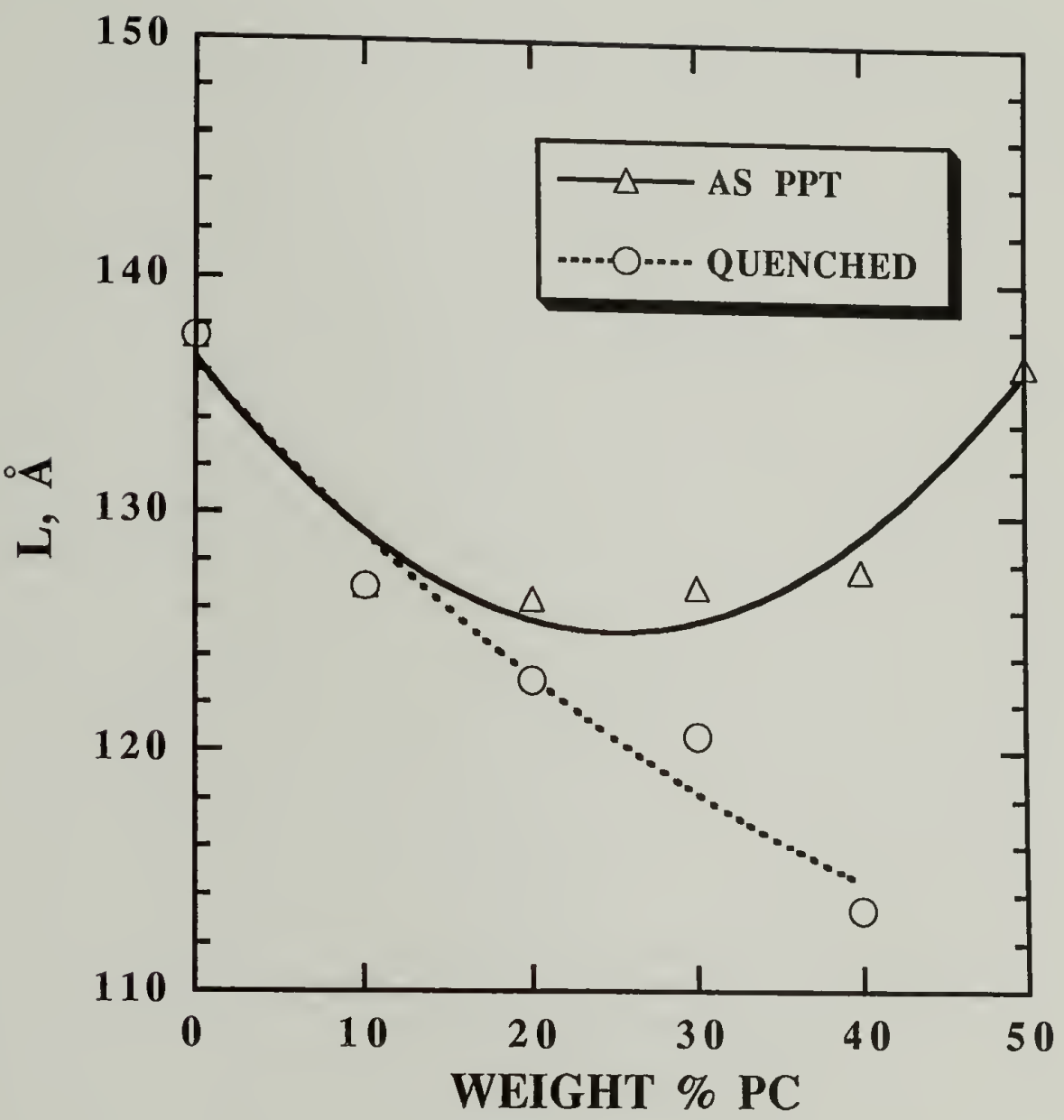

Figure 6.5. Long period measured at room temperature (in the semi-crystalline/semicrystalline state) for as precipitated and quenched blends.

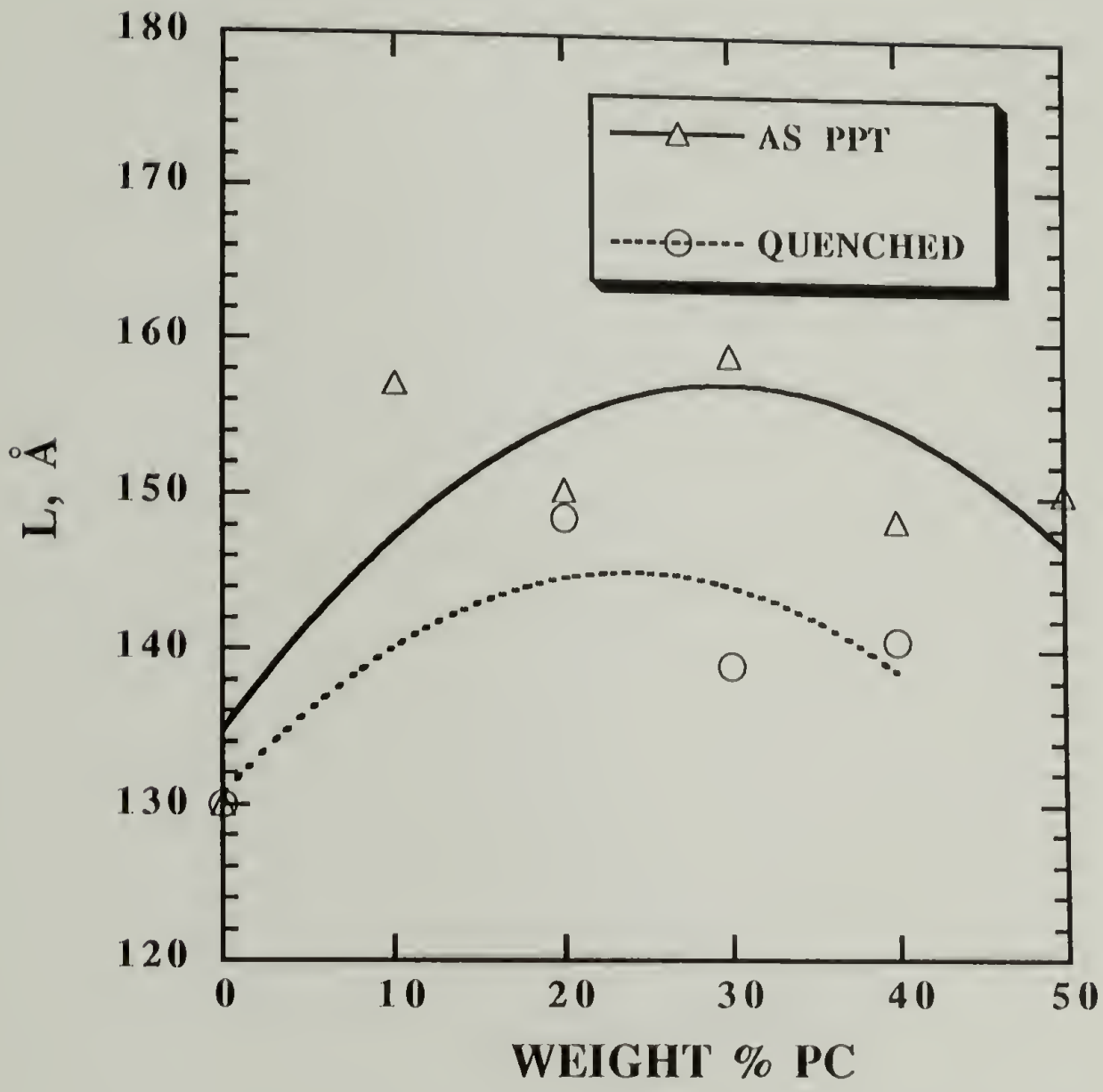

Figure 6.6 Long period measured at 75 °C (in the semicrystalline/ amorphous state) for as precipitated and quenched blends.

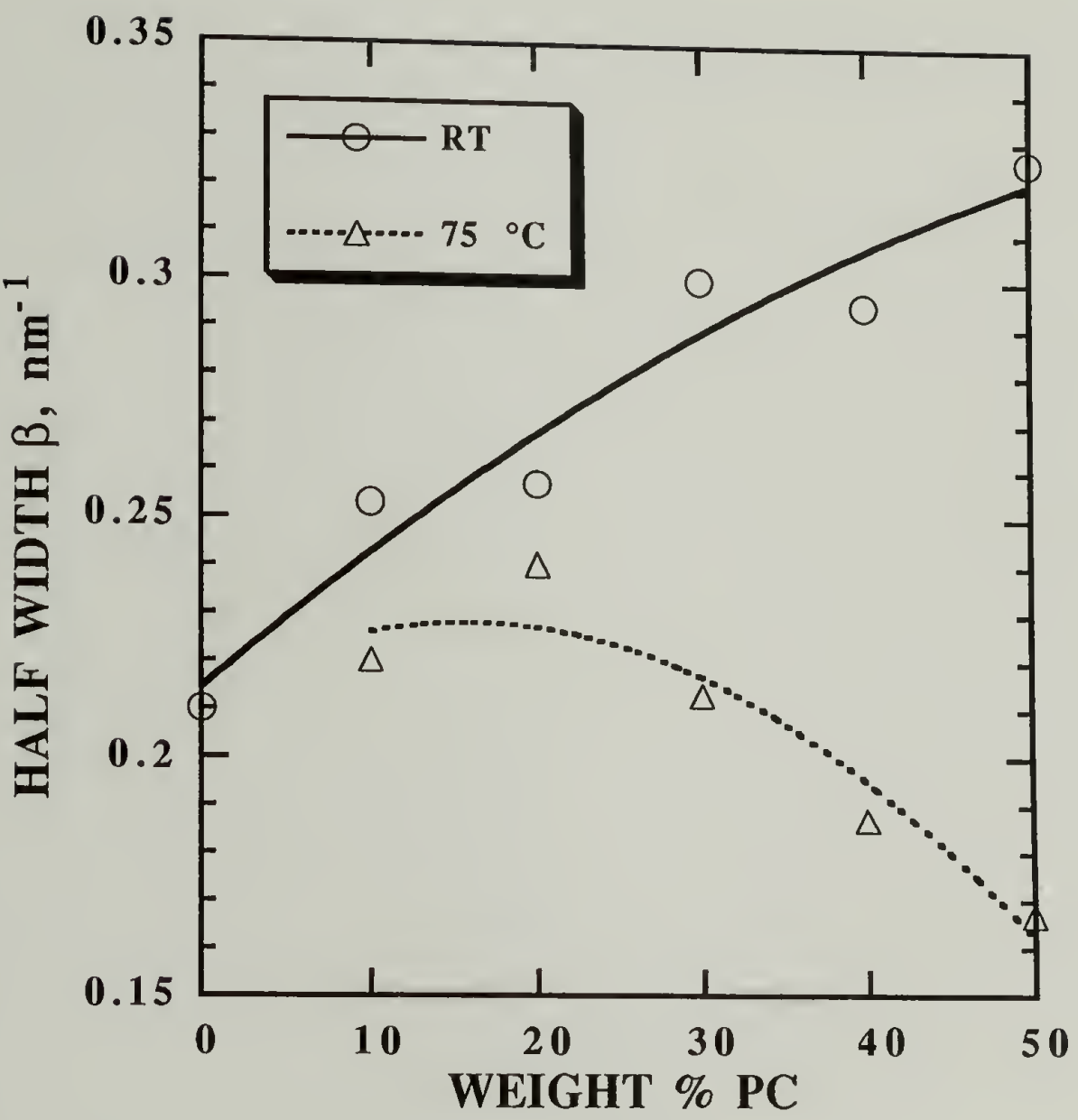

Figure 6.7 Peak width at half height of the Lorentz-corrected SAXS profiles for as precipitated blends measured at RT and 75 °C.

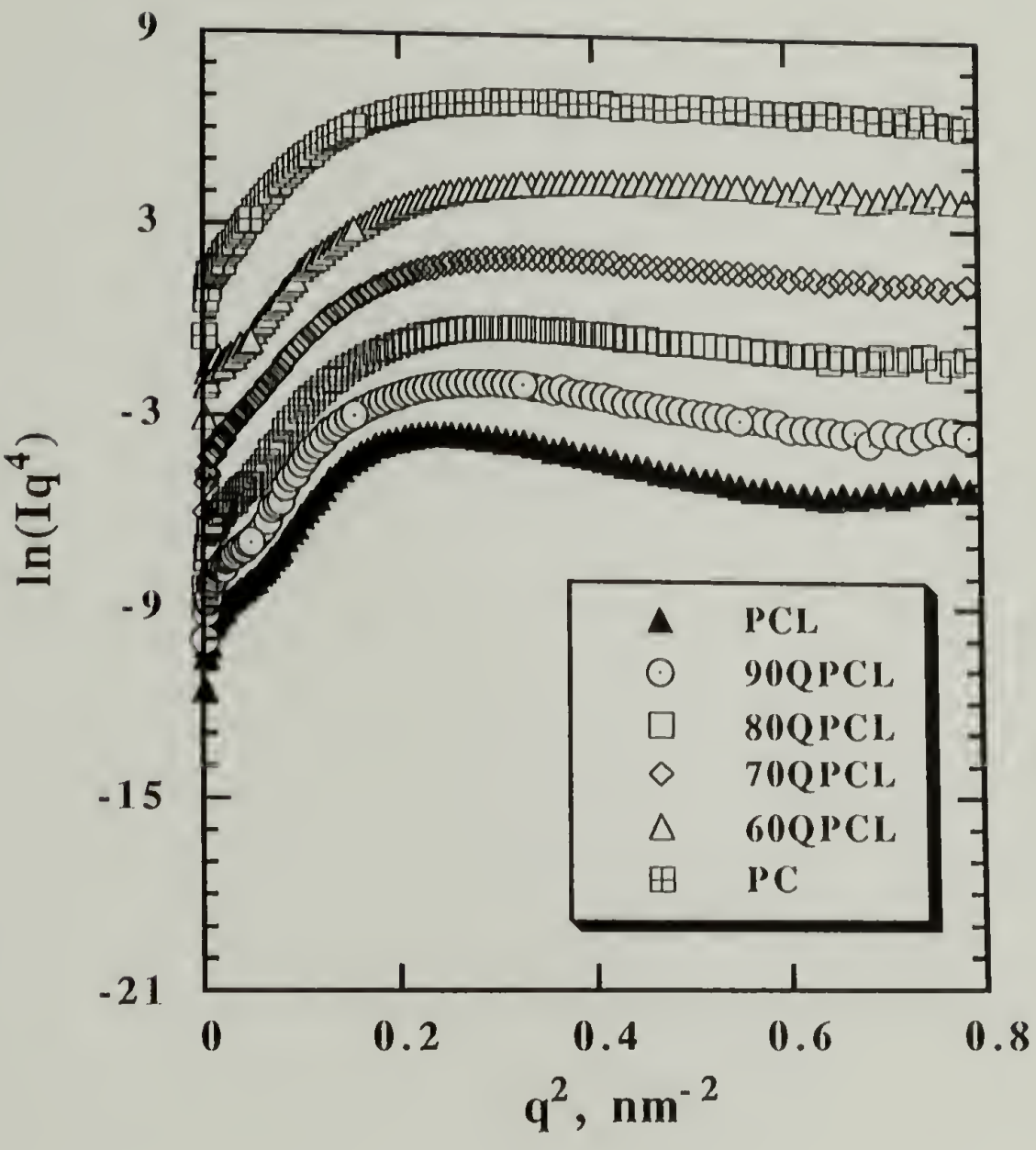

Figure 6.8 Porod plots (at RT) for pure PCL, quenched PCL-rich blends and pure PC.

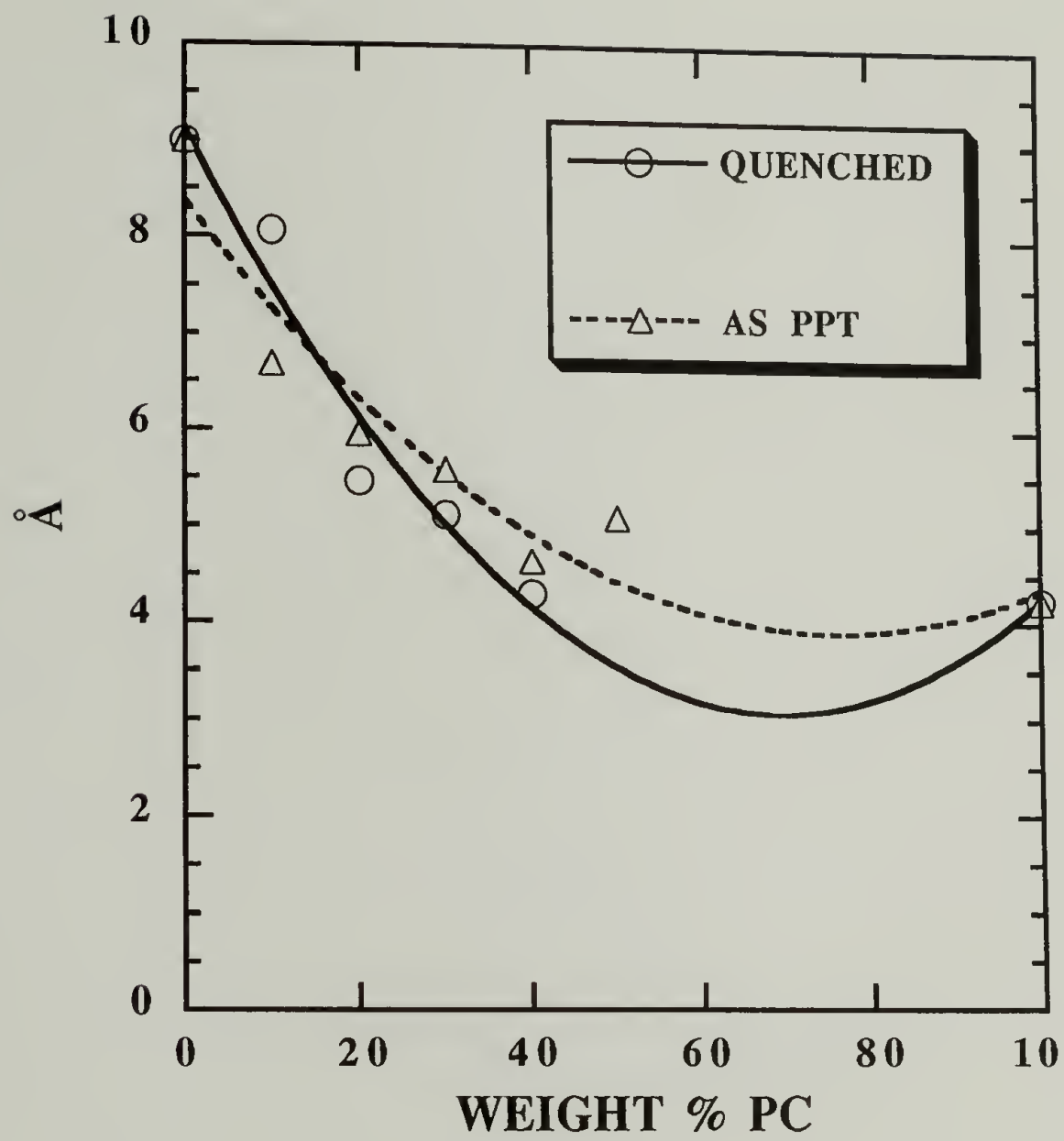

Figure 6.9 Interfacial thickness for quenched and as precipitated blends measured at RT.

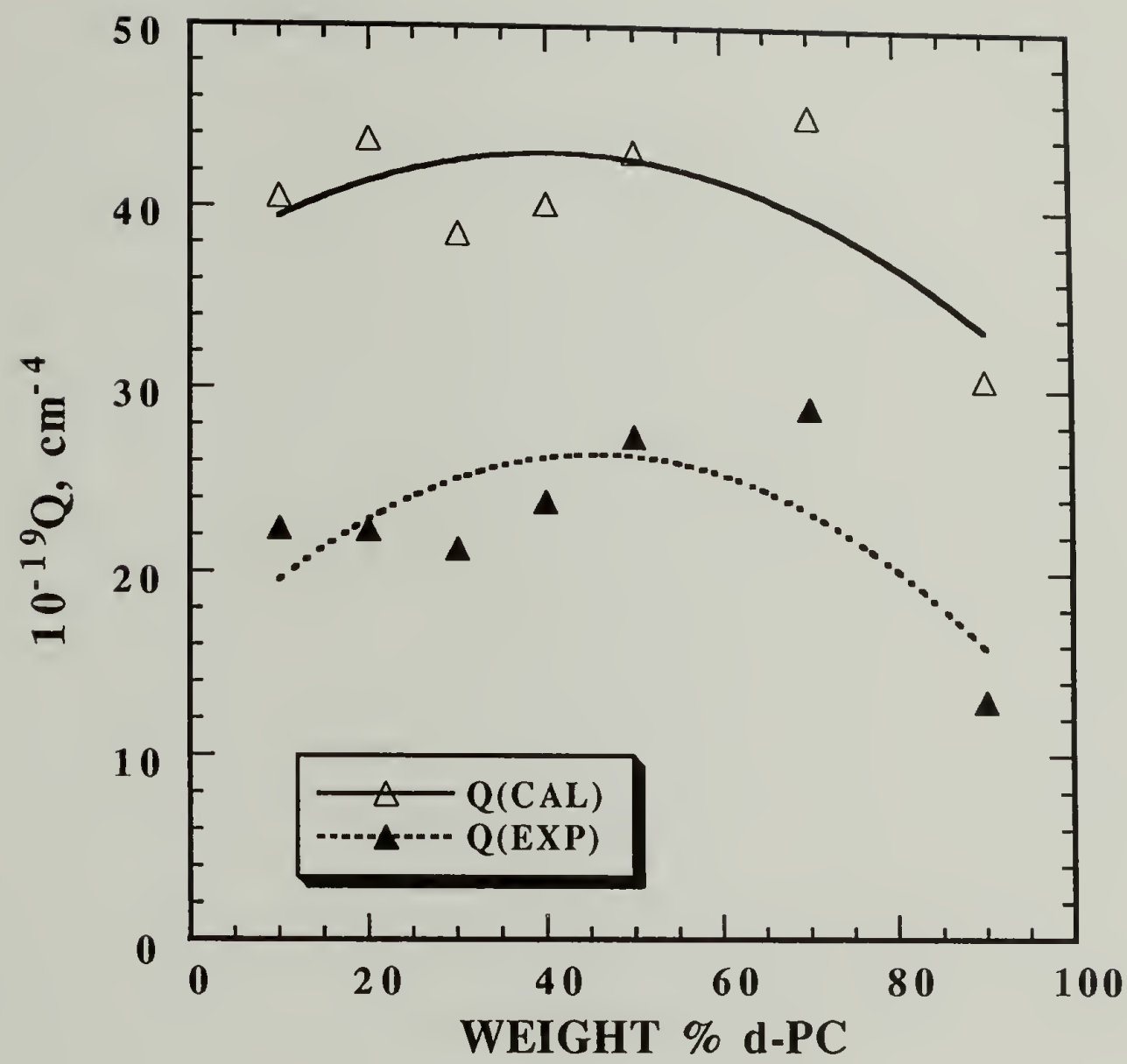

Figure 6.10 Comparison of the experimentally measured absolute invariant (EXP) to the calculated invariant (CAL) in the semi-crystalline/semicrystalline state.

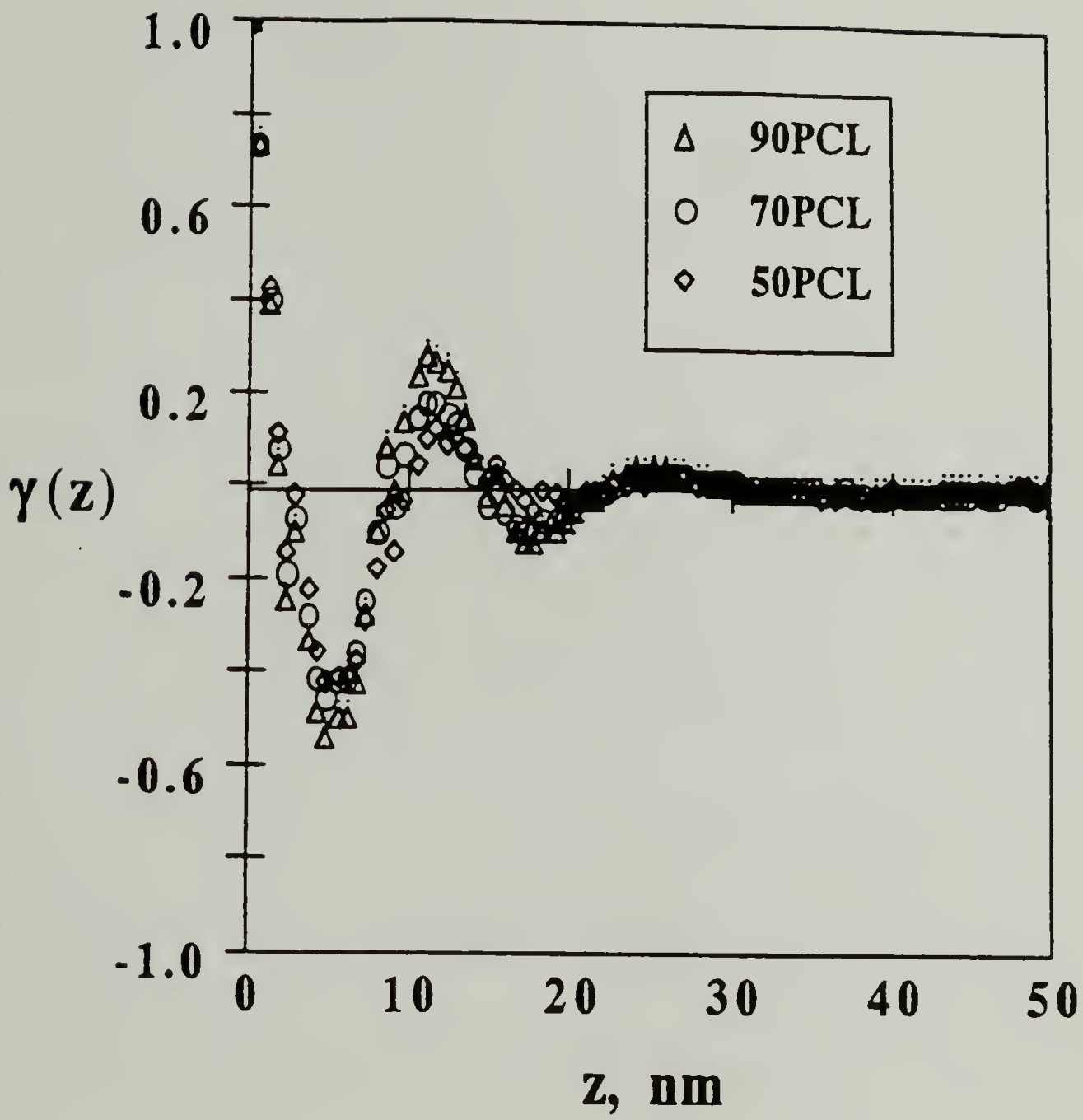

Figure 6.11 Correlation function evaluated at RT for the as precipitated PCL-rich blends.

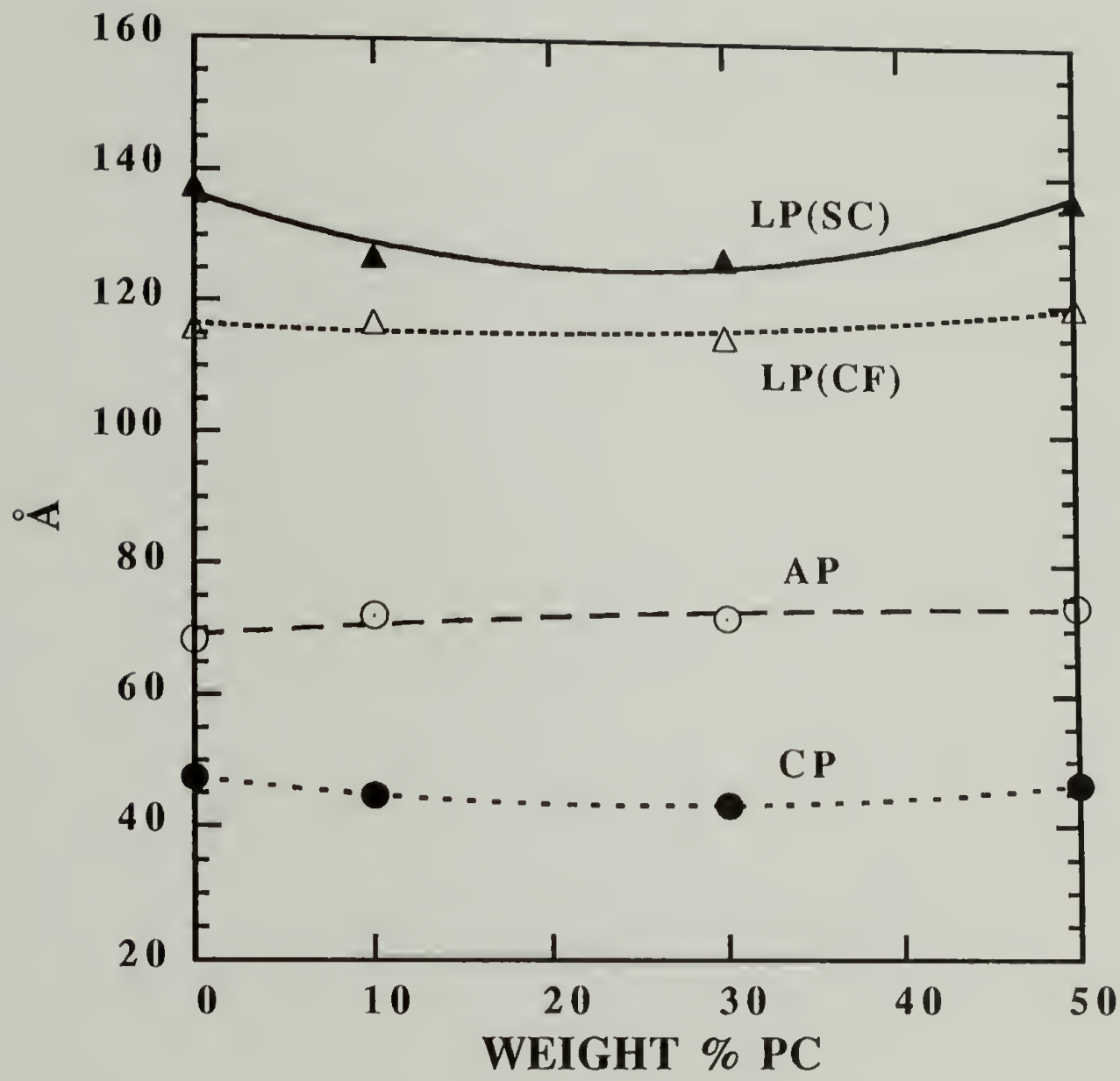

Figure 6.12 Correlation function results for the as precipitated blends measured at RT. LP(SC) = long period directly calculated from SAXS, LP(CF) = obtained from the correlation function, AP = amorphous-phase thickness, CP = crystal-phase thickness.

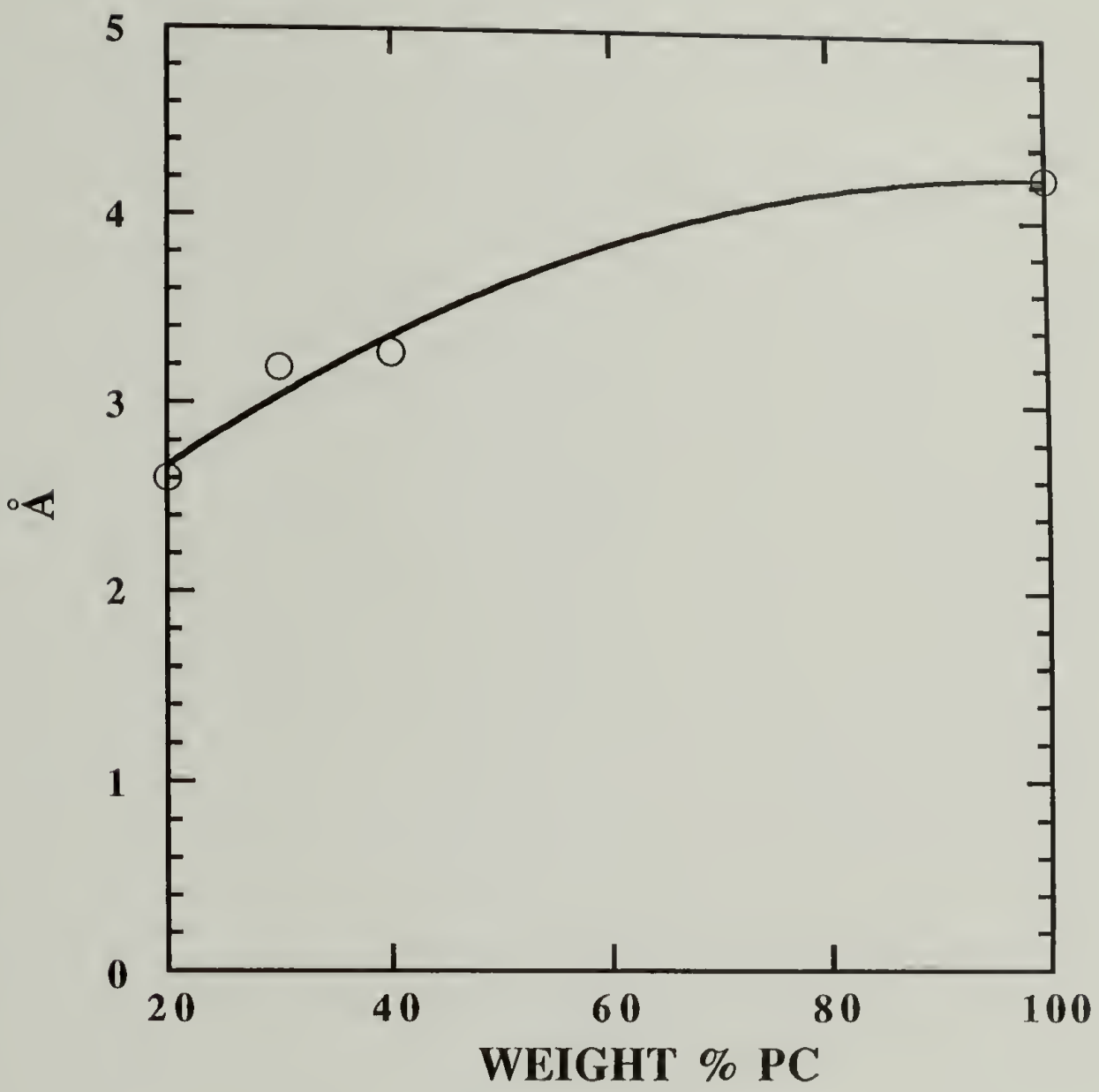

Figure 6.13 Interfacial thickness obtained at 75 °C for the quenched PCL-rich blends.

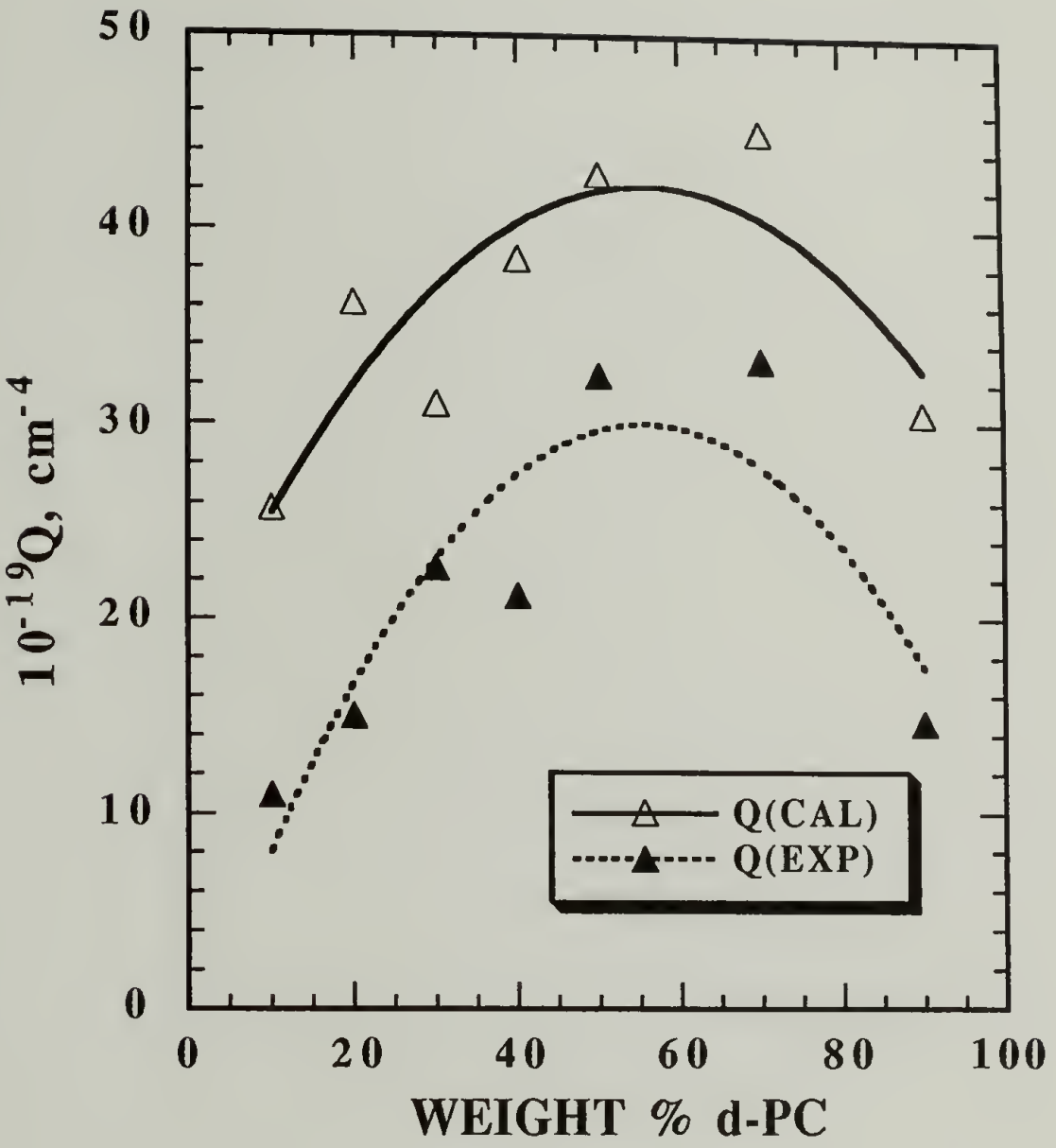

Figure 6.14 Comparison of the experimentally measured absolute invariant (EXP) to the calculated invariant (CAL)in the semi-crystalline/amorphous state.

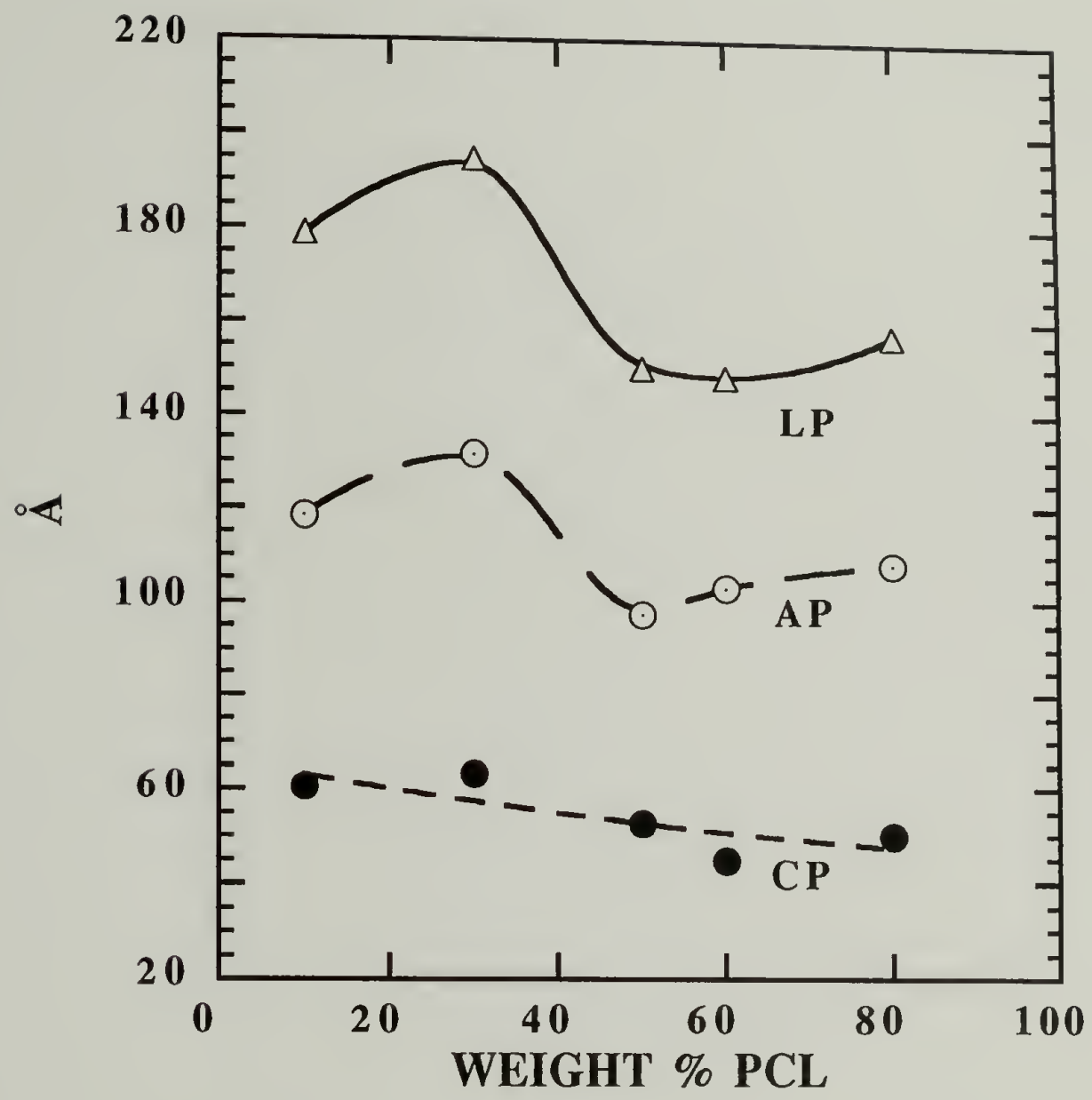

Figure 6.15 Correlation function results for d-PC/PCL blends in the semicrystalline/amorphous state. LP = PC long period, CP = PC crystalline-phase thickness, AP = PC amorphous-phase thickness.

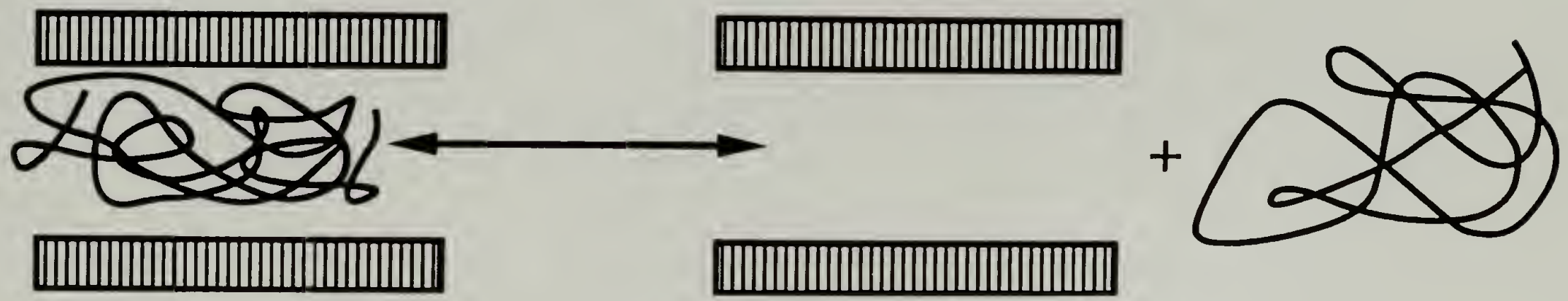

Figure 6.16 Competition between entropy and mobility governs the mode of lamellar incorporation.

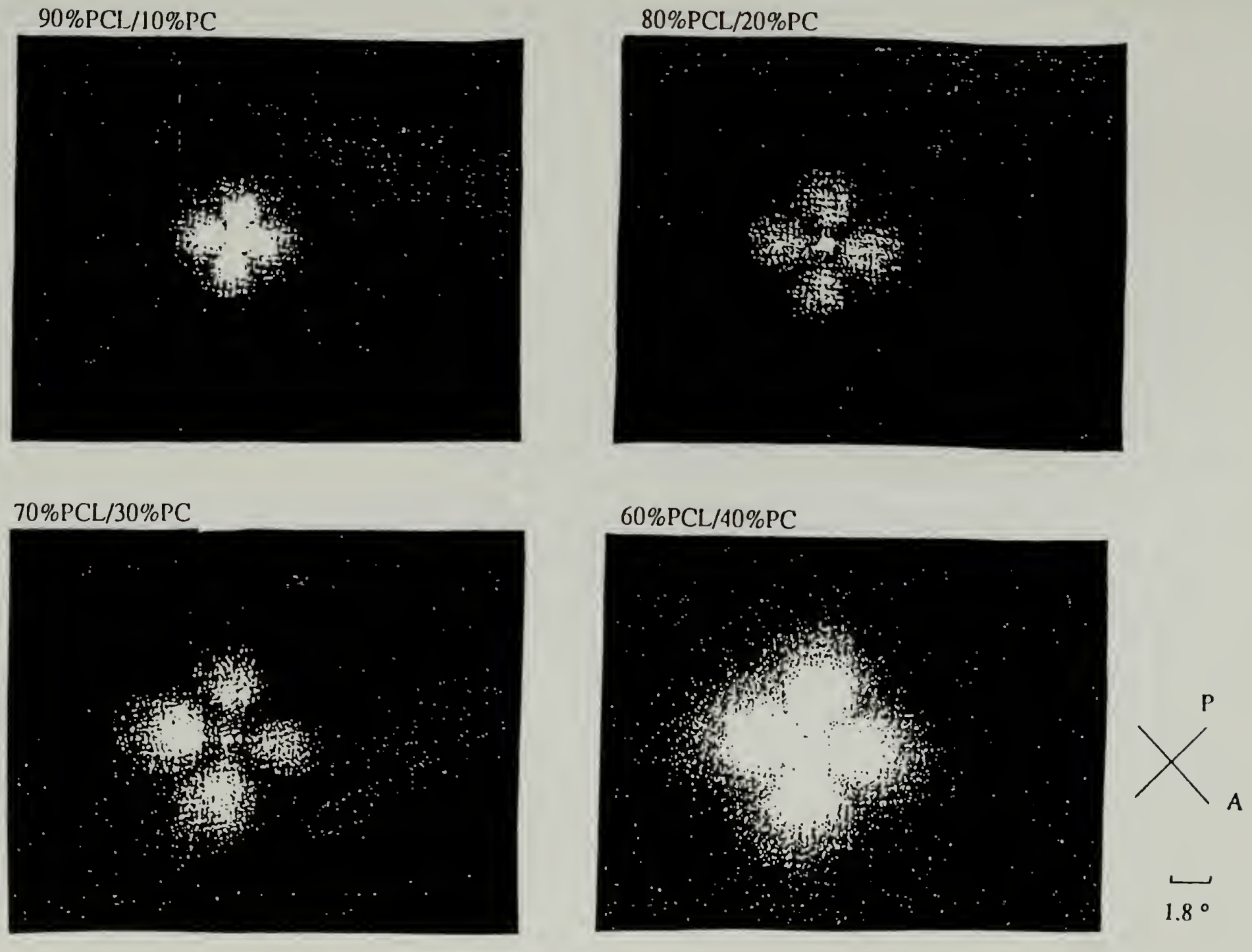

Figure 6.17 Small-angle light scattering (SALS) patterns for PCL-rich blends recorded at RT.

CHAPTER 7

GENERAL CONCLUSIONS AND FUTURE WORK

Unique to the PCL/PC blends is the multitude of phase transitions which could produce very rich and complex crystalline structures. The macromolecular plasticizer effects of PCL on PC are clearly manifested in the marked depression of the T_g of the blends relative to that of the pure PC. Correspondingly, the nucleating effects of PC on PCL crystallization are readily observable in the athermal and isothermal crystallization kinetics. Combination of the small-angle scattering results and the thermal analysis findings has provided invaluable insight into the complex structural evolution and organization of the PCL/PC blends at both the microscopic and macroscopic levels. However, there are many questions still remain unanswered and many phenomena remain unexplored. Therefore, the purpose of this chapter is to identify some important areas which would warrant further examinations.

Results derived from the preceding chapters could serve as a foundation for more fundamental investigations into the miscibility, crystallization kinetics and mechanisms, and morphologies of semicrystalline/semicrystalline blends. In addition to the traditional variables of composition and temperature, the degree of crystallinity could profoundly influence the crystallization kinetics and morphologies. It has been postulated that the degree of miscibility is an important determinant of crystallizability and supermolecular structure formation. Another dominant factor is the competition between kinetics and thermodynamics which ultimately controls the final structure and hence the properties of the material. Based on the guiding principle of structure-property relationships, the following research program is proposed to further advance our understanding of semi-crystalline/semicrystalline blends.

7.1 Crystallization Kinetics Studies of PC

Results derived from the DSC and synchrotron SAXS studies indicated that the PCL crystallization kinetics and mechanisms are strongly influenced by the physical state and the structure of PC in the blends. Additionally, it is postulated that the PCL and PC crystallization may be coupled in which the mobility of the amorphous phase continuously changes during the course of the crystallization. It is proposed that the crystallization studies be extended to PC in which the non-isothermal crystallization kinetics are probed by both small-angle and wide-angle X-ray scattering (SAXS and WAXS) using synchrotron radiation. Both rapid and slow cooling programs should be used in the study.

Since PC and PCL exhibit different crystalline structures and hence different crystalline reflections, WAXS is ideally suited for independently monitoring the evolution of PC and PCL crystallinity. Two experimental protocols may be designed to elucidate the complex crystallization mechanism. The first study will involve cooling the samples from above the melting point of PC to below the melting point of PCL to promote both PCL and PC crystallization. The second is a two-stage crystallization study in which the samples are first cooled to and held at 80 °C until PC crystallization is completed as reflected by the invariant in the SAXS and WADS intensities. PCL crystallization is then initiated by cooling the samples to below the PCL melting point. Results derived from this study may confirm the hypothesis that PCL crystallization could catalyze further PC crystallization.

7.2 Morphological Investigations

Quantitative SAXS analysis suggested that the mode of lamellar incorporation is governed by the competition between entropy and mobility. The universality of this intriguing result should be tested in other semicrystalline/amorphous blend systems.

SAXS should be performed on samples annealed at various temperatures to confirm the interlamellar exclusion-inclusion principle. In addition to varying the annealing temperature, the blend T_g may be modified with the addition of a low molecular weight plasticizer. By tuning the blend T_g, the mobility of the amorphous phase may be changed and consequently the mode of lamellar incorporation.

Indisputably, it is an extremely challenging task to elucidate and predict the lamellar organization of semicrystalline/semicrystalline blends. Quantitative interpretation of the scattering profiles is complicated by the superposition of the lamellar scattering resulting from the two different crystalline structures. Transmission electron microscopy (TEM) may be useful in providing additional insight into the lamellar and spherulitic arrangements in the semicrystalline/semicrystalline state. Selective imaging of one specific type of crystal is possible with dark field TEM. More refined analysis incorporating the effects of interfaces may be used to model the scattering invariant. Additionally, morphological models deduced from the TEM results could be used to simulate the small-angle scattering profiles which could yield useful morphological parameters. The synergism of electron microscopy and small-angle scattering should be exploited to unravel the complex crystalline structural organization of semicrystalline/semicrystalline blends.

7.3 Crystallization and Phase Separation

Competition between liquid-liquid phase separation and crystallization could often lead to a formation of very complex morphologies. Structural investigations have been conducted on systems where both phenomena are observed. However, the nature and structure of the amorphous phase in a semicrystalline/amorphous blend have never been systematically examined. SANS results based on the two-correlation length analysis suggested clustering in the amorphous phase of a semicrystalline/amorphous blend. This finding should be augmented and corroborated with solid-state NMR measurement.

Domain size in heterogeneous systems may be obtained by monitoring and analyzing the progression of the ^1H spin diffusion, which is based on the transfer of magnetization mediated by homonuclear decouplings between neighboring nuclei. Combination of small-angle scattering studies and solid-state NMR spectroscopy could provide additional insight into the structure of the amorphous phase of a semicrystalline/amorphous blend.

7.4 Miscibility and Crystallizability

In a blend system where both components could undergo crystallization, the degree of miscibility is expected to exert an important force in determining the crystallization kinetics and the degree of crystallinity. Theoretically, it is known that the interdiffusion coefficient of the crystallizing component(s) in the melt is a function of the interaction parameter χ. In a highly miscible system, it is envisioned that a polymer molecule has to diffuse from a highly entangled melt to form an ordered phase. In the case of a less miscible or partially miscible system, the crystallizing component can easily diffuse from an "inhomogeneous" (less entangled) melt to form an ordered structure. Since the χ parameter is related to diffusion and which determines crystal growth, systems with different degree of miscibility should be investigated. It has been observed that aliphatic polyesters with varying number of methylene units exhibit different degree of miscibility with PC. The crystallization rate of both components in the polyester/PC blends should be monitored and compared to those found in a totally immiscible blend system such as the polyethylene/PC blends. In order to account for the differences in mobility, a normalized parameter, defined as $\theta = [(T_c-T_g)/(T_m-T_g)]$, where T_c, T_g, and T_m, are the crystallization, glass transition and melting temperatures, respectively, should be used for the comparison.

7.5 Physical Property Correlation

Central to any blend study is the examination of the modification of the properties resulted from mixing of the two polymers. The ultimate properties are known to be profoundly influenced by the blend morphologies. Direct measurements of these properties may be obtained by examining the stress-strain behavior. More elaborate evaluations such as the J-integral measurement may be used to assess the fracture toughness. By varying the composition and the annealing conditions, the mode of lamellar incorporation and the degree of crystallinity of both components in a semicrystalline/semicrystalline blend may be controlled. It is of fundamental interest to generate a mapping between the structure and the mechanical properties of the blends.

APPENDIX: PUBLICATIONS

1. "Small-Angle Scattering Investigations of Poly(ε-caprolactone)/Polycarbonate Blends. 1. Small-Angle Neutron and X-ray Scattering Study of Crystalline Blend Morphology", *Macromolecules*, **26**, 5365 (1993).
   (with R.S. Stein, G.D. Wignall and H.E. Yang).

2. "Small-Angle Scattering Investigations of Poly(ε-caprolactone)/Polycarbonate Blends. 2. Small-Angle X-ray and Light Scattering Study of Semicrystalline/Semicrystalline and Semicrystalline/Amorphous Blends", *Macromolecules*, in press.
   (with R.S. Stein, J.S. Lin and G.D. Wignall).

3. "Small-Angle Scattering Investigations of Crystalline Morphologies of Poly(ε-caprolactone)/Polycarbonate Blends", Materials Research Society Proceedings, in press.
   (with R.S. Stein, G.D. Wignall and J.S. Lin).

4. "Evolution of Crystalline Structures of Poly(ε-caprolactone)/Polycarbonate Blends. 1. Isothermal Crystallization Kinetics As Probed By Synchrotron Small-Angle X-ray Scattering", Submitted to *Macromolecules*.
   (with R.S. Stein, B. Chu and G. Wu).

5. "Evolution of Crystalline Structures of Poly(ε-caprolactone)/Polycarbonate Blends. 2. Athermal and Isothermal Crystallization Kinetics", In Preparation.
   (with R.S. Stein).

6. "Phase Behavior and Miscibility of Poly(ε-caprolactone)/Polycarbonate Blends", In Preparation.
   (with R.S. Stein).

7. "Small-Angle Scattering Studies of Polymer Blend Morphologies"
   To Be Submitted to *Acta Polymerica.*
   (with R.S. Stein).

BIBLIOGRAPHY

Aubin, M. and Prud'homme, R.E. *Macromolecules* **21**, 2945 (1988).

Balta-Calleja, F.J. and Vonk, C.G. *X-Ray Scattering of Synthetic Polymers*; Elsevier, Amsterdam, 1989.

Barham, P.J. and Keller, H.H. *J. Polym. Sci., Phys. Ed.* **27**, 1029 (1989).

Bates, F.S. *J. Appl. Cryst.* **21**, 681 (1988).

Beaucage, G., Ph.D. Thesis, University of Massachusetts, Amherst, 1991.

Bittiger, H. and Marchessault, R.H. *Acta. Cryst.* **B26**, 1923 (1970).

Blundell, D.J. *Acta Crystallogr.* Sect. **A26**, 472, 476 (1970).

Bonart, V.A. *Die Makromolekulare* **92**, 146 (1966).

Branddrup, J. and Immergut, E.H. *Polymer Handbook*, 2nd ed., Wiley, New York, 1975.

Braun, G. and Kovacs, A.J. In *Physics of Non-Crystalline Solids*; Prins, J.A. Ed.; North-Holland, Amsterdam, 1965.

Cheung, Y.W.; Stein, R.S.; Wignall, G.D. and Yang, H.E. *Macromolecules* **26**, 5365 (1993).

Chu, B.; Wu, D.Q. and Howard, R. *Rev. Sci. Instrum.* **60**, 3224 (1989).

Coleman, M.M. and Zarian, J. *J. Polym. Sci., Polym. Phys. Ed.* **17**, 837 (1979).

Coleman, M.M. and Painter, P.C. *J. Appl. Spect. Reviews* **20(3&4)**, 255 (1984).

Couchman, P.R. and Karasz, F.E. *Macromolecules* **11**, 117 (1978).

Cruz, C.A.; Paul, D.R., and Barlow, J.W. *J. Appl. Polym. Sci.* **23**, 589 (1979).

Cruz, C.A.; Barlow, J.A. and Paul, D.R. *Macromolecules* **12**, 726 (1979).

Debye, P.; Anderson, H.R. and Brumberger, H. *J. Appl. Phys.* **28**, 6 (1957).

de Gennes, P.G. *Scaling Concepts in Polymer Physics*; Cornell University, Ithaca, 1979.

Dubner, W.S.; Schultz, J.M. and Wignall, G.D., *J. Appl. Cryst.* **23**, 469 (1990).

Elsner, G.; Koch, M.J.; Bordas, J. and Zachman, H.G. *Makr. Chem.* **182**, 1262 (1981).

Fox, T.G. and Flory, P.J. *J. Polym. Sci.***14**, 315 (1954).

Gerasimov, V.I. and Tsvankin, D.Y. *J. Polym. Sci., Polym. Phys. Ed.* **12**, 2035 (1974).

Glatter, O. and Kratky, O. *Small Angle X-Ray Scattering*; Academic Press; New York, 1982.

Godard, P.; Dekoninck, J.M. and Devlesavedr, J. *J. Polym. Sci., Polym. Chem.* **24**, 3315 (1986).

Gordon, M. and Taylor, J.S. *J. Appl. Chem.***2**, 493 (1952).

Hahn, B.R.; Herrmann, S. and Wendorff, J.H. *Polymer* **28**, 201 (1987).

Han, C.C.; Baurer, B.J.; Clark, J.C.; Muroga, Y.; Okada, M.; Tran-Cong, Q. and Sanchez, I.C. *Polymer* **29**, 2002 (1988).

Hoffman, J.D., Davis, G.T. and Lauritzen Jr, J.I. in "Treaties on Solid State Chemistry" (Ed. N.B. Hanny), Vol. 3, Plenum, New York, 1976, P. 497.

Hosemann, R. and Bagchi, S.N. *Direct Analysis of Diffraction by Matter;* North-Holland, Amsterdam, 1962.

Imai, M.; mori, K.; Mizukami, T; Kaji, K. and Kanaya, T. *Polymer* **33(21)** 4457 (1992).

Jonza, J.M. and Porter, R.S. *Macromolecuels* **19**, 1946 (1986).

Keith, H.D. and Padden, F.J. *J. Appl. Phys.* **24**, 2490 (1963).

Keith, H.D. and Padden , F.J. *J. Appl. Phys.* **35**, 1270, 1286. (1964)

Khamatta, F.B., Ph.D. Thesis, University of Massachusetts, Amherst, 1976.

Khamatta, F.B.; Warner, F.; Russell, T.B. and Stein, R.S. *J. Polymer Sci., Phys. Ed.* **14**, 1391 (1976).

Koleske, J.V. In *Polymer Blends*; Paul, D.R. and Newman, S., Ed.; Academic Press, New York, 1978.

Koningsveld, R. Private Communications .

Korberstein, J.T.; Morra, B. and Stein, R.S. *J. Appl. Cryst.* **13**, 34 (1980).

Kovacs, A.J. *Adv. Polym. Sci.***3**, 394 (1963).

Mandelkern, L. *Crystallization of Polymers;* McGraw-Hill, New York, 1964.

Mercier, J.P. *Polym. Sci. Eng.* **30(5)**, 270 (1990).

Moritani, M.; Inoue, T. and Kawai, H. *Macromolecules* **3(4)**, 433 (1970).

Morra, B.S., *Ph.D. Thesis*, University of Massachusetts, Amherst, 1980.

Nishi, T. and Wang, T.T. *Macromolecules* **8**, 909 (1975).

Nojima, S.; Tsutsui, H. and Urushihara, A. *Polym. J.* **18**, 451 (1986).

Olabisi, O. *Macromolecules* **8(3)** 316 (1975).

Philips, P.J. and Rensch G. *J. Polym. Sci. Polym. Phys. Ed.***27**, 155 (1989).

Porod, G. *Kolloid-Z* **124(2)**, 83 (1951).

Porod, G. *Kolloid-Z* **125(2)**, 108 (1952).

Roe, R.J. *J. Appl. Cryst.* **15**, 182 (1982).

Russell, T.P., Ph.D. Thesis, University of Massachusetts, Amherst, 1979.

Russell, T.P.; Ito, H. and Wignall, G.D. *Macromolecules* **21**, 1703 (1988).

Russell, T.P.; Lin, J.S. Spooner, S. and Wignall, G.D., J, *Appl. Cryst.* **21**, 629 (1988).

Russell, T.P. and Stein, R.S. *J. Polym. Sci., Polym. Phys. Ed.* **21**, 999 (1983).

Shibayama, M.; Yang, H.E.; Stein, R.S. and Han, C.C. *Macromolecules* **18** 2179 (1985).

Solc, K. Ed. *Polymer Compatibility and Incompatibility: Principles and Practices*; Harwood Academic, New York, 1982.

Song, H.H.; Stein, R.S.; Wu, D.Q.; Ree, M.; Philips, J.C.; Legrand, A and Chu, B. *Macromolecules* **21**, 1180 (1988).

Song, H.H.; Wu, D.Q.; Chu, B.; Satkowski, M.; Ree, M.; Stein, R.S. and Philips, J.C. *Macromolecules* **23**, 2380 (1990).

Stauffer, D. *Introduction to Percolation Theory*; Taylor and Francis, London, 1985.

Stein, R.S. and Rhodes, M.B. *J. Appl. Phys.* **26**, 3072 (1965).

Strobl, G.R. and Schneider, M. *J. Polym. Sci., Polym. Phys. Ed.*18, 1343 (1980).

Tabar, R.J., *Ph.D. Thesis*, University of Massachusetts, Amherst, 1983.

Tanaka, H. and Lovinger, A.J. *Macromolecules* **1987**, 20, 2683.

Tashiro, K; Satkowski, M.M.; Stein, R.S.; Li, Y; Chu, B. and Hsu, S.L. *Macromolecules* **25**, 1809 (1992).

Utracki, L.A. *Adv. Polym. Technol.***5**, 33 (1985).

Varnell, D.F.; Runt, J.P. and Coleman, M.M. *Macromolecules* **14**, 1350 (1981).

Vonk, C.G. and Kortleve, G. *Kolloid Z. Z. Polym.* **19**, 220, (1967).

Warner, F.P.; Stein, R.S. and Macknight, W.J. *J. Polym. Sci., Polym. Phys. Ed.***15**, 2113 (1977).

Wignall, G.D. and Bates, F.S. *J. Appl. Cryst.* **20**, 28 (1987).

Wignall, G.D.; Farrar, M. and Morris, S. *J. Mater. Sci.*. **25**, 69 (1990).

Wignall, G.D.; Lin, J.S. and Spooner, S. *J. Appl. Cryst.* **23**, 241 (1990).

Wittmann, J.C. and Lotz, B. *J. Polym. Sci. Polym. Phys. Ed.***19**, 1837 (1981).

Wittmann, J.C.; Hodge, A. M. and Lotz, B. *J. Polym. Sci. Polym. Phys. Ed.* **21**, 2495 (1983).

Wunderlich, B. *Macromolecular Physics*; Vol 2, Academic Press, New York, 1976.